Advancing sepsis treatment: synthesis and evaluation of multi-target drugs with antimicrobial, antioxidant and anticoagulant properties.

WEST, J.E.

2024

Advancing Sepsis Treatment: Synthesis and Evaluation of Multi-Target Drugs with Antimicrobial, Antioxidant and Anticoagulant Properties

Jordan Emma West

This thesis is given in partial fulfilment of the requirements of
Robert Gordon University
for the degree of
Master of Research

December 2024

Declaration

I hereby declare that the work presented in this thesis is my own, except where otherwise acknowledged, and has not been given in any form for another degree or qualification at any other academic institution. Information derived from the published or unpublished work of others has been acknowledged in the text, and a list of references is given.

Jordan West

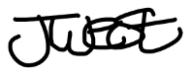

Abstract

Author: Jordan West

Degree: Master of Research

Title: Advancing Sepsis Treatment: Synthesis and Evaluation of Multi-Target Drugs with Antimicrobial, Antioxidant and Anticoagulant Properties.

Sepsis is a complex disease that affects individuals of all ages but is particularly dangerous for vulnerable populations, such as newborns, the elderly, and those with weakened immune systems. It is triggered by infection, leading to hyperinflammation, oxidative stress (OS), excessive blood coagulation, and, in severe cases, death. Globally, sepsis accounts for approximately 11 million deaths each year, with around 245,000 cases reported annually in the UK. The intricate clinical nature of sepsis renders single-target therapies, such as antibiotics, fluid resuscitation, and vasopressors, ineffective in many cases. This project aims to develop a series of multi-target drugs (MTDs) to address the various pathologies of sepsis, specifically targeting infection, OS, and abnormal blood coagulation.

A total of 11 MTD (JW1-JW11) compounds were synthesised, incorporating Naphthalimido and phenolic groups, with yields ranging from 23% to 92%. These compounds were fully characterised using high-resolution mass spectrometry (HRMS) and nuclear magnetic resonance (NMR; ^{1}H and ^{13}C).

Their antimicrobial properties were evaluated through standard 96-well plate microdilution to determine the minimum inhibitory concentration (MIC) and time-kill kinetics assays to assess bacterial survival over time against *Escherichia coli* and *Staphylococcus aureus*. Compounds JW6 and JW10 exhibited the lowest MIC among the synthesised compounds, measuring 125 µg/mL against *E. coli* and 250 µg/mL against *S. aureus*. Time-kill kinetics assays confirmed that JW6 and JW10 contain bactericidal properties, as no bacterial growth was observed after 24 hours at a dosage of twice the MIC. Antioxidant activity was investigated using Ferric Reducing Antioxidant Power (FRAP) and 2,2-diphenyl-1-picrylhydrazyl (DPPH) assays, with all compounds showing antioxidant activity. JW6, JW7, and JW10 demonstrated strong activity in the DPPH assay, with lead compounds JW6 and JW10 exhibiting IC_{50} values of 40.70 µM and 38.90 µM, respectively. In the FRAP assay, JW10 exhibited 1.25 Trolox equivalent (TE). The clot lysis assay was performed to investigate the anticoagulant properties. Compounds JW1, JW4, JW9, and JW11 demonstrated the strongest fibrinolytic activity, achieving a 50% clot lysis time of 68-78 minutes compared to the control (Pooled Normal Plasma + Phospholipids + tPA), which had a 50% clot lysis time of 70 minutes ($p < 0.05$). Compounds JW3, JW5, JW7, and JW8 showed the lowest maximum absorbance of 0.2, indicating reduced clot density compared to the control (PNP+Pl), with an absorbance of 0.4 at 405 nm.

The antibacterial and antioxidant properties of the compounds highlight their potential as MTD candidates for sepsis treatment. Further investigations into specific drug targets and mechanisms of action are required. By addressing the multifaceted nature of sepsis through simultaneous targeting of infection, OS, and blood clotting, these compounds provide ideal candidates for further

optimisation, particularly JW6 and JW10. Future research will include mechanisms of action studies and *In vivo* testing to assess the toxicity of the compounds. This study underscores the relevance of the MTD strategy in managing complex diseases such as sepsis, where single-target therapies may be insufficient.

Keywords: Sepsis, Naphthalimide, Antimicrobial, Antioxidant, Anticoagulant, Multi-target strategy.

Table of Contents

Abbreviations

2,2-Diphenyl-1-Picrylhydrazyl (DPPH)
Absorbance (ABS)
Acute Respiratory Distress Syndrome (ARDS)
Adenosine Diphosphate (ADP)
Activated Protein C (APC)
Antimicrobial Peptides (AMPs)
Antimicrobial Resistance (AMR)
Antithrombin (AT)
Atmospheric Solids Analysis Probe (ASAP)
Butyrylcholinesterase (BuChE)
C-Reactive Protein (CRP)
Clinical Laboratory Standards Institute (CLSI)
Colony-Forming Units (CFU)
Damage-Associated Molecular Patterns (DAMPs)
Deuterated Dimethyl Sulfoxide (DMSO-d_6)
Dimethyl Sulfoxide (DMSO)
Disseminated Intravascular Coagulation (DIC)
Ferric Reducing Antioxidant Power (FRAP)
Fibroblast Growth Factor Receptor (FGFR)
Full Width at Half Maximum (FWHM)
High-Resolution Mass Spectrometry (HRMS)
Human Leukocyte Antigen (HLA)
Hydrogen Atom Transfer (HAT)
Interferons (IFNs)
Interleukins (ILs)
Mass-to-Charge Ratio (m/z)
Minimum Inhibitory Concentration (MIC)
Multi-Target Drug (MTD)
Muller Hinton Agar (MHA)
Muller Hinton Broth (MHB)
Multi-Organ Dysfunction Syndrome (MODS)
Naphthalimidopropylamine (NPA)
Negative Ion Nanoelectrospray Ionisation (nES)
Neutrophil Extracellular Traps (NETs)
NOD-Like Receptors (NLRs)
Nuclear Factor-Kappa-Light-Chain-Enhancer of Activated B Cells (NF-κB)
Nuclear Magnetic Resonance (NMR)
Optical Density (OD)
Oxidative Stress (OS)
Parts Per Million (ppm)
Pathogen-Associated Molecular Patterns (PAMPs)
Pathogen Recognition Receptors (PRRs)
P-Selectin Glycoprotein Ligand-1 (PSGL-1)
Phospholipids (PL)
Platelet-Leukocyte Aggregates (PLAs)
Plasminogen Activator Inhibitor-1 (PAI-1)
Pooled Normal Plasma (PNP)
Procalcitonin (PCT)

Protease-Activated Receptors (PARs)
Reactive Nitrogen Species (RNS)
Reactive Oxygen Species (ROS)
Sepsis-Induced Coagulopathy (SIC)
Sequential Organ Failure Assessment (SOFA)
Single Electron Transfer (SET)
Thin Layer Chromatography (TLC)
Thrombin-Activatable Fibrinolysis Inhibitor (TAFI)
Tissue Factor (TF)
Tissue Factor Pathway Inhibitor (TFPI)
Tissue Plasminogen Activator (tPA)
Toll-Like Receptors (TLRs)
Trolox Equivalent (TE)
Tumour Necrosis Factor-Alpha (TNF-α)
Vascular Endothelial Growth Factor Receptor (VEGFR)
Von Willebrand Factor (vWF)

1. Introduction

1.1 What is Sepsis?

Sepsis is a life-threatening clinical condition with a complex pathophysiology that arises when our immune response to infection becomes dysregulated [1]. The presence of pathogens and other pathogenic molecules entering the bloodstream ultimately triggers widespread hyper-inflammation [1,2], which in severe cases leads to tissue and organ damage, which may cause death [3]. The human innate and adaptive immune system rapidly responds to invasive pathogens by releasing inflammatory mediators, propagating immune cells, and re-locating them into the tissues where the pathogens are present [4]. This prevents the microbial multiplication and its spread [4]. Since the release of inflammatory mediators is tightly regulated by the immunological homeostasis in our body [5], the inflammatory response subsides once the pathogen is eliminated or brought under control [3,4].

However, in patients who develop sepsis, this process becomes uncontrolled and results in excessive production of inflammatory mediators, including cytokines such as Tumour Necrosis Factor-alpha (TNF-α), interleukins (IL-1, IL-6), prostaglandins, histamine, and nitric oxide (NO) [1,2,3]. Although these inflammatory molecules are crucial in initiating and aiding inflammation to protect the body from infection-causing pathogens, their excessive release can lead to biological pathways that contribute to self-damaging vital tissues [80]. As a result of ongoing tissue damage, vital organs such as the liver, lungs, and heart may begin to fail, potentially leading to septic shock and, in severe cases, death within hours of sepsis development [3]. Therefore, early identification and intervention are critical to reducing the high mortality rate associated with this condition [1].

Sepsis is characterised by a complex interaction between infection and inflammation [1,3], which is not yet completely understood [1,6]. Therefore, the definition of sepsis continues to evolve as our understanding of its pathophysiology advances. Initially, sepsis was defined primarily as an infection-related condition, with its first formal definition established during a conference held by the American College of Chest Physicians and the Society of Critical Care Medicine in the early 1990s [9]. A later conference in 2001, where the condition was defined as sepsis, severe sepsis and septic shock [9]. However, modern definitions now emphasise the complexity of its mechanisms, including hyperinflammation, OS, and multiple pathological processes [1,3].

The Third International Consensus Definitions for Sepsis and Septic Shock (Sepsis-3) [4]:

> Sepsis is defined as life-threatening organ dysfunction caused by a dysregulated host response to infection.
>
> Septic Shock is a subset of sepsis in which particularly profound circulatory, cellular, and metabolic abnormalities are associated with a greater risk of mortality than with sepsis alone.

This distinction between sepsis and septic shock is vital for guiding clinical management, as septic shock requires more intensive therapeutic interventions due to its higher associated mortality risk [4]. The dysregulated immune response in sepsis activates several interconnected biological pathways, including the complement system, the coagulation cascade, and innate and adaptive immune systems (Figure 1). Although the complement system is primarily designed to enhance pathogen clearance, its excessive activation in sepsis can aggravate tissue injury [65]. Similarly, dysregulation of the coagulation pathways, commonly referred to as sepsis-induced coagulopathy (SIC; Figure 1), often results in disseminated intravascular coagulation (DIC), which also intensifies organ dysfunction. This can result in organ-specific failures, such as acute respiratory distress syndrome (ARDS; Figure 1), particularly affecting the lungs [6].

As sepsis progresses, persistent inflammation and immune imbalance can lead to multi-organ dysfunction syndrome (MODS; Figure 1), characterised by the failure of two or more organ systems [6]. The development of MODS significantly increases the risk of mortality, representing the most severe phase of sepsis and septic shock. At this stage, critical organs such as the kidneys, lungs, liver, and cardiovascular system are commonly affected, marking the terminal progression of the disease [6].

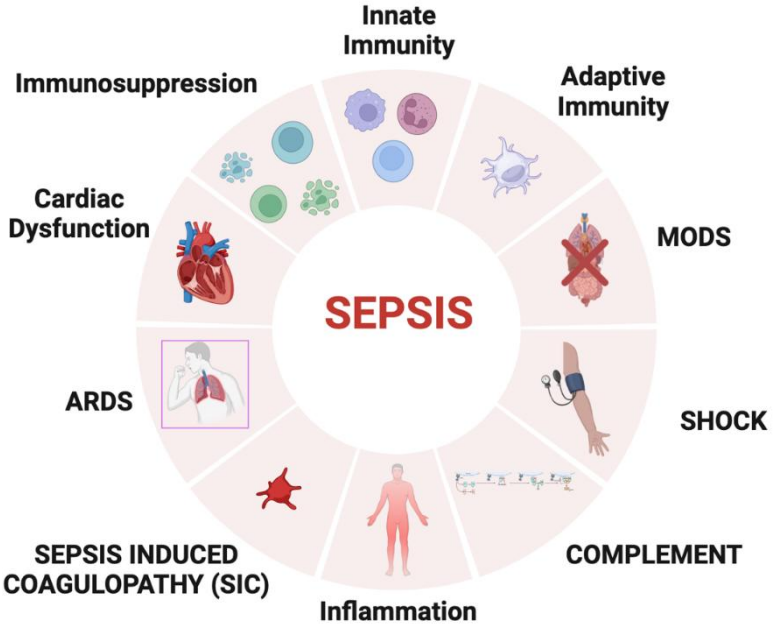

Figure 1 Pathophysiology of Sepsis: Key Mechanisms and Associated Complications [6]

The infection may arise from any area, most commonly the lungs, urinary tract, skin, or gastrointestinal tract [7]. Those who develop sepsis are more likely to have a pre-existing condition, such as a weakened immune system or lung disease. Other risk factors include those 65 years or older, children under one year, sepsis survivors, recently hospitalised or those with chronic conditions [7].

1.2 Sepsis Pathophysiology

1.2.1 Microbial Invasion and Initial Immune Response

Sepsis can result from bacterial, viral, or fungal infections. Bacteria are the most common causative pathogens and can enter the body through wounds, the respiratory tract, the urinary tract, or the bloodstream [7,8]. The main agents responsible for sepsis include Gram-negative and Gram-positive bacterial strains (Table 1).

Table 1 Predominant Causative Agents of Sepsis [8]

Gram-positive bacterial strains	*Staphylococcus aureus* *Streptococcus pyogenes*
Gram-negative bacterial strains	*Escherichia coli* *Klebsiella spp*. *Pseudomonas aeruginosa*

Once the pathogen breaches the body's defences, the immune system activates a localised inflammatory response to control the infection. Unlike the controlled response to localised infections, sepsis disrupts the balance between pro-inflammatory and anti-inflammatory processes [6]. Upon recognition of pathogen-associated molecular patterns (PAMPs) and damage-associated molecular patterns (DAMPs) of the pathogens, the host immune system launches a widespread response. This recognition triggers the release of numerous factors, including cytokines, pathogen-related molecules, and various mediators, which collectively activate the coagulation cascade and complement system [6, 12]. PAMPS and DAMPS activate receptors known as pathogen recognition receptors (PRRs), such as toll-like receptors, (TLR) nucleotide-binding and oligomerisation domain (NOD)-like receptors (NLRs), and retinoic acid-inducible gene (RIG)-I-like receptors (RLRs) on monocytes and antigen-presenting cells (APC) surfaces [64]. This initiates sepsis *via* gene transcription; these genes are involved in inflammation, adaptive immunity and cell metabolism. The upregulation of both inflammatory pathways also results in tissue damage, progressing to multi-organ failure. In the later stages of sepsis, immunoparalysis can also arise due to the immunosuppression caused by the downregulation of cell surface molecules, exhaustion of T cells and an increase in immune cell apoptosis, leaving the patient susceptible to nosocomial infections [10,11].

As the PAMPS and DAMPS bind to the APCs and monocytes, TLR signal transduction is induced, and nuclear factor-kappa-light-chain-enhancer of activated B cells (NF-κB) is translocated into the nucleus of the cell [64]. This prompts the expression of early activation genes, including several pro-inflammatory ILs such as IL-1, IL-12, IL-18, TNF-α, and interferons (IFNs) (Figure 2). Subsequently, negative feedback and downregulation of adaptive immune system factors cause further activation of cytokines such as IFN-γ, IL-6, IL-8, complement system and coagulation cascade. The above processes can be

seen in the early stages of sepsis, characterised by increased pro- and anti-inflammatory cytokines (Figure 2) [6,11].

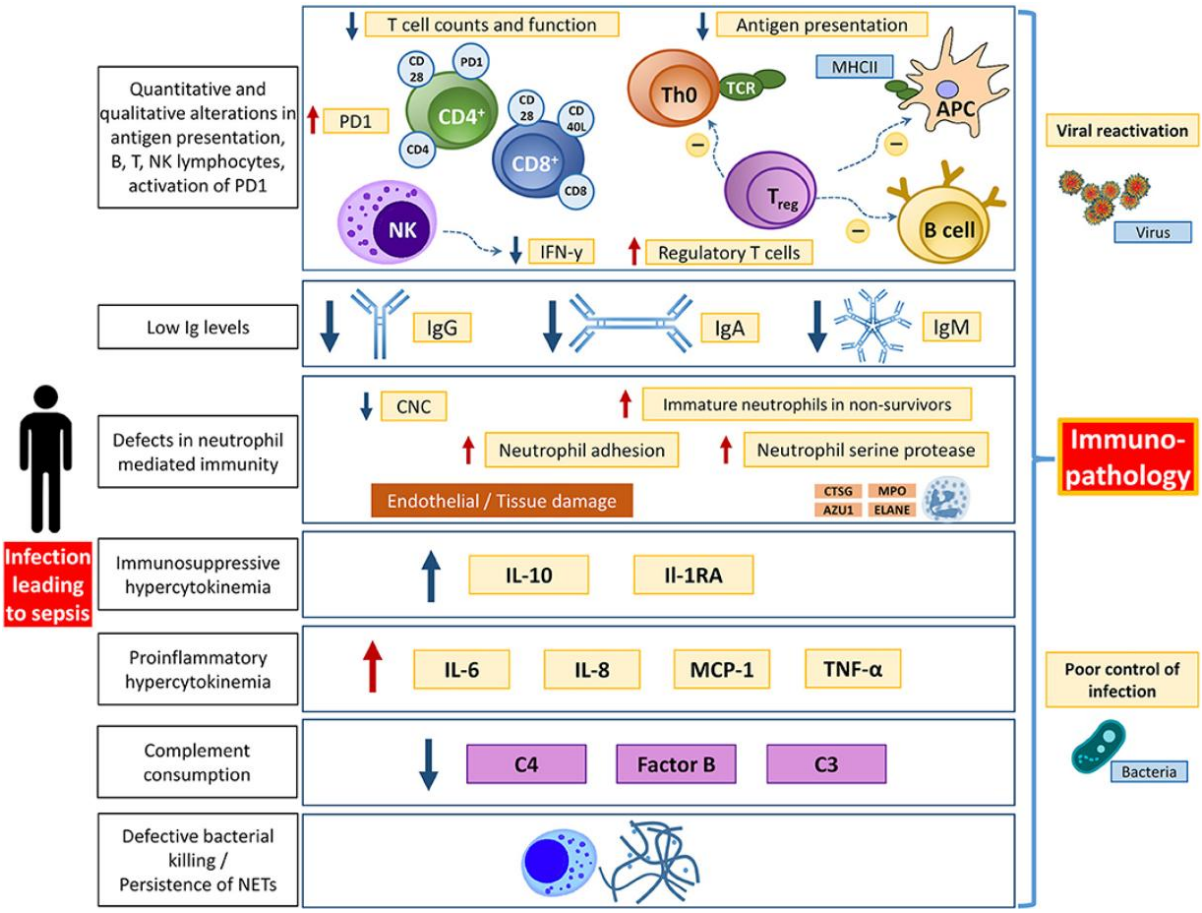

Figure 2 Overview of the immunological dysfunction in sepsis and the response of different cell types, including T Cells, IL, and APC (sourced form 6).

Neutrophils form the first line of defence against invading pathogens [12]. During bacterial infection, immature and mature neutrophil forms are released by the bone marrow *via* granulocyte maturation [6, 12]. When PAMPS and DAMPS activate the immature neutrophils, they reduce phagocytosis and oxidative burst capacity [6]. Patient deterioration is often concurrent with elevated levels of these cells, which is also associated with the release of neutrophil extracellular traps (NETs). NETS are comprised of decondensed chromatin with nuclear and granular proteins and can halt several pathogens, including bacteria (Gram-negative and positive), viruses and parasites. NET release can be triggered by chemokines and cytokines, platelet agonists and antibodies. A high abundance of NETS may result from overproduction or insufficient degradation, which is associated with endothelial damage and hypercoagulation (Figure 2) [11,12].

To design an effective and safe therapy to prevent sepsis, it is vital that we understand how infection develops and the way in which the immune system responds. The early identification of pathogens through PAMPs and DAMPs and the later activation of immune pathways play a critical role in the progression from localised infection to systemic inflammation [64]. Targeting these early

immune signalling pathways, such as through the modulation of TLRs, inhibition of inflammatory cytokines like TNF-α and IL-6, and regulation of the coagulation cascade therapeutics, can prevent the immune system from becoming overwhelmed. Moreover, therapies that address the damaging effects of excessive NET formation and prompt and appropriate antibiotic use are key to mitigating tissue damage and reducing the risk of multi-organ failure [(6)].

1.2.2 Endothelial Dysfunction and Vascular Permeability

In sepsis, microvascular dysfunction initiates endothelium activation and changes to the proinflammatory phenotype of endothelial cells (ECs). Many different pathogens and products act upon the endothelium *via* various mechanisms. In addition to direct pathogen-induced endothelium activation, non-specific activation can also occur due to DAMPS, which plays an essential role in the inflammatory process [12,13].

After proinflammatory stimulation, ECs lose their anticoagulant function, and coagulation is then promoted due to the decreased expression on the cell surface of thrombomodulin and heparan sulphate with increased tissue factor (TF) expression [13]. The coagulation cascade can be triggered by the upregulation of pathogen-activated endothelial cells, tissue factor-bearing monocytes, and leukocyte-derived microparticles [13].

The cytokine storm caused by hyperinflammation also damages the endothelium, disrupting vascular tone, homeostasis, and permeability [64]. ECs share many common characteristics, such as regulating blood flow and controlling passage in and out of the bloodstream but also have organ-specific features. Due to the heterogeneity of the different microvascular beds (tiny blood vessels of organs), the ECs must adapt to each organ's specific needs [1]. Therefore, the endothelial lining of blood vessels is crucial for upholding vascular health, and it is supported by the endothelial cytoskeleton and a protective layer known as the glycocalyx, which helps regulate multiple vascular functions [18]. Harmful species such as reactive oxygen species (ROS) and bacterial endotoxins can disrupt the integrity, causing damage to the ECs and glycocalyx shedding, where the EC's protective layer is degraded. The shedding of this protective barrier contributes to vascular dysfunction [1,14,16].

ARDS (Figure 1) is a severe lung condition that arises as the lungs become inflamed and filled with fluid, causing difficulty breathing and reduced oxygen levels in the blood [14]. ARDS results from damage to the EC lining in the blood vessels located in the lung. This damage disrupts the endothelial barriers regulating the passage between lung tissue and the bloodstream [2]. During inflammation, the proinflammatory cytokines are released, increasing pulmonary permeability and allowing larger fluid volumes to leak into the lung tissue [18]. This causes increased pulmonary vascular permeability, allowing the accumulation of protein-rich fluid in the alveoli and interstitial space [6]. This fluid accumulation interferes with the normal function of the lungs, gas exchange, and inflammation. It causes severe breathing difficulties that may ultimately lead to acute respiratory failure diagnosed in patients who develop sepsis [14].

1.2.3 Coagulation and DIC

Platelets contain receptors for PAMPs and DAMPS, such as TLR4, activated by certain factors, including bacterial endotoxins [20]. During sepsis, platelet reactivity is increased and further amplified by elevated hormone levels (e.g., epinephrine and 5-hydroxytryptamine) [16]. Sepsis is additionally linked with increased thrombin generation due to the coagulation cascade. Thrombin activates the platelets through the protease-activated receptors (PAR), further contributing to the coagulant state [15].

The activated platelets undergo several processes. Dense granules rich in adenosine diphosphate (ADP) fuse with the platelet cell membrane, prompting further activation through P2Y1 AND P2Y12 receptors [17]. Meanwhile, alpha granules release P-selectin, which activates leukocytes by P-selectin glycoprotein ligand-1 (PSGL-1) binding, chemokine release and procoagulant factors. Platelet aggregation then leads to micro/macro thrombi formation by activating the GPIIb/IIIa receptor and bridging by fibrinogen and von Willebrand Factor (vWF) [16]. Both are elevated during sepsis, and vWF aids platelet adhesion to the endothelium [15,16].

The endothelium becomes damaged during sepsis due to numerous factors, such as direct pathogen interactions, inflammatory response, OS and coagulation cascade [6]. Regarding coagulation activation, TF expressed on monocytes and endothelial cells is promoted by direct pathogen interactions, and inflammatory mediators initiate the coagulation cascade extrinsic pathway [20]. This process can lead to blood clot formation, causing further damage to the endothelium. Meanwhile, thrombin, a key factor in the coagulation cascade, is generated promoting platelet activation. Platelet activation contributes to further thrombin generation through the release of procoagulant factors during degranulation [66]. Thrombin activation of endothelial cells can also result in hyperpermeability and inflammation [6].

Moreover, hypofibrinolysis is also associated with sepsis and is mediated through a thrombin-activatable fibrinolysis inhibitor (TAFI), which improves clot stability by reducing lysis [15, 16]. However, due to these clotting processes described above, significant changes in fibrin clot dynamics occur, such as a reduction in fibrin fibre diameter, increased network density and greater clot turbidity [13]. Thrombocytopenia often occurs during sepsis; however, the mechanism that causes sepsis-induced thrombocytopenia is not fully understood. It is likely related to low platelet production, increased consumption and sequestration [13]. In the initial stages of sepsis, platelet activation and aggregation with leukocytes form platelet-leukocyte aggregates (PLAs). PLAs can also release platelet-activating NETs, further contributing to thrombocytopenia. The infection from which sepsis originates can also be a factor in platelet activation and, therefore, thrombocytopenia [67]. Bacterial species, including *S. aureus*, *E. coli*, and *Streptococcus pneumoniae*, can bind to and activate platelet receptors (e.g., TLRs) or plasma proteins. Additionally, indirect platelet activation can be stimulated by antimicrobial peptides, which cause inflammation by tissue damage and cell destruction [13]. With pneumococcal infections, an increase in platelet clearance is caused by desialylation, a process involving the release of neuraminidase and galactose residue exposure. In Gram-negative and Gram-

positive infections, platelets can also become the target of antibodies or be reduced by the onset of DIC (Figure 3) [13,17,67].

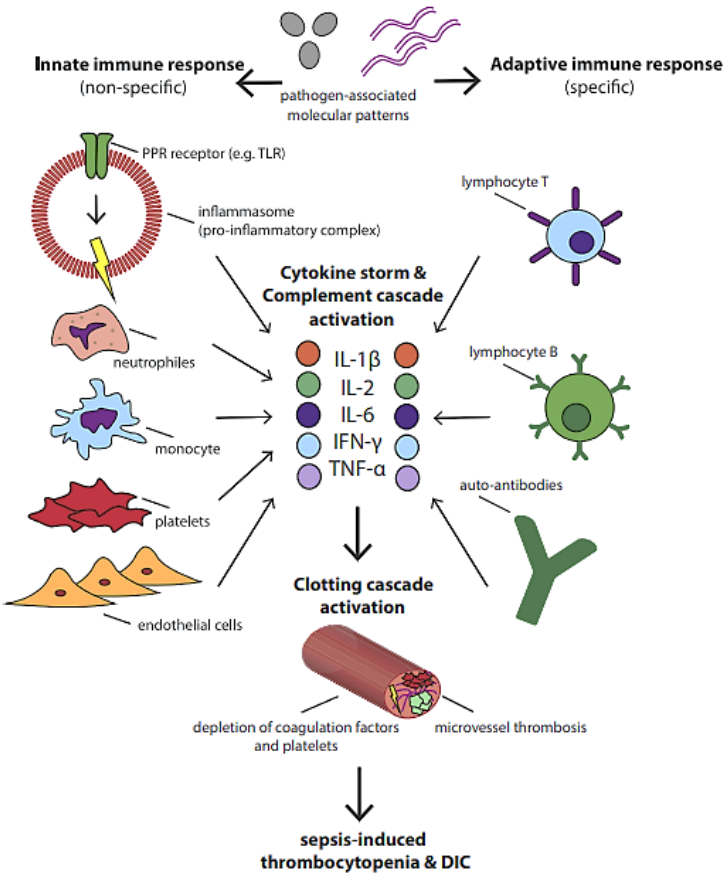

Figure 3 Components of Sepsis-induced thrombocytopenia and the progression to DIC (Sourced from 13)

DIC is an acquired thrombohemorrhagic syndrome characterised by the widespread dysfunctional activation of the coagulation process (Figure 3). This results in fibrin clot formation in small blood vessels (microangiopathic thrombosis), reducing essential coagulation factors and platelets [13]. Along with sepsis, DIC can also be triggered by non-infectious factors such as malignant disease or trauma. One of the significant issues in DIC is the loss of localised control in the coagulation pathway, where excessive thrombin is generated without inhibition, exacerbating the process [17].

The pathophysiology of DIC is complex and multifaceted as it involves several mechanisms working simultaneously. The triggering event initiates the process, whether it is trauma, sepsis, or cancer, producing the excessive release of TF. The overproduction then leads to high thrombin levels, which converts fibrinogen to fibrin strands, causing further activation of clotting factors (factor VIII, IX and XI) [18, 19]. Aggregation of activated platelets initiates primary and secondary haemostasis, which stimulates the coagulation pathway via TF/Factor VIIa (Figure 4) and prompts inflammation through Factor XIIa, kallikrein, bradykinin and C3a [13].

Platelets play a crucial role in coagulation. They support the generation of thrombin *via* numerous cellular pathways [16]. Complement-mediated reactions contribute by lysing cells and pathogens. As the cells are lysed, they release DAMPS and PAMPs, further promoting coagulopathy [6].

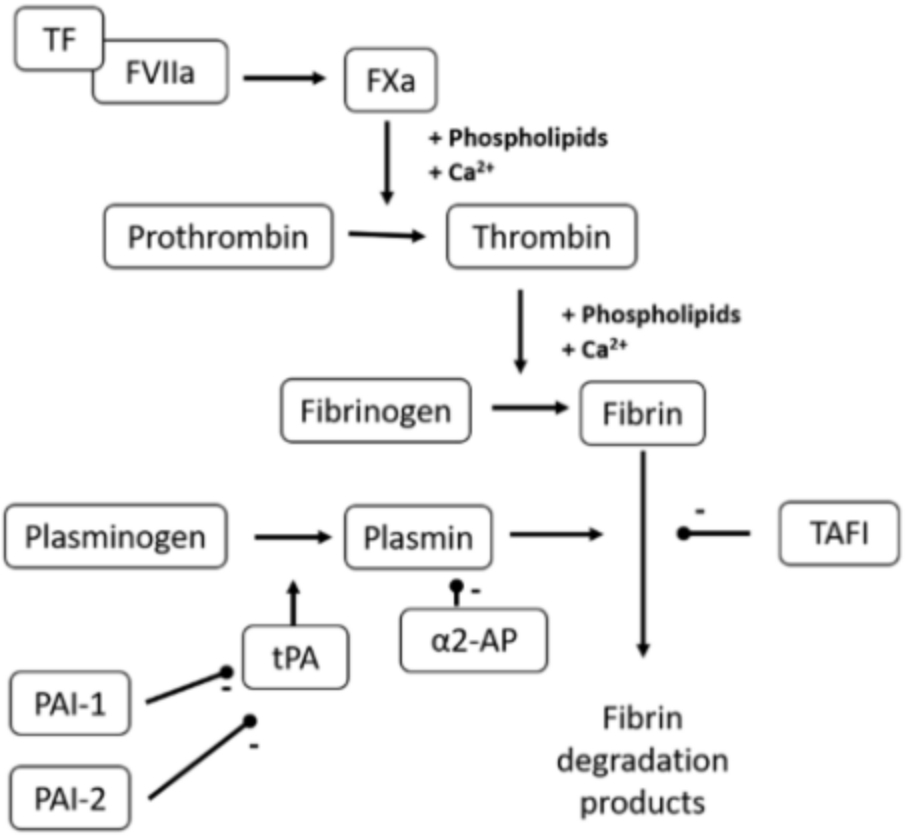

Figure 4 Overview of the fibrinolytic process [sourced form 40].

As the fibrin clots form (Figure 4), the fibrinolytic pathway activates to counteract the fibrin accumulation. However, antifibrinolytic factors such as plasminogen activator inhibitor (PAI-1) and TAFI can impair the fibrinolytic process. The body's natural anticoagulants, tissue factor pathway inhibitor (TFPI), antithrombin (AT), and activated protein C (APC) activity are impaired and unable to effectively control the procoagulant state [13, 18, 19].
Coagulation abnormalities are closely linked with inflammation. Inflammation triggers the coagulation process, while dysfunction in the coagulation process increases inflammation. The pro-inflammatory cytokines IL-1, IL-6, TNF-α, elastase, and cathepsin G play a prominent role in the body's response to sepsis [13, 19].

Research advances in DIC have shown that additional factors such as NETs, extracellular vesicles, and shedding of the endothelial glycocalyx are involved in the inflammatory-coagulation response. These findings help to understand the harmful cycle that can inflict severe damage on organs and the body, resulting in poor patient outcomes [20].

1.2.4 Immune System Dysregulation

During pathogen invasion, the innate and adaptive immune cells enter the tissues, preventing the microbial spread and maintaining immunological haemostasis. In sepsis, the pro- and anti-inflammatory processes are simultaneously activated in response to the binding of PAMPs to PRRs [6]. The activation of PRRs then prompts intracellular signalling, which stimulates transcription factors (such as NF-κB) and interferon regulatory factor pathways to produce inflammatory cytokines [6,21,64].

Sepsis causes the immune system to alter immune cell production, function, and apoptosis. When innate immune cells are activated, they prompt the release of several pro-inflammatory cytokines (IL-1, IL-2, IL-6, IFN-gamma, and TNF-α), shown in Figure 3 [21]. The interplay of cytokine storm and complement system activation exacerbates the inflammatory pathway, resulting in tissue damage and progressive organ failure. Restoring normal immune function promptly will result in the overactivation of the immune system by extensive anti-inflammatory and immunosuppressive responses, leaving the patient at greater risk of secondary infections [21,22].

Various cell types within the innate and adaptive immune systems contribute to sepsis's dysfunction. Neutrophils are vital to the body's host defence against invading pathogens. In sepsis, neutrophils have altered chemotaxis, where cells struggle to migrate to infection sites, impaired phagocytic ability, and defective ROS production, which delays their ability to break down engulfed microbes [21]. Furthermore, neutrophils can show altered pro-inflammatory cytokine secretion, disrupting the balance between fighting infection and further immune dysfunction [21,22]. Production of NETs is also exacerbated; excessive production can negatively affect autoinflammation and contribute to organ damage [12,21].

In sepsis, reduced expression of monocyte human leukocyte antigen (HLA)-DR is commonly observed [21]. HLA-DR is a key factor in antigen presentation, and a reduction in these molecules is associated with a decrease in the immune response to bacterial endotoxins, resulting in a weakened immune response and a greater risk of secondary infection [22]. The risk of secondary infections is increased due to apoptosis of APCs in sepsis, which contributes to immune dysfunction and T-cell anergy (T-cells become unresponsive) [21].

In summary, the innate and adaptive immune systems are disrupted during sepsis, leading to immunosuppression and excessive inflammation. This causes challenges when developing new immunotherapies as targeting one aspect can lead to negative outcomes and may worsen other aspects, creating uncertain outcomes for the patient.

1.3 Diagnostics and Therapeutics

Sepsis management relies heavily on early diagnosis, antibiotic administration, fluid resuscitation, vasopressors, and infection source control, such as drainage or surgical removal [6]. Delays in treatment or incorrect diagnosis can lead to poor patient outcomes and higher mortality. The sepsis six protocol is carried out across the UK to treat adult sepsis. This six-step process should be implemented within one hour of suspected sepsis [23].

1. Administer Oxygen (maintain O_2 saturation above 94%)
2. Fluid Resuscitation (support organ perfusion and blood pressure)
3. Take Blood Cultures (identify pathogen)
4. Administer broad-spectrum antibiotics
5. Measure Serum Lactate
6. Monitor Urine Output

When the sepsis six protocol is conducted promptly, significant reductions in mortality rates and improved patient outcomes have been seen. Raising awareness of sepsis and informing the public of signs and symptoms is vital in reducing the global burden of sepsis. Early identification and diagnosis significantly improve patient survival [23]. Typical symptoms of sepsis include fever, chills, sweating, soreness, swelling, diarrhoea, nausea, cough, sore throat, shortness of breath, stiff neck, changes in skin, urination, and altered mental status. Other common symptoms include hypothermia, tachycardia, tachypnoea, hypotension, and signs of organ dysfunction [24].

Supportive and adjunctive therapies include haemodynamic management to stabilise the circulatory system (mainly in septic shock) via fluids, which must be carefully monitored to avoid hypervolemia. Fluid volume must be administered and adjusted depending on the body's reaction. Vasopressors may also be administered to maintain and restore blood pressure and organ perfusion. Modulation of the host response aims to influence the immune and inflammatory response through vasopressin, Glucocorticoids (e.g., hydrocortisone), and blood purification [6,13].

Scoring systems such as the sequential organ failure assessment (SOFA) are used in conjunction to help diagnose sepsis. Biomarkers used include procalcitonin (PCT), which has elevated levels associated with bacterial infections, and C-reactive protein (CRP), which indicates inflammation. These biomarkers are used to help diagnose sepsis but are not specific to the condition, so they are limited in use [21,68].

1.3.1 Emerging Concepts and Therapeutic Targets in Sepsis

The discovery of antibiotics has declined extensively, combined with the rise in antimicrobial resistance (AMR); this leaves a daunting future for treating many conditions and infections, including sepsis. Selecting the correct antibiotic therapy is critical for patients with suspected sepsis to ensure effective treatment and improve patient outcomes. The National Institute for Health and Care Excellence (NICE) published guidelines on recommended antibiotic administration in the UK, which should be reviewed and adjusted once the infection source and strain have been identified [33]. For newborn babies (< 28 days) with suspected sepsis, the guidelines recommend treatment with intravenous antibiotics benzylpenicillin and gentamicin within the first 27 hours. Also, effective antibiotics against Listeria, such as ampicillin or amoxicillin, are advised for children under three months. For those with suspected community-acquired sepsis under 18 years, ceftriaxone 80 mg/kg once a day with a maximum dose of 4 g daily is advised. For patients 18 years and over, empirical intravenous antibiotics from local formulary that align with local guidelines are advised. These may include cefepime, meropenem, and piperacillin-tazobactam, all critical antibiotics used in the treatment of sepsis due to their broad range of activity against several susceptible and resistant pathogens [25,26].

However, the increase in antibiotic-resistant bacteria threatens the effectiveness of antibiotics and public health. Resistance can occur due to natural factors, and by the overuse and misuse of antibiotics in human medicine and agriculture, resulting in the bacteria developing resistant mechanisms. Multi-drug-resistant bacteria increase the risk of higher morbidity, leading to longer hospital stays and increased healthcare costs. The lack of new and successful antibiotics leaves limited treatment options for these resistant infections. Coupled with the global rise in AMR this significantly threatens public health and standard treatments for even common infections. Therefore, the World Health Organisation (WHO) stresses the severity of the increasing resistance rates through the Global Antimicrobial Resistance and Use Surveillance System (GLASS) Report: 2022, developed to track and inform on this issue [27]. The report indicates an increase in the prevalence of antibiotic-resistant strains, reporting a 35% resistance rate for methicillin-resistant *S. aureus* and a 42% resistance rate for *E. coli* against third-generation cephalosporins in 76 countries [27]. This demonstrates the need for new antimicrobial treatments and how the proposed MTD strategy would aid in combatting AMR, reducing resistance in bacteria, and preventing further development by providing an alternative treatment strategy.

Natural and synthetic antimicrobial peptides (AMPs) are an upcoming advancement in the search for novel antibiotics. They are small innate immune system proteins with antimicrobial, viral, and fungal activity and are gaining attention due to their clinical potential. However, due to their limited specificity to bacterial cells, there are cytotoxicity concerns towards non-target host cells. To limit their toxicity, concurrent administration with other antimicrobials may provide a synergistic approach and reduce toxicity [28]. There are several AMPs currently in clinical trials, highlighting their antimicrobial potential. AMPs have various mechanisms, including immune modulation, intracellular bacterial inhibition, and direct activity on the cell membrane [28, 29]. Although AMPs show potential with their antimicrobial activity, they only address and treat the

infection, leaving septic patients vulnerable to existing damage and continuous inflammation.

Several clinical trials for immunotherapy in septic patients have been carried out. Researchers observe how modulating the immunological response can restore immune function and balance to help prevent further organ failure. First, they want to restore the inflammatory response and improve immune function by maintaining immune homeostasis—using specific antibodies on inflammatory mediators such as TNF-α and TLR4. Injecting neutralising monoclonal anti-cachectin/TNF-α monoclonal antibodies one hour before bacterial invasion in baboons prevented shock. When injected two hours before, organ dysfunction and mortality were prevented. Deficiency or blockage of TLR4 can be beneficial in protecting animals from septic shock and reducing mortality [30].

A clinical trial using high-dose glucocorticoid steroids as a sepsis treatment showed significantly decreased mortality rates. Another study later contradicted this study, observing the effects of short-term high-dose glucocorticoids associated with a declining secondary infection and increased mortality. Low to moderate doses of the steroids did not show any clinical advantages in sepsis or septic shock. Further research into the use of these steroids as a beneficial treatment for sepsis must be carried out to validate whether they are a potential treatment [6].

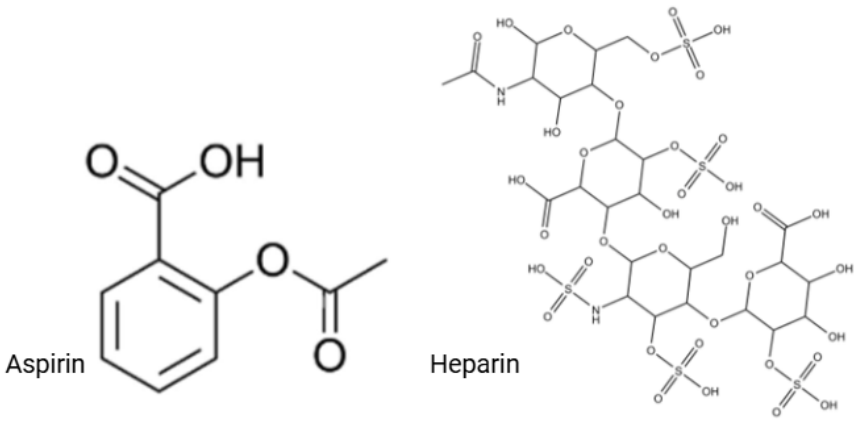

Figure 5 Structure of Aspirin [92] and Heparin [93]

Aspirin (Figure 5) is a widely used drug with anti-inflammatory and antiplatelet properties. Aspirin is being studied as an anti-inflammatory treatment for sepsis due to its ability to aid in controlling inflammation by inhibiting cyclooxygenase enzymes, which may reduce excessive inflammation [89]. However, the dosage and timing of administration must be explored further to maximise the benefits and reduce risk to patients [90].

In sepsis, anticoagulants are not routinely used but have become a growing area of research. Treatments, such as heparin (Figure 5), are being investigated for their ability to reduce clot formation and increase blood flow in septic patients. However, the use of anticoagulants in sepsis must be carefully

considered to maintain the coagulation balance and avoid further harm to the patient. Further studies are required to establish the benefit of anticoagulant therapy in sepsis to optimise patient outcomes [91].

1.4 Multi-Target Drug (MTD)

In previous years, in drug development, it has been the basis that one molecule is designed for one target. However, in the last decade, the drug development industry has been evolving, moving from one target – one drug to the multi-target approach. Most diseases, including neurodegenerative disease, human immunodeficiency viruses (HIV), cancer and diabetes, have complex pathologies for which the single target approach is somewhat inadequate (Figure 6). In these cases, further medications are required, leading to increased complications and a negative effect on patient compliance, healthcare costs and, therefore, quality of life. Despite the direct impact on the patient, there is also a greater risk of adverse side effects due to drug-to-drug interactions in the case of combination therapy (Figure 6) [31].

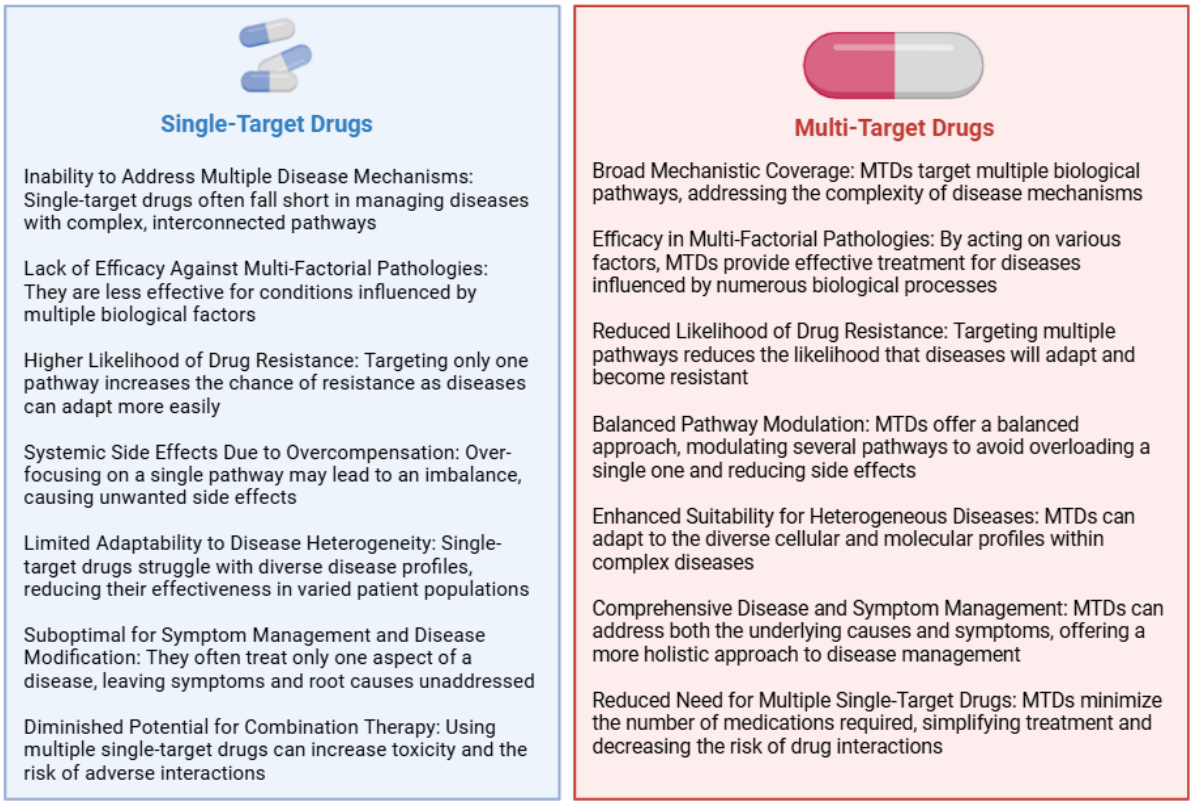

Figure 6 Overview of the disadvantages of single-target drugs and advantages of MTD in treating complex conditions [31].

The multi-target approach has been successfully implemented in many complex diseases. In 2017, 21% of the Food and Drug Administration's (FDA) new molecular entities were MTD [86]. The successful application of the MTD approach in multiple conditions demonstrates its versatility and potential. Lenvatinib (Figure 7) is a kinase inhibitor in cancer therapy, targeting multiple pathways that contribute to tumour progression. This includes vascular endothelial growth factor receptor (VEGFR), the Fibroblast Growth Factor Receptor (FGFR), and the Platelet-Derived Growth Factor Receptor (PDGFR). Lenvatinib has been approved for radioiodine-resistant thyroid cancers [87]. Additionally, MTD strategies have been developed for neurodegenerative disease. Memoqion (Figure 7) is a multifunctional compound designed to address neuroinflammation and OS by

inhibiting acetylcholinesterase and b-amyloid aggregation in Alzheimer's disease. Thus, showing promising results in preclinical models [88].

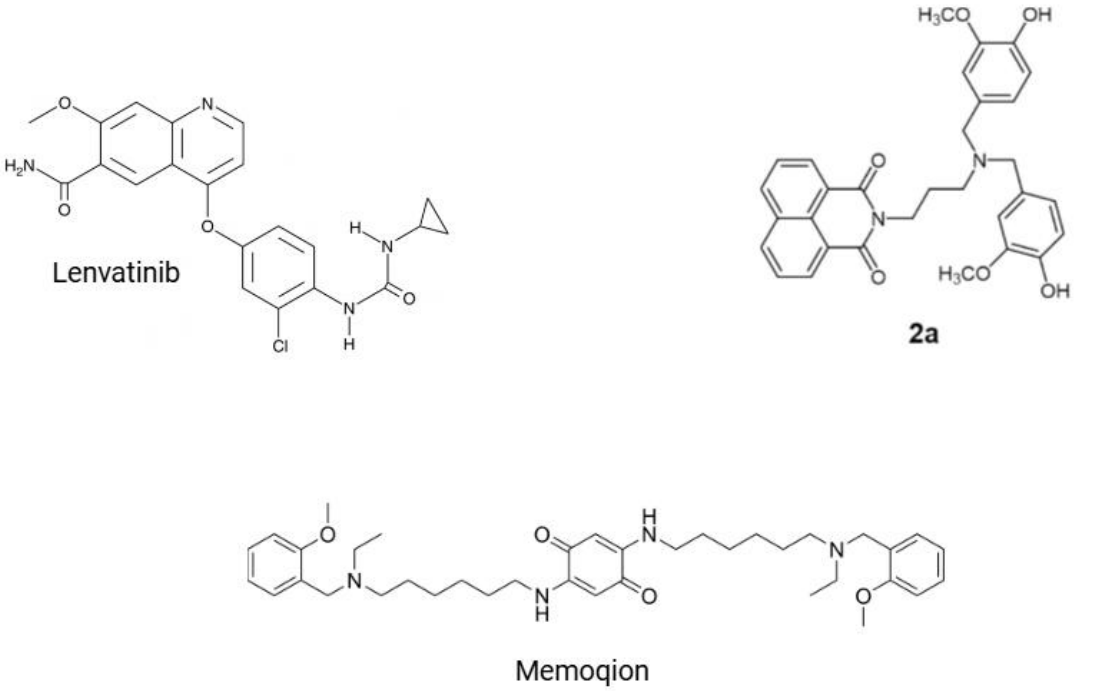

Figure 7 Structures of current and potential MTD examples, Lenvatinib [87], Memoqion [88] and 2a [33].

Previous research at Robert Gordon University in developing a Vanillin-MTD for Alzheimer's treatment showed compelling neuroprotective effects in *In vitro* studies. According to the study [33], lead compound 2a (Figure 7) exhibited potent antioxidant activity in the DPPH assay with an IC_{50} of 16.67 µM, 0.49 TE in the FRAP assay and 10-fold greater than the standard Trolox in the ORAC assay. Additionally, 2a again showed a 10-fold greater inhibition of BuChE compared to the known inhibitor, neostigmine. This paper, therefore, highlights compound 2a as a potential MTD while demonstrating the benefits and applications of this concept for other complex diseases.

The multifaceted nature and complex interplay of various biological systems requires an advanced treatment that can target multiple aspects simultaneously that a single target drug cannot (Figure 6). The treatment of multiple pathways simultaneously provides a more effective and vigorous approach, helping to support the body's systems and reversing or preventing further damage to the body. In contrast to current treatments used in sepsis, where numerous therapies are used in combination, the MTD approach may also provide a safer and more practical option to reduce toxicity due to combination therapy. Therefore, the larger therapeutic window the MTD provides makes it a safer option for the patient [31].

However, the MTD approach is still a relatively new concept and, therefore, comes with challenges. Since the drug contains multiple pharmacophores, it may have issues with its bioavailability and drug uptake, which may harm the efficacy

and stability of the compound, leaving a challenge for pharmaceutical chemists. In addition, the pathophysiology of sepsis is not fully understood, and there are limited diagnostic and therapeutic options, therefore adding further complications to the advancement of new treatments. Advances in novel treatments are based on current and past research outcomes; overall, the challenges and lack of successful novel therapeutics for the condition emphasise the need for new research and promising therapeutic studies [31].

As previously stated, sepsis is a life-threatening and complex condition which develops from a dysregulated host response to an infection, resulting in widespread inflammation, tissue damage and organ failure. Due to the heterogeneity of sepsis and the condition's involvement in processes such as OS, coagulopathy, and microbial invasion, a multi-target therapeutic could be a potentially life-saving and cost-effective approach. The proposed MTD will provide antimicrobial, anti-inflammatory, and anticoagulant components while simultaneously treating multiple aspects of sepsis (Figure 8). In contrast, current treatment focuses on independently managing the infection, inflammation, or blood clotting.

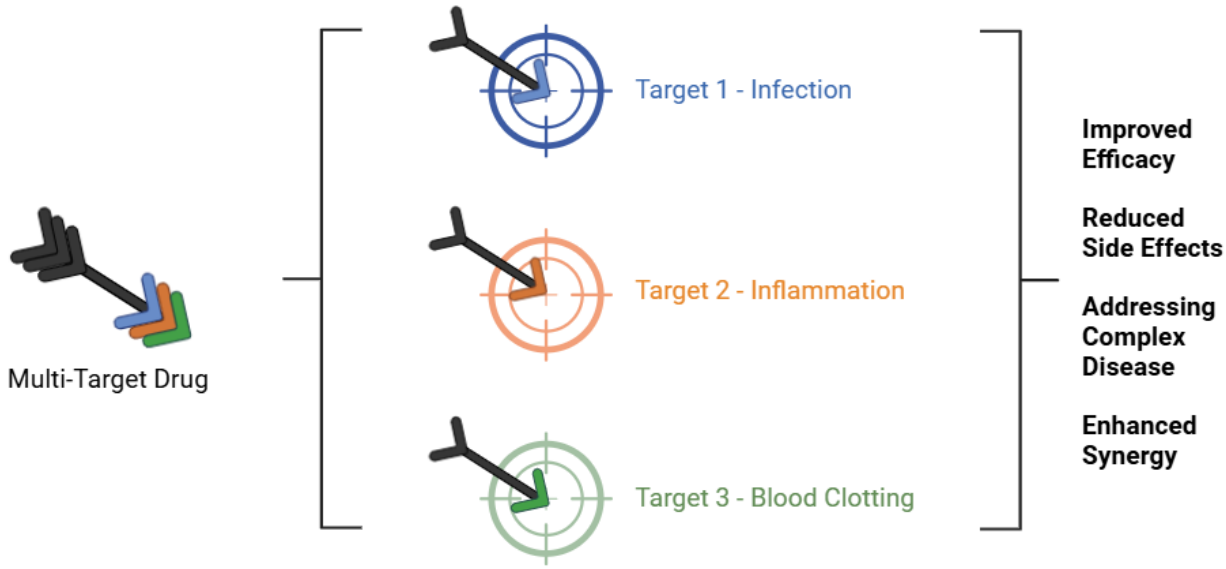

Figure 8 MTD Approach and Targets

The compound's antimicrobial component would target the triggering infection, control it, and reduce the spread. The antioxidant component would help mitigate inflammation by neutralising ROS and reducing tissue damage by restoring the oxidation balance. Finally, the anticoagulant component would help restore the coagulation/fibrinolysis balance, reduce blood clot formation, and protect the blood vessels and organs from further damage. Integrating these components in a single drug would offer a comprehensive therapeutic for sepsis by addressing the condition's multifactorial nature (Figure 8). Targeting the triggering infection and reducing later damages due to excessive inflammation and blood clotting *via* the antioxidant and anticoagulant components would synergistically reduce organ damage and mortality of patients while providing further understanding and treatment of sepsis.

This study synthesises new MTD compounds using the linked combination, which connects two structures *via* a linking chain. Other synthetic combinations include fused, where the two structures are directly linked, or merged, where the structure is overlapped (Figure 9). The linked MTD structure will have a naphthalimide base designed with an aminopropyl chain bridge (Figure 10). Secondary compounds will consist of various aromatic aldehydes.

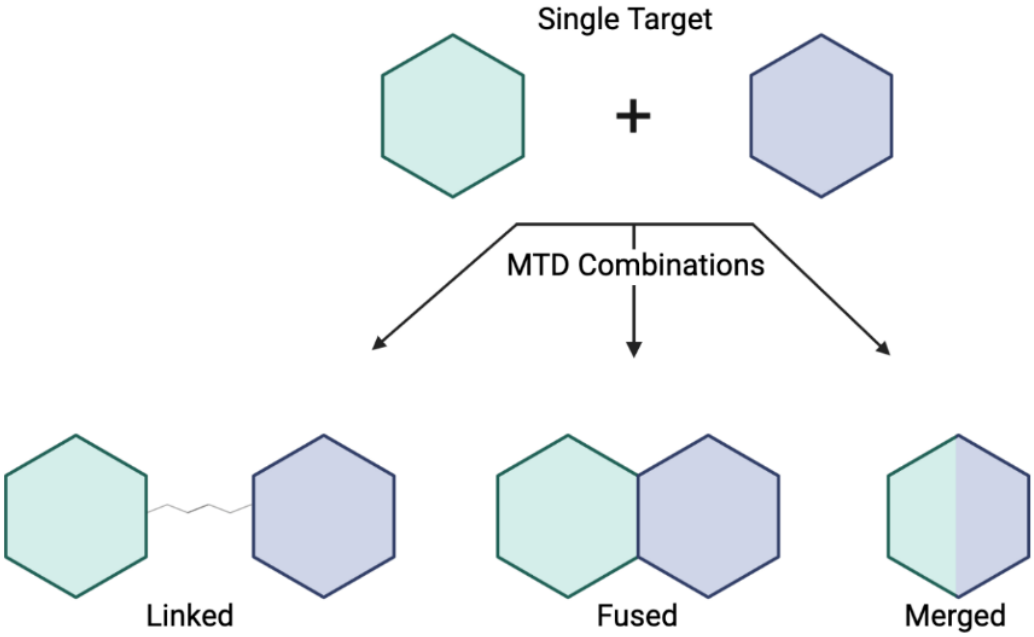

Figure 9 Methods of MTD Synthesis

The described synthesis and derivatisation protocols below provide a strong framework for creating a diverse library of MTD compounds, each with unique structural and electronic properties. This diversity enables extensive exploration of their potential application and reactivity.

1.4.1 Design of MTD

Naphthalimide is the base compound for each novel compound (Figure 10). Naphthalimide has previously been researched for its therapeutic activity, specifically its antioxidant and anti-inflammatory properties [36]. Naphthalimide and its corresponding derivatives are extensively studied in anti-tumour and anti-cancer research for their DNA intercalating ability and toxicity towards cancer cells [36]. However, these properties are undesirable in sepsis treatments. Structural modifications are necessary to optimise the therapeutic effect of naphthalimide while reducing its toxicity. Incorporating the secondary aromatic aldehydes into the synthesis process may enhance the bioactivity of naphthalimide and potentially reverse their toxic effects, thereby improving their suitability for treating sepsis.

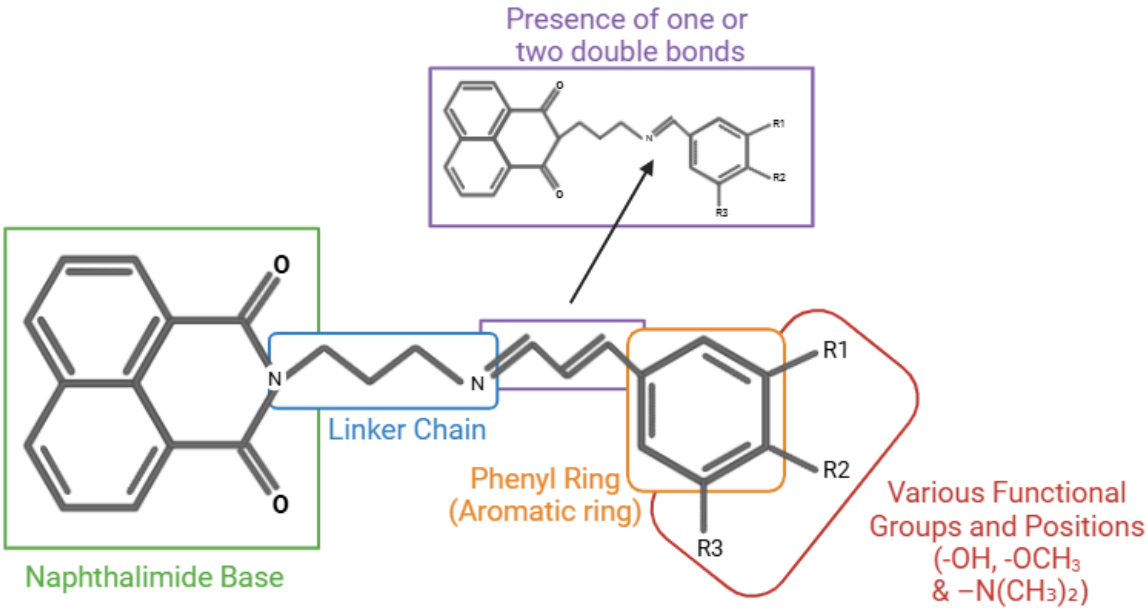

Figure 10 Structure and components of the MTD library

The MTD library design (Figure 10) involves a constant naphthalimide base with a propylamine linker chain. The structure of the compounds differs due to the range of secondary compounds used and can be characterised by one or two double bonds in the aldehyde chain and varying functional groups (R1-3: Figure 10).

The secondary compounds have been selected due to their various functional groups and potential properties (Figure 11). The selected phenolic and cinnamic aldehyde derivatives share a common structure consisting of an aromatic ring with an aldehyde group (-CHO). Many of the compounds additionally contain a hydroxyl group (-OH), methoxy group (-OCH_3), or dimethyl amino group (Figure 10). The addition of these functional groups influences compound reactivity and chemical properties. Therefore, they are promising candidates for developing novel antimicrobial, antioxidant, and anticoagulant therapies.

Many of these compounds are naturally occurring, such as Coniferaldehyde, which can be found in lignin in plant cell walls, or Vanillin, which is derived from

vanilla beans. These aromatic aldehydes are commonly found as secondary metabolites in plants, which are involved in defensive mechanisms. Extensive research has also been undertaken on a variety of these compounds and has shown promising antimicrobial and antioxidant results [33,53]; the work of this project will include the optimisation of their potential activity through the combination with Naphthalimidopropylamine (NPA) (Figure 12) to increase and optimise the synthesis of the novel library of compounds and assess the advantage and activity of the various functional groups [36,37].

The aromatic rings serve as an electron reservoir, allowing the phenolic compounds to effectively stabilise free radicals, which contributes to their ROS-scavenging activity. The position and number of hydroxyl groups can significantly impact the compound activity [36]. The phenolic moiety (aromatic ring with hydroxy substitute) has several different methods to which its antioxidant activity is due, but the primary mechanism is free radical scavenging *via* hydrogen donation [39]. Additional substitutes on the aromatic ring will impact the moiety's radical scavenging ability due to alterations in structure and stability. Additionally, hydroxyl groups have potential antimicrobial functions, such as interacting with the cell membrane structure, destabilising the membrane, and inhibiting catalytic activity [37,39]. Methoxy groups enhance the compounds' antioxidant activity by stabilising the free radical intermediate after donating an electron and show antimicrobial potential by increasing the compound's lipophilicity, allowing for penetration of microbial membranes and cell walls. The dimethyl amino group increases the compound's lipophilicity and membrane permeability, enhancing its ability to penetrate microbial cells and exert antibacterial effects. This group can donate electrons, helping stabilise free radicals in combination with the aromatic system, thereby enhancing antioxidant activity [36,38].

The additional double bond on the extended carbon chain characterises compounds JW 7-10 (Figure 10 & 11). Therefore, incorporating these compounds provides a wide therapeutic and research range by providing information on the group structure, position, and combination regarding antimicrobial, antioxidant, and anticoagulant function. Combining these compounds through linked synthesis with NPA provides a versatile and effective MTD that can potentially treat infection and inflammation and promote blood clot lysis.

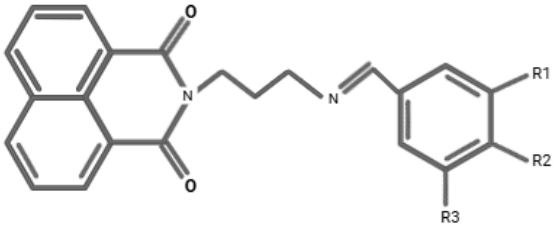

JW1: R1 = H R2 = H R3 = H **JW2**: R1 = H R2 = OH R3 = H **JW3:** R1 = OH R2 = OH R3 = H
JW4: R1 = OH R2 = OH R3 = OH **JW5:** R1 = H R2 = OCH_3 R3 = H **JW6:** R1 = OCH_3 R2 = OH R3 = H
JW7: R1 = OCH_3 R2 = OH R3 = OCH_3

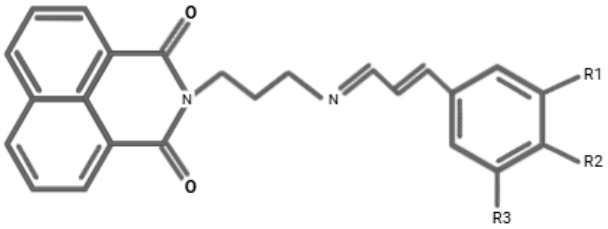

JW8: R1 = H R2 = H R3 = H **JW9:** R1 = H R2 = OCH_3 R3 = H **JW10:** R1 = OCH_3 R2 = OH R3 = H
JW11: R1 = H R2 = NC_2H_6 R3 = H

Starting Material (NPA + Derivative)

JW1 - Benzaldehyde JW2 - 4-Hydroxybenzaldehyde JW3 - 3,4-Dihydroxybenzaldehyde
JW4 - 3,4,5-Trihydroxybenzaldehyde JW5 - 4-Anisaldehyde JW6 - Vanillin
JW6 - Syringaldehyde JW7 - 4-Anisaldehyde JW8 - Trans Cinnamaldehyde JW9 - 4-Methoxycinnamaldehyde
JW10 - Coniferaldehyde JW11 - 4-(Dimethylamino)cinnamaldehyde

Figure 11 MTD Library (JW1 - 11) and Respective Parent Compounds

2. Aims and Objectives

The research project aims to synthesise a library of novel compounds (Naphthalimide-bearing) with antimicrobial, antioxidant and anticoagulant properties and then characterise their different mechanisms of action (as MTDs). This will be achieved by completing the specific objectives below:

1. Design and synthesise multi-target drug molecules incorporating the lead Naphthalimide-bearing compound (i.e., NPA Figure 12) (Section 1.4.1 & 3.2).

2. Perform structural characterisation on the library of compounds using various qualitative methods such as ^{1}H and ^{13}C NMR. HRMS will be employed for molecular weight and structural determination (Section 4.1).

3. To perform *in vitro* investigations and evaluations of the antibacterial properties (e.g., MIC and minimum bactericidal concentration (MBC)) of the newly synthesised compounds on selected sepsis-causing bacteria (e.g., *S. aureus* and *E. coli*) (Section 4.2).

4. Investigate/evaluate the antioxidant potential of the novel compounds using various *in vitro* methods, such as DPPH and FRAP (Section 4.3).

5. To determine the anti-coagulant activity of the compounds by employing the clot lysis assay (Section 4.4).

6. To compare a range of structural modifications, including chain length and various functional groups, on the library's antimicrobial, antioxidant, and anticoagulant activities.

Focusing on these expanded objectives, the project aims to comprehensively evaluate the synthesised multi-target compounds, highlighting their potential as effective treatments for sepsis through combined antimicrobial, antioxidant, and anticoagulant mechanisms.

3. Materials and Methods

3.1 Compound Characterisation Techniques

Thin Layer Chromatography (TLC)

A small amount of test solution dissolved in methanol (Fisher Scientific, USA) was spotted onto silica gel-coated plates, dried and placed in a TLC chamber with a small volume of Dichloromethane (Fisher Scientific, USA) and Methanol at a 90:10 ratio. The solvent was allowed to migrate up the plate, and the plate was removed once the solvent reached ~1 cm from the top. The plate was dried, and spots were visualised under UV light.

Nuclear Magnetic Resonance (NMR)

For analysis, 20 mg of each compound was dissolved in 0.7 mL deuterated Dimethyl sulfoxide (DMSO D_6) (Fisher Scientific, USA), ensuring compounds were fully dissolved before transferring to 5 mm optical density (OD) thin-walled NMR tubes. ^{1}H and ^{13}C analysis was carried out using Bruker Avance III 400MHz NMR and TopSpin 4.4.0 processing software.

High-Resolution Mass Spectrometry (HRMS)

HRMS for each compound was carried out at the Mass Spectrometry Centre at Swansea University. Depending on the sample properties, two distinct ionisation techniques were employed: negative ion nanoelectrospray ionisation (nES) for samples JW1-3, 7, 9, and 10 and positive ion Atmospheric Solids Analysis Probe (ASAP) for samples JW4-6, 8, and 11 [(85)].

For nES analysis, an Advion Triversa NanoMate coupled with a Thermo LTQ Orbitrap XL mass spectrometer was used. Sample preparation for nES involved dissolving in 350 µL of methanol followed by a 1:1000 dilution into Methanol containing diethanolamine. For analysis, the NanoMate operated at a gas pressure of 0.45 psi with an applied voltage of -1.4 kV, delivering an infusion flow rate of approximately 250 nL/min. The Orbitrap mass spectrometer was configured with a capillary temperature of 200°C, a capillary voltage of -30 V, and a tube lens voltage of -100 V, with mass spectra acquired over a range of *m/z* 150 to 2000 and a resolution greater than 60,000 full width at half maximum (FWHM).

ASAP analysis used a Waters Xevo G2-S time-of-flight (TOF) mass spectrometer. Samples JW4-6, 8, and 11 were analysed in solid form and introduced via a glass capillary inserted into the probe. For ASAP analysis, the vaporisation temperature was sample-dependent, and a corona discharge current of 3 µA was applied, with the source temperature set at 80°C and nitrogen desolvation gas flowing at 600 L/hr. Mass spectra were recorded over a range of *m/z* 50 to 2000, with a resolution exceeding 30,000 FWHM.

3.2 Organic Synthesis Protocol

The MTD compounds were synthesised using an organic synthesis protocol previously reported by Scipioni et al. [55]. Where the core structure NPA is produced, providing a link for a further condensation reaction with a secondary aromatic aldehyde to produce a Schiff base (R1R2C=NR3). The final compounds were then characterised and evaluated for their antimicrobial, antioxidant and anticoagulant properties.

NPA synthesis (Figure 12) is the foundational step in creating a diverse library of MTD compounds. The synthesis of NPA was carried out by reacting 1,8-naphthalic anhydride (Sigma-Aldrich, USA) with 1,3-diaminopropane (Sigma-Aldrich, USA in ethanol (Fisher Scientific, USA) under reflux conditions, followed by further derivatisation with various aromatic aldehydes (Figure 14).

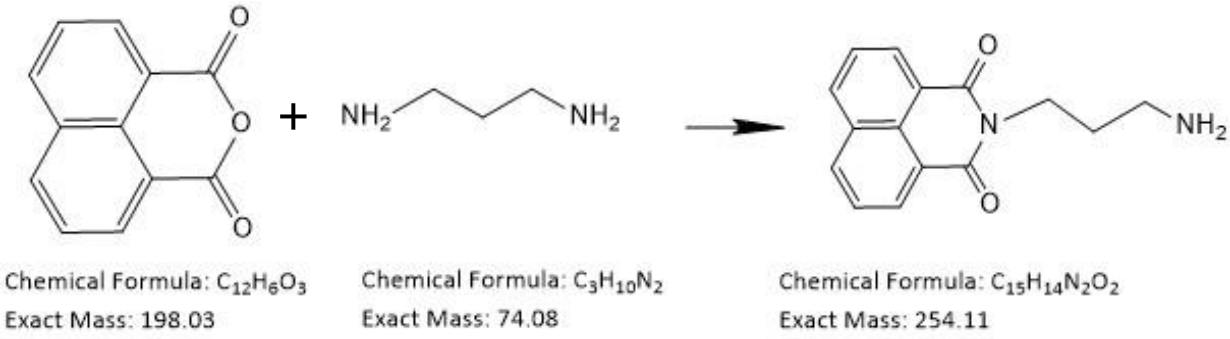

Figure 12 Synthesis of Naphthalimidopropylamine (NPA)

A round-bottom flask containing 1,8-naphthalic anhydride and 1,3-diaminopropane in ethanol was heated in an oil bath for 2 hours while TLC monitored the progress of the reaction. Once the reaction was completed (confirmed by TLC), the reaction mixture was filtered through a glass fiber filter (Grade C), and the remaining product in the filter paper was washed with neat ethanol by gently pouring over the product to remove any residual liquid or unreacted materials. The solid product was then dried in a vacuum oven set at 40°C for 24 h. The structure and purity of the synthesised NPA were confirmed using NMR and HRMS.

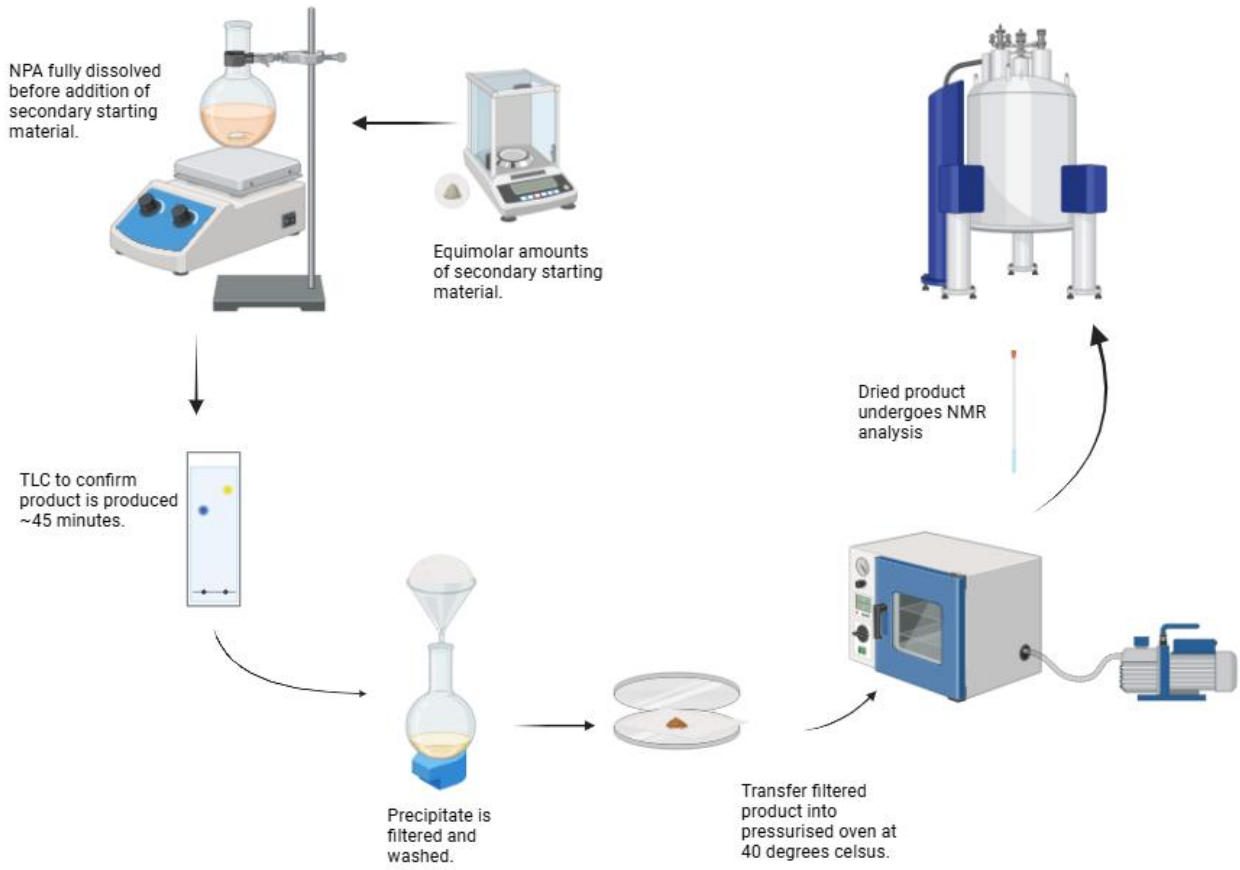

Figure 13 General overview of MTD synthesis and characterisation via NMR analysis.

Synthesis of MTD compounds (Figure 13)
NPA was further reacted with various cinnamaldehyde and benzaldehyde derivatives to generate a library of new compounds (JW1-11) (Figure 14). The general synthetic method is described below.

In a round-bottom flask containing methanol (20 mL), 0.2 g (0.00083 mmol) of NPA was dissolved with gentle heating. An equimolar amount of the selected secondary compound (0.00083 mmol) was added to the solution, dissolved through gentle heating, and left at room temperature for 2 hours. Once the reaction was completed (confirmed by TLC), the reaction mixture was filtered through a GFC filter, and the remaining product in the filter paper was washed with neat methanol by gently pouring over the product to remove any residual liquid or unreacted materials. The solid product was then dried in a vacuum oven set at 40°C for 24 h. The structure and purity of the synthesised NPA were confirmed using NMR and HRMS.

JW1 - NPA + Benzaldehyde

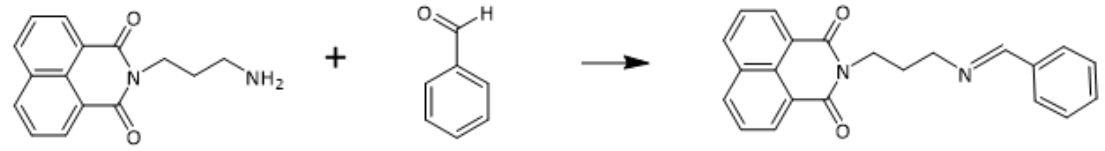

Chemical Formula: $C_{15}H_{14}N_2O_2$
Exact Mass: 254.11
Napthalimidopropylamine

Chemical Formula: $C_9H_{10}O_4$
Exact Mass: 182.06
Benzaldehyde

Chemical Formula: $C_{22}H_{18}N_2O_2$
Exact Mass: 342.14
(*E*)-2-(3-(benzylideneamino)propyl)
-1*H*-benzo[*de*]isoquinoline-1,3(2*H*)-dione

JW2 - NPA + 4-Hydroxybenzaldehyde

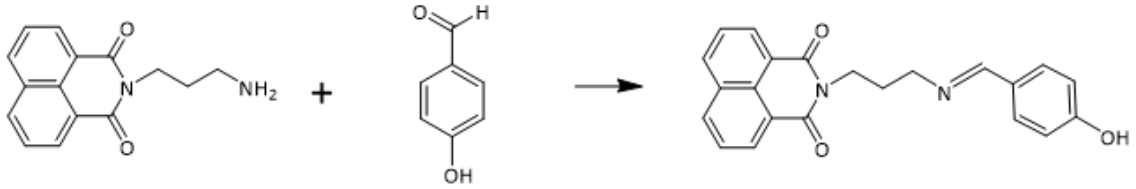

Chemical Formula: $C_{15}H_{14}N_2O_2$
Exact Mass: 254.11
Napthalimidopropylamine

Chemical Formula: $C_7H_6O_2$
Exact Mass: 122.04
4-hydroxybenzaldehyde

Chemical Formula: $C_{22}H_{18}N_2O_3$
Exact Mass: 358.13
(*E*)-2-(3-((4-hydroxybenzylidene)amino)
propyl)-1*H*-benzo[*de*]isoquinoline-1,3(2*H*)-dione

JW3 - NPA + 3,4-Dihydroxybenzaldehyde

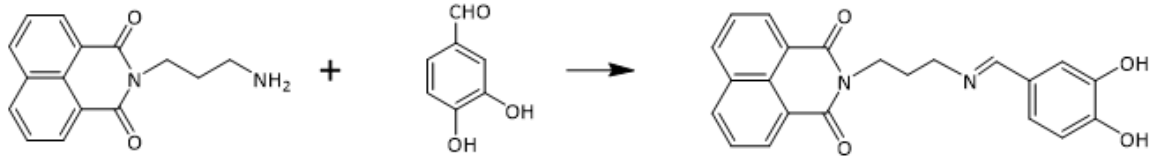

Chemical Formula: $C_{15}H_{14}N_2O_2$
Exact Mass: 254.11
Napthalimidopropylamine

Chemical Formula: $C_7H_6O_3$
Exact Mass: 138.03
3,4-Dihydroxybenzaldehyde

Chemical Formula: $C_{22}H_{18}N_2O_4$
Exact Mass: 374.13
(*E*)-2-(3-((3,4-dihydroxybenzylidene)amino)
propyl)-1*H*-benzo[*de*]isoquinoline-1,3(2*H*)-dione

JW4 - NPA + 3,4,5-Trihydroxybenzaldehyde

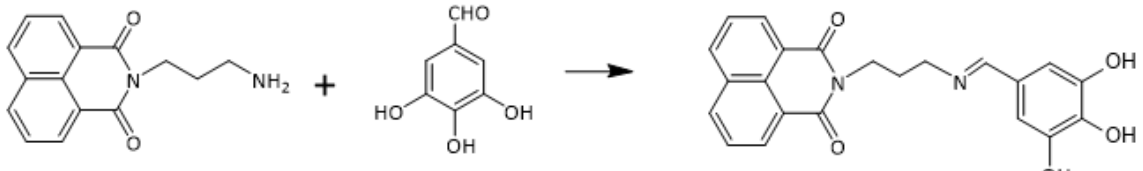

Chemical Formula: $C_{15}H_{14}N_2O_2$
Exact Mass: 254.11
Napthalimidopropylamine

Chemical Formula: $C_7H_6O_4$
Exact Mass: 154.03
3,4,5-Trihydroxybenzaldehyde

Chemical Formula: $C_{22}H_{18}N_2O_5$
Exact Mass: 390.12
(*E*)-2-(3-((3,4,5-trihydroxybenzylidene)amino)
propyl)-1*H*-benzo[*de*]isoquinoline-1,3(2*H*)-dione

JW5 - NPA + 4-Anisaldehyde

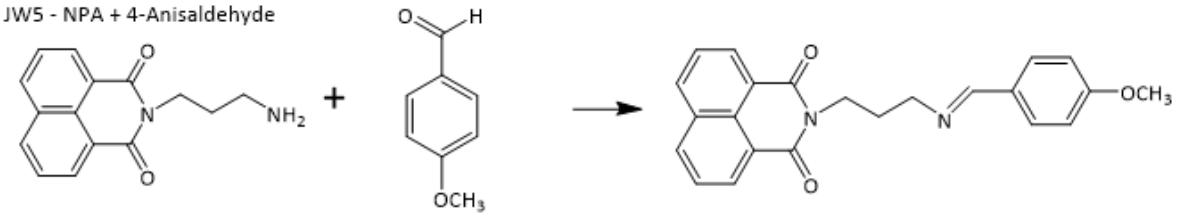

Chemical Formula: $C_{15}H_{14}N_2O_2$
Exact Mass: 254.11
Napthalimidopropylamine

Chemical Formula: $C_8H_8O_2$
Exact Mass: 136.05
4-Anisaldehyde

Chemical Formula: $C_{23}H_{20}N_2O_3$
Exact Mass: 372.15
(*E*)-2-(3-((4-methoxybenzylidene)amino)propyl)-1*H*-benzo[*de*]isoquinoline-1,3(2*H*)-dione

JW6 - NPA + Vanillin

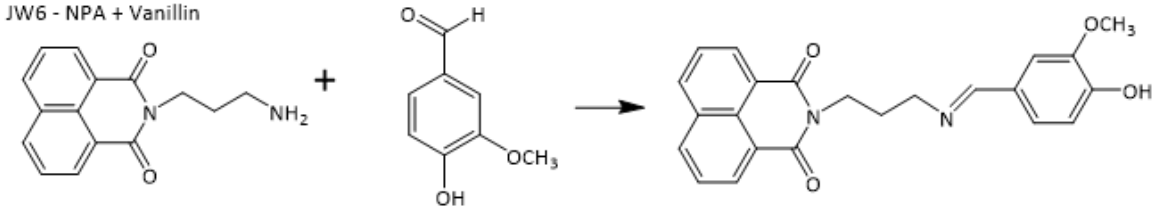

Chemical Formula: $C_{15}H_{14}N_2O_2$
Exact Mass: 254.11
Napthalimidopropylamine

Chemical Formula: $C_8H_8O_3$
Exact Mass: 152.05
Vanillin

Chemical Formula: $C_{23}H_{20}N_2O_4$
Exact Mass: 388.14
(*E*)-2-(3-((4-hydroxy-3-methoxybenzylidene)amino)propyl)-1*H*-benzo[*de*]isoquinoline-1,3(2*H*)-dione

JW7 - NPA + Syringaldehyde

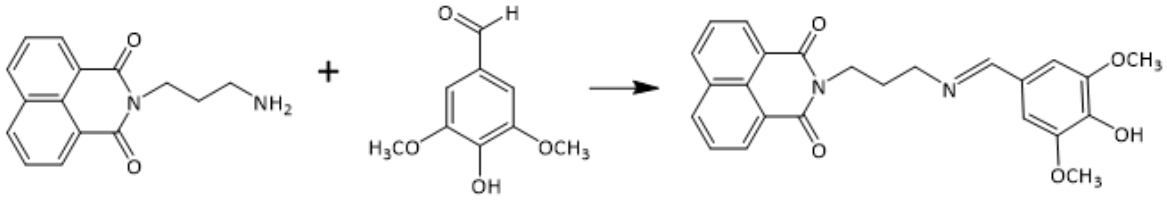

Chemical Formula: $C_{15}H_{14}N_2O_2$
Exact Mass: 254.11
Napthalimidopropylamine

Chemical Formula: $C_9H_{10}O_4$
Exact Mass: 182.06
Syringaldehyde

Chemical Formula: $C_{24}H_{22}N_2O_5$
Exact Mass: 418.15
(*E*)-2-(3-((4-hydroxy-3,5-dimethoxybenzylidene)amino)propyl)-1*H*-benzo[*de*]isoquinoline-1,3(2*H*)-dione

JW8 - NPA + Trans Cinnamaldehyde

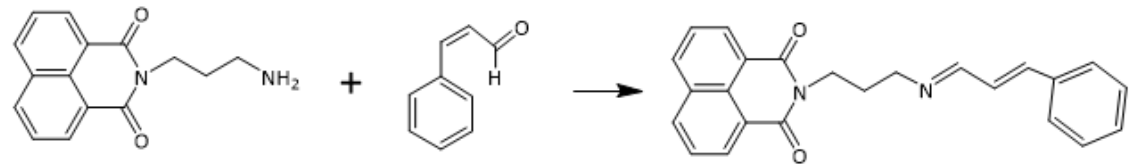

Chemical Formula: $C_{15}H_{14}N_2O_2$
Exact Mass: 254.11
Napthalimidopropylamine

Chemical Formula: C_9H_8O
Exact Mass: 132.06
Trans Cinnamaldehyde

Chemical Formula: $C_{24}H_{20}N_2O_2$
Exact Mass: 368.15
2-(3-(((1*E*,2*E*)-3-phenylallylidene)amino)propyl)-1*H*-benzo[*de*]isoquinoline-1,3(2*H*)-dione

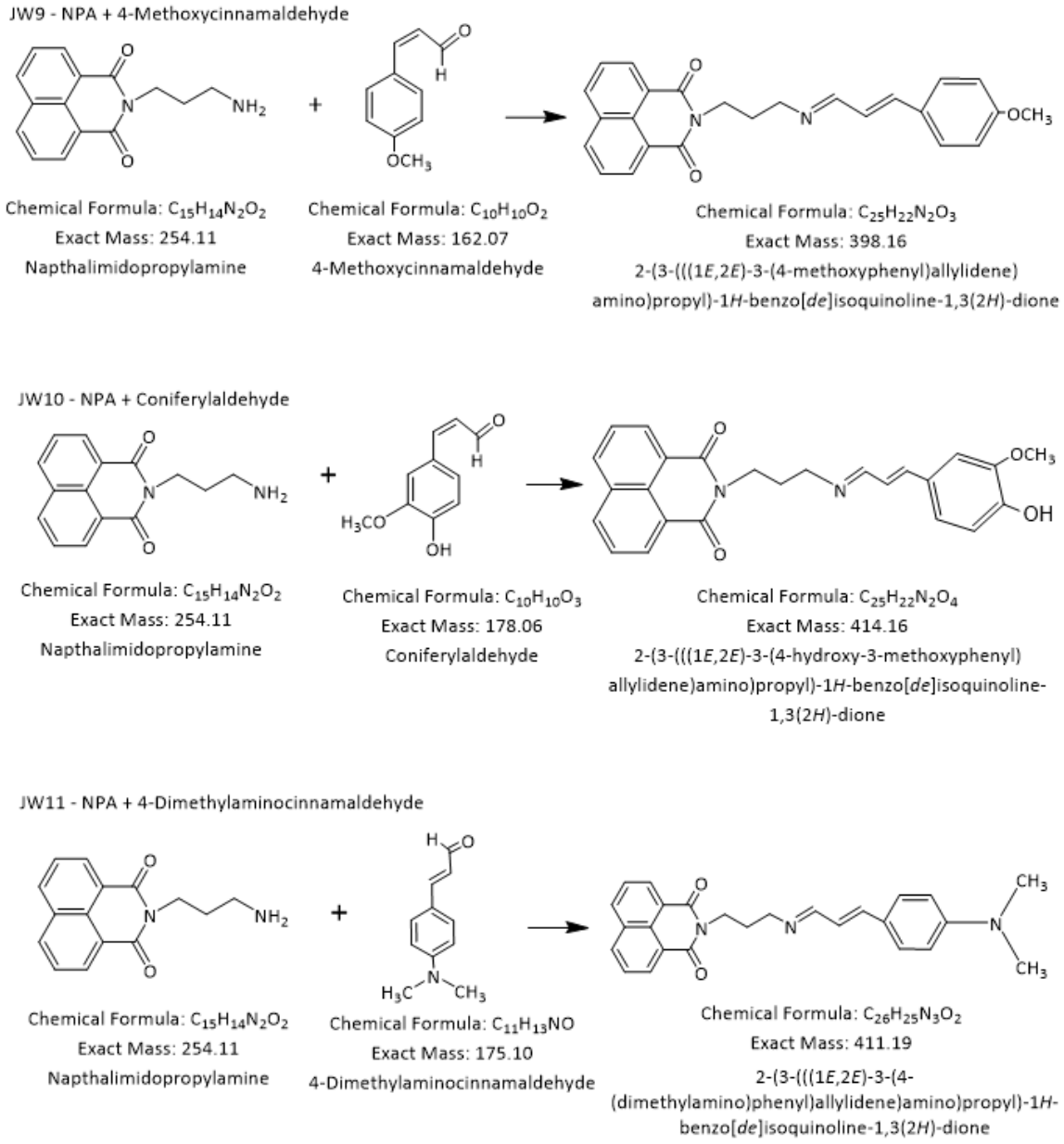

Figure 14 Full library of novel MTD compounds synthesis, structure, and mass.

3.3 Antimicrobial Methods

Antimicrobial Investigations

E. coli (4174) and *S. aureus* (6571) were purchased from the National Collection of Industrial, Food and Marine Bacteria (NCIMB), UK. These strains were specifically selected for their relevance to the study of AMR and their role in sepsis [8]. *E. coli* is a Gram-negative bacterium known for its involvement in urinary tract infections (UTIs), bloodstream infections, and sepsis. *S. aureus* is a Gram-positive bacterium often associated with severe infections like sepsis, pneumonia, and skin and soft tissue infections [8]. Including both strains in this study provides insight into two major pathogens implicated in sepsis, allowing for the evaluation of antimicrobial efficacy against both Gram-negative and Gram-positive organisms.

Muller Hinton broth (MHB) and Muller Hinton Agar (MHA) were purchased from Fischer Scientific, UK. For each bacterial investigation, bacterial suspensions were adjusted to the optical density of 0.08-0.13 at 625 nm for 0.5 McFarland standard (1.5×10^8 CFU/mL) using a spectrophotometer (Jenway 7315) following the guidance provided by the Clinical Laboratory Standards Institute (CLSI) for antimicrobial susceptibility testing [43].

96 Well Plate Microdilution

A stock solution of compounds was prepared in 100% DMSO at a concentration of 10 mg/mL. The solution was filtered using a 0.22 µm syringe filter before performing a 2-fold serial dilution (DMSO as solvent) for 10 dilutions (19-10,000 µg/mL). Overnight cultures of *E. coli* and *S. aureus* were grown in MHB, and the OD of bacterial suspensions were adjusted to match a 0.5 McFarland standard. Aliquots of 100 µL of each dilution of the compounds were added to sterile 1.5 mL size microcentrifuge tubes. Subsequently, 900 µL bacterial suspensions were added into each microcentrifuge tube, where the final DMSO concentration of the suspension was set at 10% (final compound concentration 1.9-1000 µg/mL). The suspension was mixed by gentle vortex, and 200 µL of each dilution was pipetted in triplicate to a 96-well plate. Time 0 absorbance was read at 625 nm using the Epoch plate reader, and then the plate was incubated for 24 hours at 37°C. Absorbance was read at 625 nm after 24 hours; data was analysed using GraphPad prism to generate a MIC curve. A 2-fold serial dilution of gentamycin (1.5-200 µg/mL) was plated in triplicate as a positive control and MHB only as a negative control.

Resazurin Assay

Following the final absorbance reading from the 96-well microdilution assay (at 24 h), 30 µL of sterile resazurin (Sigma-Aldrich, USA) solution (0.2% W/V) was added to each well of the 96-well plate and incubated for a further 60 minutes at 37 °C. Images of the plate were taken and compared with MIC values from the microdilution assay to confirm antibacterial activity.

Time Kill Kinetics Assay

An aliquot of 1 mL overnight bacterial culture and 9 mL test compounds (0.5xMIC, 1xMIC & 2xMIC) were dispensed into sterile universal bottles and shaken at 100 rpm in a temperature-controlled incubator set at 37 °C. At 0, 1, 2, 4, 6 and 24 hours, a 10 µL sample from each universal bottle was transferred

in a fresh universal containing 9.99 mL sterile saline and gently vortexed. An aliquot of 100 µL of this dilution was aseptically spread evenly on MH agar plates and was incubated at 37 °C for 24 hours. Once incubated, colonies of each plate were counted to determine the viability of the bacteria at each time point. Controls for assay were performed by substituting the test compound with gentamycin for the positive control and MHB for the negative control, following the same protocol.

To evaluate the bactericidal activity of JW6 and JW10, varying concentrations were tested against *S. aureus* and *E. coli*. The concentrations were based on multiples of their respective MICs, specifically 0.5× MIC, 1× MIC, and 2× MIC.

Concentrations of JW6 and JW10 used in the time-kill kinetics assay:

For ***S. aureus***, concentrations of 125 µg/mL (0.5 × MIC), 250 µg/mL (1 × MIC), and 500 µg/mL (2 × MIC) were tested.

For ***E. coli***, concentrations of 62.5 µg/mL (0.5 × MIC), 125 µg/mL (1 × MIC), and 250 µg/mL (2 × MIC) were tested.

3.4 Antioxidant Methods

2,2-Diphenyl-1-picrylhydrazyl (DPPH) Assay

Fresh DPPH solution was prepared daily at 0.1mM, dissolving 0.0039 g of DPPH (394.2 g/mol) (Sigma-Aldrich, USA) and adjusted to 100 mL with methanol. The solution was stored in the refrigerator and kept in the dark. The serial dilution (2-fold) of the test compounds was prepared starting at 10 mM - 26 µM in DMSO, and 50 µL of the test sample was pipetted into corresponding wells in the 96-well plate. Aliquots of 50 µL methanol were pipetted into corresponding wells as the negative control, followed by 100 µL DPPH added to all wells. The plate was then stored in a dark space for 30 minutes at room temperature. Absorbance measurement read at 490 nm using iMark™ microplate absorbance reader. All concentrations are divided by 3 for the final plate volume. The % ABS (absorbance) was calculated by dividing the absorbance value at each sample concentration by the average absorbance of the negative controls, then multiplying by 100. A graph was generated with the concentration in the x-axis and % ABS in the y-axis. The linear part of the curve was isolated using at least 3 points with a range including 50% ABS. The IC_{50} (50% ABS) was calculated using the line equation.

Ferric Reducing Antioxidant Power (FRAP) Assay

All assay reagents were purchased from (Sigma-Aldrich, USA). The FRAP reagent was prepared by mixing 25 mL of acetate buffer, 2.5 mL of TPTZ, and 2.5 mL of ferric chloride solution. A 300 mM acetate buffer was prepared by dissolving 2.7066 g sodium acetate (anhydrous) in dH_2O (~950 mL) and adding approximately 16.85 mL of glacial acetic acid. The solution's pH was adjusted with small volumes of glacial acetic acid to 3.6. Once pH 3.6 was reached, the solution was brought to a final volume of 1 litre with dH_2O and stored at 4°C until needed.

The following solutions were prepared daily to ensure their stability and effectiveness for experimental use:
A 10 mM solution of TPTZ (2,4,6-Tris(2-pyridyl)-s-triazine) was prepared by dissolving 0.0156 g of TPTZ in 40 mM HCl and adjusting the volume to 5 mL.
A 20 mM ferric chloride solution was prepared by dissolving 0.0270 g of ferric chloride ($FeCl_3*6H_2O$) in dH_2O and adjusting the volume to 5 mL.

Test samples were serially diluted (2-fold) using methanol at a 2 mM - 62.5 µM concentration range. A 2-fold serial dilution of Trolox was prepared starting at 2 mM - 62.5 µM in methanol. In the 96-well plate, 10 µL of each sample, methanol (negative control), and Trolox were added, followed by a 190 µL FRAP reagent. The plate was incubated in the dark at room temperature for 30 minutes, and the absorbance was measured at 595 nm using iMark™ microplate absorbance reader. The samples were expressed as Trolox Equivalents (TE).

3.5 Anticoagulant Methods

Clot Lysis Assay

Pooled normal plasma (PNP) was removed from a -80 °C freezer and thawed at 37°C. Thrombin and tPA were removed from the -80 °C freezer and stored on ice until use.

Phospholipids (Rossix, Molndal, Sweden) were diluted to 200 µM (x12.5 final plate concentration) from stock (0.5 mM) with TBST buffer.

CaCl2 was diluted to 106 mM (x10 higher), and thrombin was diluted to 1 U/ml (x10 higher) using TBST buffer to prepare the activation mix. Then, 750 µL of each CaCl2 (10.6mM) and thrombin (µg/mL) were mixed to produce an activation mix.

tPA (Sigma Aldrich, St Louis, USA) was diluted to 3.6 µM using TBST buffer.

Compounds were diluted to 20 µM with TBST buffer.

TBST buffer, PNP, phospholipids, tPA and compounds were added to label microcentrifuge tubes (1.5 mL) as follows in Table 2 (total volume of each tube 150 µL):

Table 2 Example of the reaction mixture and volumes used in the clot lysis assay (µL).

SAMPLE		**TBST Buffer**	**PNP**	**Phospholipid**	**tPA**	**Compound**
1	Buffer	150	/	/	/	/
2	plasma only	93.7	56.3	/	/	/
3	plasma + PL	78.7	56.3	15	/	/
4	Plasma + PL + tPA	63.7	56.3	15	15	/
5	JW2 20	63.7	56.3	15	/	15
6	JW2 20+tPA	48.7	56.3	15	15	15
7	JW2 15	63.7	56.3	15	/	15
8	JW2 15+tPA	48.7	56.3	15	15	15

From each tube, 40 µL was added in triplicate to a half-volume 96-well plate. Aliquots (10 µL) of activation mix were added to each well and placed immediately into the plate reader (Varioskan LUX plate reader using Skan It software (version 7.0)) for 4 hours with 1-minute absorbance intervals at 405 nm.

4. Results and Discussion
4.1 MTD Characterisation
4.1.1 NMR
NMR spectroscopy is a powerful and widely employed tool for confirming and characterising newly synthesised organic compounds. Using the magnetic properties of atomic nuclei, NMR provides valuable insights into the structure, concentration, purity, and chemical environments. Researchers in various fields rely on NMR for characterisation, mixture composition monitoring, quantifying unknown compounds, and dynamic studies.

NMR provides 3 types of essential data: first, the chemical shift, which is the variation in the resonance frequency of nuclei, typically hydrogen or carbon, relative to a reference compound in a magnetic field [41]. There is a shift in a compound's nuclei resonance frequency when the electron's magnetic field interacts with the nucleus's magnetic field. The shift, also known as the chemical shift (δ), is proportional to the external electrons' magnetic field, expressed in parts per million (ppm). This is the greatest characteristic of the NMR data, as the chemical shift allows the determination of the structure and functional groups present in the NMR signal [41].

The second of the 3 essential data types is the distance between two peaks, known as J-coupling. This provides information on the splitting patterns of the chemical bonds and interactions between hydrogen atoms in the sample. When identifying splitting patterns, the 'n + 1' rule where n is equal to the number of neighbouring protons (Figure 15). Therefore, singlets have no proton coupling; doublets have one coupled proton; triplets have two proton couples [41,42].

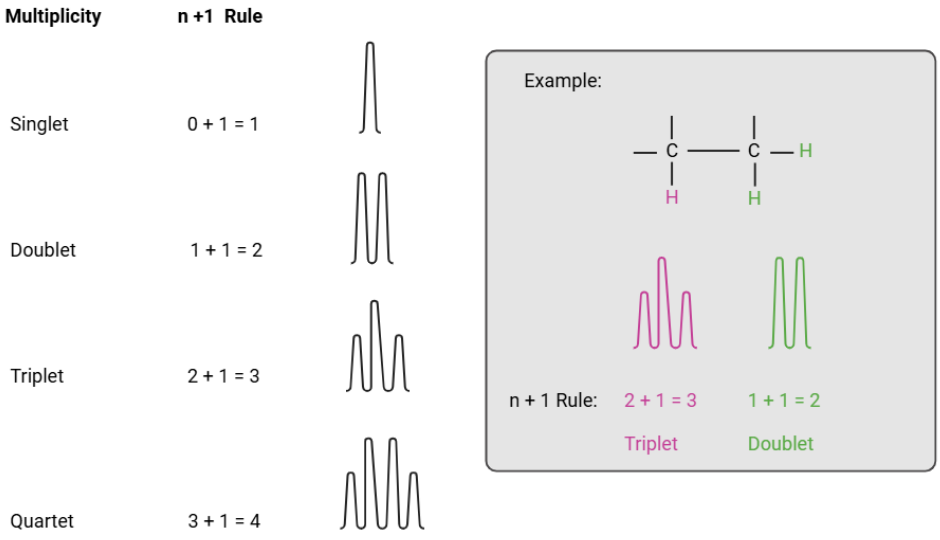

Figure 15 Diagram of NMR correlation peaks and associated n + 1 rule describing multiplicity of peaks.

Finally, the integration signals are determined by the area under the peak proportional to the number of hydrogens that generate the peak. The integration allows for determining the relative number of protons contributing to each peak. Often presented as ratios, these values help identify the compound's structure and functional groups using the specific proton counts [42].

The 11 synthesised compounds in this research were structurally characterised using NMR (^{1}H and ^{13}C) spectroscopy and HRMS. Each compound contains an NPA (naphthalimidopropyl) group linked to another group *via* an imino bond (Figure 10). The ^{1}H NMR spectroscopy provides insight into the unique hydrogen environments of each compound, producing characteristic peaks based on hydrogen atom environments. The ^{13}C NMR offers structural information on the carbon backbone without the splitting patterns seen in ^{1}H NMR due to decoupling [42]. To represent the library of synthesised compounds and as an example, the full characterisation of compound JW2 is discussed in detail below.

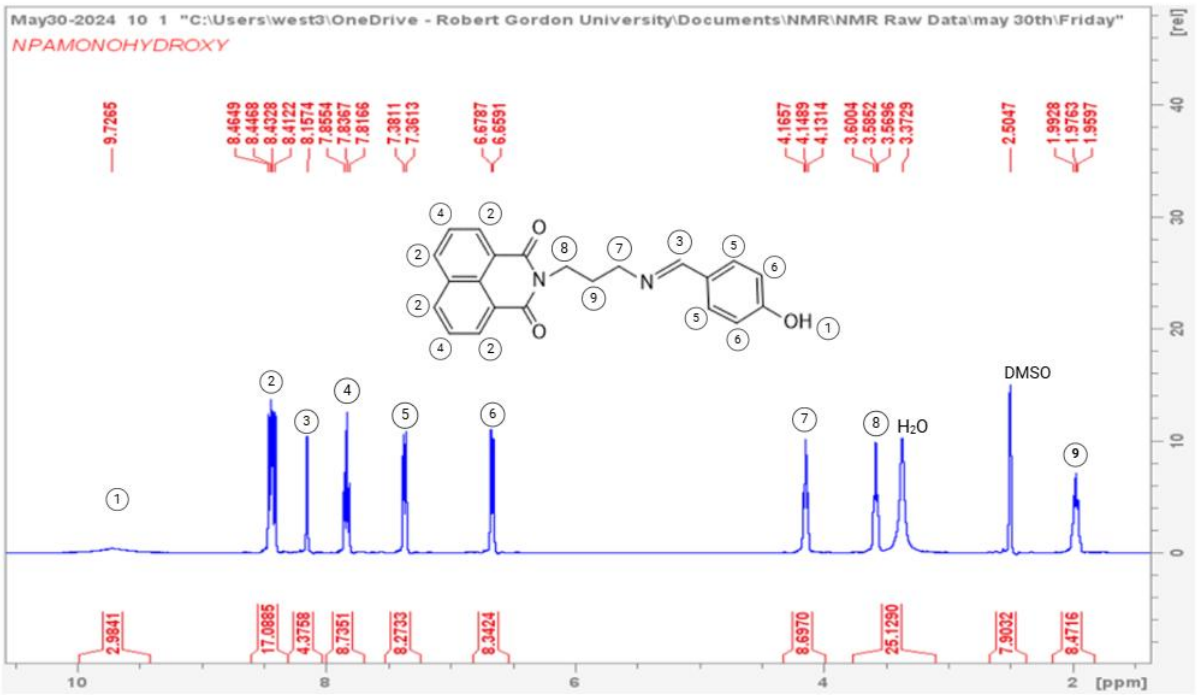

Figure 16 ^{1}H NMR JW2

In the ^{1}H NMR for JW2 (Figure 16), the Naphthalimide moiety protons of the aromatic rings are represented by two sets of signals: multiplet at 8.46-8.41 ppm with integration for 4 protons (No.2) and triplet peak 7.85-7.81ppm integration for 2 protons (No.4). The protons of the propylamine linker chain present as a triplet (No.7 & 8) and multiplet (No.9) peaks 4.16-4.13 ppm, 3.60-3.56 ppm and 1.99-1.95 ppm each integrating for 2 protons. The N=C at the end of the linker chain is represented by a singlet at 8.15 ppm integration for 1 proton (No.3). As the nitrogen atom is highly electronegative, it causes de-shielding of the proton, moving the signal further downfield. Two doublets represent the protons of the phenyl ring, each at 7.38-7.36 ppm and 6.67-6.65 ppm, integrating for 2 protons each (No.5 & 6). The protons adjacent to the hydroxyl group (OH), denoted as No.6 in Figure 16, have a more significant shielding effect due to the electron-donating ability of the hydroxyl group, causing the peak to present further upfield. The hydroxyl group presents a broad peak at 9.71 ppm (No.1), commonly seen with hydroxyl groups due to the rapid proton exchange and hydrogen bonding.

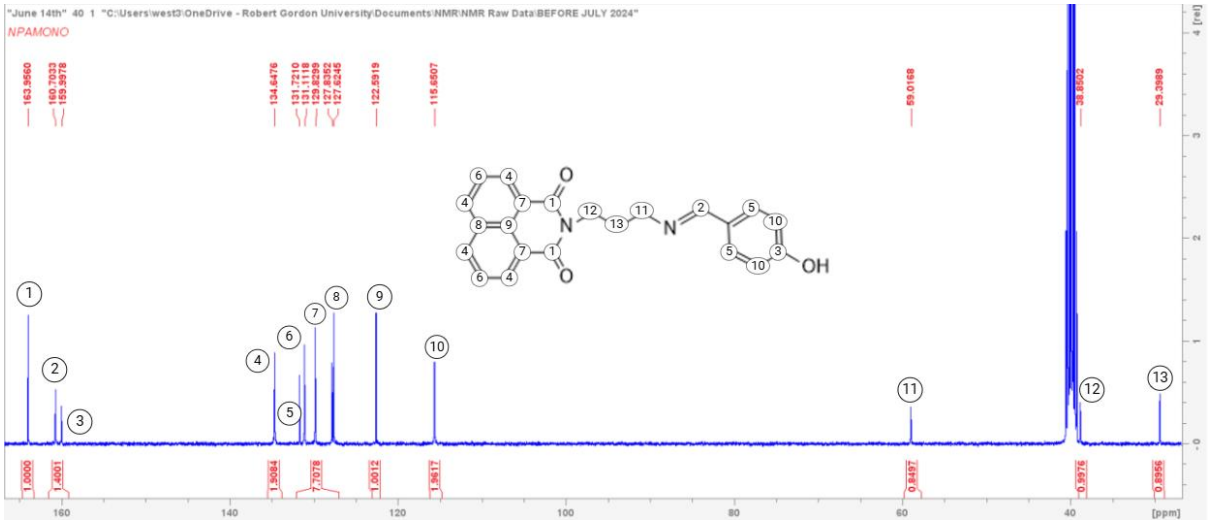

Figure 17 ^{13}C NMR JW2

In the ^{13}C NMR for JW2 (Figure 17), the carbons of the naphthalimide moiety are represented by peaks 4, 6 ,7 ,8 and 9, ranging between 134–122 ppm. The carbonyl groups of naphthalimide are represented by peak No.1 at 163 ppm. The imine group (N=C) appears at 159 ppm (No.2). The carbon-bearing hydroxyl group appears at 160 ppm (No.3). The linker propylamine chain presents at 59-29 ppm (No.11-13), and the remaining carbons of the phenyl ring at 131 and 115 ppm (No.5 & 10). The solvent peak for DMSO D_6 can be seen at 40 ppm.

4.1.2 HRMS

Mass Spectrometry (MS) and HR-MS are powerful tools for characterising small organic molecules. The compound is broken down into small, charged fragments, which are then analysed using their mass-to-charge ratio (*m/z*). This process is presented via a series of peaks corresponding to the different ions generated, known as the mass spectrum. The peaks provide information on the structure of the compound, its molecular weight, and its fragmentation.

HR-MS works by the same principles as MS but provides greater accuracy and precision. The HR-MS can distinguish between ions within small *m/z* value ranges, providing the exact molecular formula. The application of both NMR and MS methods allows for a comprehensive characterisation and determination of the small organic compounds which are analysed in this research project. These characterisation methods provide a strong analytical approach which is used in various fields, including organic chemistry and pharmaceuticals, to obtain reliable and accurate characterisation.

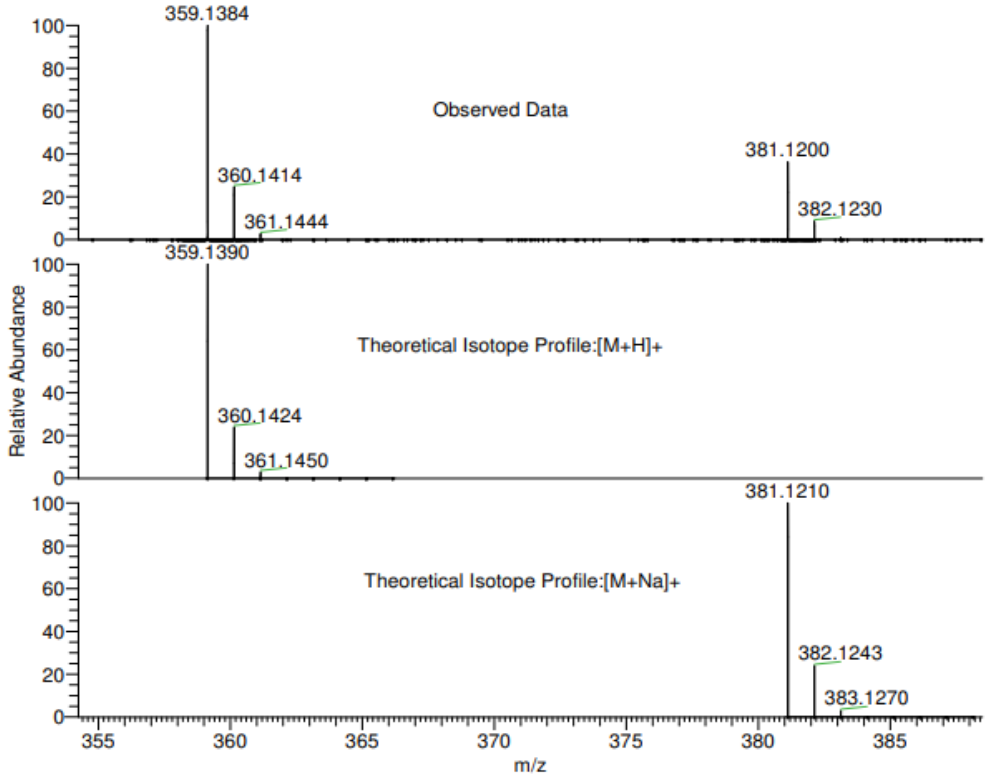

Figure 18 HRMS analysis of JW2

As shown in Figure 18, the HRMS analysis of the compound JW2 revealed a parent ion at *m/z* 359.1384 Da. This also corresponds closely with the theoretical *m/z* value of 359.1390 Da for the protonated molecular ion $[M+H]^{+,}$ as seen in Figure 18. The isotopic peaks at *m/z* 360.1414 Da and 361.1444 Da align well with the theoretical isotope profile values of 360.1424 Da and 361.1450 Da. Furthermore, peaks at *m/z* 381.1200 Da and 382.1230 Da were identified with correspondence to the sodium adduct $[M+Na]^{+}$ of the JW2 parent ion (Figure 18). The close agreement between the observed and theoretical HRMS spectra demonstrates the presence of both protonated and sodium-adducted forms of JW2, confirming the successful synthesis.

4.1.3 % Yield of JW Compounds

Table 3 List of compounds and corresponding % yield in relation to similarities and differences in structure.

Compound	**% Yield (n=1)**	Structural Features/Functional Group
JW1	25	1 Double Bond ($N=CH_2$), No additional groups on the phenyl ring.
JW2	70	1 Double Bond, Hydroxyl group on the phenyl ring para position.
JW3	85	1 Double Bond, Hydroxyl groups on the phenyl ring para and ortho position.
JW4	59	1 Double Bond, Hydroxyl groups on the phenyl ring para and ortho positions.
JW5	32	1 Double Bond, Methoxy group on the phenyl ring para position.
JW6	57	1 Double Bond, Hydroxyl group on the phenyl ring para position and Methoxy group on ortho position.
JW7	74	1 Double Bond, Hydroxyl group on the phenyl ring para position and Methoxy groups on both ortho positions.
JW8	23	2 Double Bond (N=CH-CH=N), No additional groups on the ring.
JW9	92	2 Double Bond, Methoxy group on the phenyl ring para position.
JW10	86	2 Double Bond, Hydroxyl group on the phenyl ring para position, methoxy group on ortho position.
JW11	73	2 Double Bond, Dimethylamine group on phenyl para position.

The percentage yield of a chemical reaction can be used to indicate the effectiveness and efficacy of compound synthesis. Structural features such as varying functional groups or the position of these groups in the compound can influence the reactivity, stability, and reaction pathway [(69)]. The % yield of the 11 synthesised compounds was analysed to determine the relationship between their structural characterisation and subsequent yield (Table 3).

As seen in Table 3, JW1 and JW8 have a considerably lower yield than their sister compounds. Both compounds share the same structural pattern with no additional group attached to the phenyl ring (Figure 14). The additional double bond in JW8 (Figure 14) showed no benefit to the compound's yield, suggesting that it does not facilitate further reactivity. The presence of the hydroxyl group in compounds JW2-4, JW6 and JW7 shows a substantial increase in yield (Table 3). JW5 contains a methoxy group on the para position, replacing the hydroxy group, which significantly reduced the yield to 32%, although higher than simpler compounds JW1 and JW8. This is further supported by the greater yields of JW6, JW7 and JW10, which contain a para hydroxy group and an ortho

methoxy group; the presence of the second double bond in JW10 may also play a role in increasing the reaction stability, producing a yield 1.5-fold greater than, JW6 with the same structure but one double bond. In contrast, JW9 with a singular methoxy group on the para position and two double bonds produced the greatest yield (92%), possibly due to the dual double bonds coupled with the para position of the functional group. JW11 differs from the other compounds with the presence of a dimethylamine group at the para position of the phenyl ring, increasing the yield to 73%; the dimethylamine group likely enhances the reactivity *via* nucleophilicity along with the presence of two double bonds [70].

The synthesised compound's functional groups and structural features substantially influence the reactivity and yield. Previous studies have shown that electron-donating groups, such as hydroxyl groups, can enhance reactivity by increasing the electron density at reactive sites, ultimately leading to better yield [71]. In contrast, the electron-withdrawing groups, such as methoxy groups, often reduce reactivity unless specific structural conditions are met (i.e. conjugation) to mitigate steric hindrance [81]. These observations support the observed trend in yield variations in Table 3. Further highlighting the critical role of functional group types and position on reaction efficiency. Future optimisation of the compounds will be evaluated using the analyses gathered to increase reactivity and overall yield, improve reaction efficacy, and reduce waste.

Two synthesised compounds, namely JW5 and JW7, exhibited minor impurities on TLC and NMR analysis. Such minor impurities could result from an incomplete reaction, leaving residual starting materials in the product, which is common in organic synthesis [82]. Thus, recrystallisation and rotary evaporation were employed to remove the impurities since these methods are commonly implemented to increase the purity of synthesised compounds [83]. However, the recrystallisation of these compounds, JW5 and JW7, decreased yield due to the unavoidable product loss during the purification, possibly because the product and its parent compounds share similar solubility. Synthesis of these compounds was also carried out under reflux conditions but had little to no impact on purity or yield. To maintain yield, the compounds were investigated with impurities in both antimicrobial and antioxidant investigations to establish whether these impurities would affect the potential therapeutic effect.

4.1.4 Full Characterisation of JW Compounds

Complete Characterisation of all JW compounds (ppm):
JW1 Orange Solid - 25% Yield
^{1}H NMR (DMSO D6): Solvent peak δ 2.5, 8.46-8.40 (dd, 4H Naphthalene J = 7.2 Hz, 8.28 Hz) 8.30 (s, 1H N=CH) 7.85-7.81, (t, 2H Naphthalene J = 7.6 Hz) 7.54-7.52 (d, 1H Phenyl J = 7.4 Hz) 7.38-7.35 (t, 2H Phenyl J = 7.4 Hz) 7.31-7.27 (t, 2H Phenyl J = 7.24 Hz) 4.18-4.15 (t, 2H CH_2-CH_2-**CH_2** J = 6.9 Hz) 3.67 – 3.64 (t, 2H **CH_2**-CH_2-CH_2 J = 6.4 Hz) 2.04-2.00 (m, 2H CH_2-**CH_2**-CH_2 J = 6.6 Hz)
^{13}C NMR (DMSO D6): Solvent peak δ 40, 163 (C=O) 161 (Nap N=C) 136 (Naphthalene C) 134 (AR–C) 131 – 122 (Naphthalene and Ar C) 59 (CH_2-N) 38 (N-CH_2) 29 (CH_2-CH_2-N).
HRMS: Calculated mass 342.14 for $C_{22}H_{18}N_2O_2$, $[M+H]^+$ 343.14, *m/z* found 343.14.

JW2 Yellow Solid - 70% Yield
^{1}H NMR (DMSO D6): Solvent peak δ 2.5, 9.72 (s, 1H Hydroxy) 8.46-8.41 (dd, 4H Naphthalene J = 7.2 Hz, 8.2 Hz) 8.15 (s, 1H N=CH) 7.85-7.81 (t, 2H Naphthalene J = 7.5 Hz) 7.38-7.36 (d, 2H Phenyl J = 7.9 Hz) 6.67-6.65 (d, 2H Phenyl J = 7.8 Hz) 4.16-4.13 (t, 2H CH_2 – CH_2 – **CH_2** J = 6.7 Hz) 3.60-3.56 (t, 2H **CH_2**–CH_2–CH_2 J = 6.1 Hz) 1.99-1.95 (m, 2H CH_2–**CH_2**–CH_2 J = 6.8 Hz).
^{13}C NMR (DMSO D6): Solvent peak δ 38, 163 (C=O) 160 (Nap C=N) 159 (C – OH) 134 – 122 (Naphthalene and Ar C) 115 (AR – ortho) 59 (CH_2-N) 38 (N-CH_2) 29 (CH_2-CH_2-N).
HRMS: Calculated mass 358.13 for $C_{22}H_{18}N_2O_3$, $[M+H]^+$ 359.13, $[M+Na]^+$ 381.1210, *m/z* found 359.13.

JW3 Red Solid - 85% Yield
^{1}H NMR (DMSO D6): Solvent peak δ 2.5, 8.47 – 8.41 (dd, 4H Naphthalene J = 7.1 Hz, 8.4 Hz) 8.09 (s, 1H N= CH) 7.86 – 7.82 (t, 2H Naphthalene J = 7.6 Hz) 7.12 (s, 1H Phenyl) 6.86 – 6.84 (d, 1H Phenyl J = 8.1 Hz) 6.67 – 6.65 (d, 1H Phenyl J = 8.1 Hz) 4.14 – 4.11 (t, 2H CH_2–CH_2–**CH_2**–N J = 7.1 Hz) 3.58 – 3.55 (t, 2H **CH_2**–CH_2–CH_2–N J = 6.5 Hz) 1.99 – 1.92 (m, 2H N–CH_2–**CH_2**–CH_2–N J = 6.7 Hz).
^{13}C NMR (DMSO D6): Solvent peak δ 40, 163 (C=O) 161 (Nap C=N) 134 (Ar - OH) 131 – 122 (Naphthalene and Ar C) 115 (AR – ortho) 49 (CH_2-N) 38 (N-CH_2) 29 (CH_2-CH_2-N)
HRMS: Calculated mass 374.13 for $C_{22}H_{18}N_2O_4$ $[M+H]^+$ 373.11, *m/z* found 373.11.

JW4 Orange Solid - 59% Yield
^{1}H NMR (DMSO D6): Solvent peak δ 2.5, 9.48 (s, 1H hydroxy) 8.48 – 8.41 (dd, 4H Naphthalene J = 7.2 Hz, 8.1 Hz) 8.02 (s, 1H N= CH) 7.86 – 7.82 (t, 2H Naphthalene J = 7.6 Hz) 6.66 (s, 2H Phenyl) 4.13 – 4.09 (t, 2H CH_2–CH_2–**CH_2** J = 5.0 Hz) 3.57- 3.54 (t, 2H **CH_2**–CH_2 – CH_2 J = 6.5 Hz) 1,97 – 1.90 (m, 2H CH_2–**CH_2**-CH_2 J = 6.4 Hz).
^{13}C NMR (DMSO D6): Solvent peak δ 40, 163 (C=O) 161 (C=N) 146 (Ar -OH) 143 (Ar -OH) 131 – 122 (Naphthalene and Ar C) 107 (AR – 2,6) 49 (CH_2-N) 38 (N-CH_2) 29 (CH_2-CH_2-N)
HRMS: Calculated mass 390.12 for $C_{22}H_{18}N_2O_5$, $[M+H]^+$ 389.11, *m/z* found 389.11.

JW5 White Solid - 32% Yield
^{1}H NMR (DMSO D6): Solvent peak δ 2.5, 8.44 - 8.39 (dd, 4H Naphthalene J = 7.3 Hz, 8.2 Hz) 8.20 (s, 1H N = CH) 7.83 7.80 (t, 2H Naphthalene J = 7.7 Hz) 7.47 – 7.45 (d, 2H Phenyl J = 8.2 Hz) 6.84 – 6.82 (d, 2H Phenyl J = 8.2 Hz) 4.16 – 4.13 (2H CH_2–CH_2–**CH_2** J = 6.9 Hz) 3.75 (s, 1H OCH_3) 3.62 – 3.59 (t, 2H **CH_2**–CH_2–CH_2 J = 6.4 Hz) 2.03 – 1.96 (m, 2H CH_2–**CH**$_2$–CH_2 J = 6.8 Hz).
^{13}C NMR (DMSO D6): Solvent peak δ 40, 163 (C=O) 161 (N=C) 160 (AR – OCH_3) 134 (Ar -OH) 134 – 122 (Naphthalene and Ar C) 114 (AR – 3,5) 59 (CH_2-N) 55 (OCH_3) 38 (N-CH_2) 29 (CH_2-CH_2-N)
HRMS: Calculated mass 372.15 for $C_{23}H_{20}N_2O_3$, $[M+H]^+$ 373.15, *m/z* found 373.15.

JW6 White Solid - 57% Yield
^{1}H NMR (DMSO D6): Solvent peak δ 2.5, 9.36 (s, 1H Hydroxy) 8.42-8.36 (dd, 4H Naphthalene J = 7.2 Hz, 8.2 Hz), 8.13 (s, 1H N = CH), 7.82-7.78 (t, 2H Naphthalene J = 7.8 Hz) 7.12 (s, 1H, Phenyl), 6.95-6.93 (d, 1H Phenyl J = 8.0 Hz) 6.71-6.69 (d, 1H Phenyl J = 8.0 Hz), 4.15-4.11 (t, 2H CH_2–CH_2–**CH_2** J = 6.9 Hz) 3.63 (s, 3H OCH_3) 3.60-3.57 (t, 2H **CH_2**–CH_2–CH_2 J = 6.4 Hz) 2.03-1.96 (m, 2H CH_2–**CH_2**–CH_2 J = 6.5 Hz).
^{13}C NMR (DMSO D6): Solvent peak δ 40, 163 (C=O) 161 (Nap N=C) 149 (AR – OCH3) 148 (Ar -OH) 134 – 122 (Naphthalene and Ar C) 115 (AR – 4) 109 (AR – 2) 59 (CH_2-N) 55 (OCH_3) 38 (N-CH_2) 29 (CH_2-CH_2-N)
HRMS: Calculated mass 388.14 for $C_{23}H_{20}N_2O_4$, $[M+H]^+$ 389.14, $[M+Na]^+$ 411.1315 *m/z* found 389.14.

JW7 Yellow Solid - 74% Yield
^{1}H NMR (DMSO D6): Solvent peak δ 2.5, 9.53 (s, 1H hydroxy) 8.47 – 8.37 (m, 4H Naphthalene J = 10.1 Hz) 8.11 (s, 1H N = CH) 7.87 – 7.79 (m, 2H Naphthalene J = 7.8 Hz) 7.01 (s, 2H Phenyl) 4.16 – 1.08 (t, 2H CH_2–CH_2–**CH_2** J = 6.7 Hz) 3.70 (s, 3H OCH_3) 3.66 (s, 3H OCH_3) 2.71 - 2.68 (t, 2H **CH_2**–CH_2–CH_2 J = 3.7 Hz) 1.87 – 1.80 (m, 2H CH_2–**CH_2**–CH_2 J = 6.7 Hz)
^{13}C NMR (DMSO D6): Solvent peak δ 40, 163 (C=O) 161 (N=C) 148 (AR – OCH3) 148 (Ar -OH) 134 – 122 (Naphthalene and Ar C) 105 (AR – 2,6) 59 (CH_2-N) 56 (OCH_3) 38 (N-CH_2) 29 (CH_2-CH_2-N)
HRMS: Calculated mass 418.15 for $C_{42}H_{22}N_2O_5$, $[M+H]^+$ 419.16, *m/z* found 419.15.

JW8 White Solid - 23% Yield
^{1}H NMR (DMSO D6): Solvent peak δ 2.5, 8.43 – 8.38 (dd, 4H Naphthalene J = 7.3 Hz, 8.3 Hz) 8.20 (s, 1H N = CH) 7.82-7.79 (t, 2H Naphthalene J = 7.7 Hz) 7.41 – 7.45 (d, 5H Phenyl J = 8.2 Hz) 7.03 (s, 2H C=C*) 6.80 – 6.74 (s, 1H CH = CH) 4.16-4.12 (t, 2H CH_2–CH_2–**CH_2** J = 6.9 Hz) 3.61-3.58 (t, 2H **CH_2**–CH_2–CH_2 J = 6.4 Hz) 2.02-1.95 (m, 2H CH_2–**CH_2**–CH_2 J = 6.6 Hz)
^{13}C NMR (DMSO D6): Solvent peak δ 40, 163 (C=O) 163 (N=C) 141 – 122 (Naphthalene and Ar C) 59 (CH_2-N) 38 (N-CH_2) 29 (CH_2-CH_2-N)
HRMS: Calculated mass 368.15 for $C_{24}H_{20}N_2O_2$, $[M+H]^+$ 369.16, *m/z* found 369.15.

JW9 White Solid - 92% Yield
^{1}H NMR (DMSO D6): Solvent peak δ 2.5, 8.49 - 8.47 (d, 2H Naphthalene J = 6.6 Hz) 8.43 – 8.41 (d, 2H Naphthalene J = 8.2 Hz) 8.03 – 8.01 (d, 1H N = CH J = 8.8 Hz) 7.86 – 7.84 (t, 2H Naphthalene J = 7.6 Hz) 7.48 – 7.46 (d, 2H C=C J = 8.7 Hz) 6.96 – 6.92 (t, 3H Phenyl J = 7.6 Hz) 6.67 – 6.61 (d, 1H Phenyl J = 8.8 Hz) 4.13 – 4.10 (t, 2H CH_2–CH_2–**CH_2** J = 7.1 Hz) 3.78 (s, 3H OCH_3) 3.54 – 3.51 (t, 2H **CH_2**–CH_2–CH_2 J = 6.5 Hz) 1.98 – 1.91 (m, 2H CH_2–**CH_2**–CH_2 J = 6.8 Hz)
^{13}C NMR (DMSO D6): Solvent peak δ 40, 163 (C=O) 161 (N=C) 151 (AR – OCH_3)142 (N = C- Ar) 134 – 122 (Naphthalene and Ar C) 112 (AR – 3,5) 59 (CH_2-N) 55 (OCH_3) 38 (N-CH_2) 29 (CH_2-CH_2-N)
HRMS: Calculated mass 398.16 for $C_{25}H_{22}N_2O_3$, $[M+H]^+$ 399.17, *m/z* found 399.17.

JW10 Orange Solid - 86% Yield
^{1}H NMR (DMSO D6): Solvent peak δ 2.5, 9.37 (s, 1H Hydroxy) 8.47 – 8.40 (dd, 4H Naphthalene J = 7.2 Hz, 8.2 Hz) 8.02 - 7.99 (d, 2H N=CH-CH J = 8.7 Hz) 7.85 - 7.81 (t, 2H Naphthalene J = 7.8 Hz) 7.13 (s, 1H CH=**CH**-AR) 6.92 - 6.90 (d, 2H Phenyl J = 8.5 Hz) 6.86 (s, 1H Phenyl) 4.12 - 4.09 (t, 2H CH_2–CH_2–**CH_2** J = 7.1 Hz) 3.53 - 3.50 (t, 2H **CH_2**–CH_2–CH_2 J = 6.4 Hz) 3.80 (s, 1H OCH_3) 1.96 - 1. (m, 2H CH_2–**CH_2**–CH_2 J = 2.5 Hz)
^{13}C NMR (DMSO D6): Solvent peak 40, 163 (C=O) 163 (N=C) 148 (AR – OCH_3) 148 (Ar -OH) 134 – 121 (Naphthalene and Ar C) 115 (AR – 5) 110 (AR – 2) 59 (CH_2-N) 56 (OCH_3) 38 (N-CH_2) 29 (CH_2-CH_2-N)
HRMS: Calculated mass 414.16 for $C_{25}H_{22}N_2O_4$, $[M+H]^+$ 415.16, $[M+Na]^+$ 437.1472, *m/z* found 415.16.

JW11 Brown Solid - 73% Yield
^{1}H NMR (DMSO D6): Solvent peak δ 2.5, 8.54 – 8.47 (dd, 4H Naphthalene J = 7.2 Hz, 8.2 Hz) 8.05 – 8.03 (d, 1H N = CH J = 8.8 Hz) 7.92 – 7.88 (t, 2H Naphthalene J = 7.7 Hz) 7.41 – 7.39 (d, 2H Phenyl J = 8.6 Hz) 6.91 (d, 1H CH=**CH**–Ar J) 6.75 – 6.73 (d, 2H Phenyl J = 8.6 Hz) 6.60 – 6.56 (dd, 1H CH=CH J = 5.0 Hz) 4.18 – 4,15 (t, 2H CH_2–CH_2–**CH_2** J = 7.0 Hz) 3.57-3.54 (t, 2H **CH_2**–CH_2–CH_2 J = 6.4 Hz) 3.42 (s, 3H N–CH_3) 3.00 (s, 3H N–CH_3) 2.00-1.94 (t, 2H CH_2– **CH_2**–CH_2 J = 7.0 Hz)
^{13}C NMR (DMSO D6): Solvent peak δ 40, 163 (C=O) 163 (N=C) 151 (Dimethylamine) 148 (Ar -OH) 142 – 122 (Naphthalene, C=C and Ar C) 112 (Ar) 59 (CH_2-N) 40 (CH_3) 38 (N-CH_2) 29 (CH_2-CH_2-N)
HRMS: Calculated mass 411.19 for $C_{26}H_{25}N_3O_2$, $[M+H]^+$ 412.20, *m/z* found 412.20.

NPA Yellow Solid - 47% Yield
^{1}H NMR (DMSO D6): Solvent peak δ 2.5, 8.48– 8.42 (dd, 4H Naphthalene J = 7.3 Hz, 8.2 Hz) 7.87-7.83 (t, 2H Naphthalene J = 7.6 Hz) 4.10-4.06 (t, 2H N - CH_2 J = 6.8 Hz) 2.58 (s, 1H CH_2-NH_2) 1.73 – 1.69 (t, 2H CH_2=CH_2-NH_2 J = 12.6 Hz)
^{13}C NMR (DMSO D6): Solvent peak δ 40, 163 (C=O) 134 - 122 (Naphthalene) 45 (CH_2-N) 32 (N-CH_2) 20 (CH_2-CH_2-N)
HRMS: Calculated mass 254.11 for $C_{15}H_{14}N_2O_2$, $[M+H]^+$ 255.11, $[M+Na]^+$ 277.0947, *m/z* found 255.11.

In summary, the synthesis of all 11 compounds was successfully achieved, with most compounds showing a good reaction yield and purity with the exception of JW1, 5, 7 and 8. The characterisation by NMR and HRMS confirmed the structure of the synthesised compounds, allowing the research to progress. The following sections will assess the compounds' antimicrobial, antioxidant, and anticoagulant properties and potential as therapeutic agents.

4.2 Antimicrobial Investigations

Evaluating the antimicrobial properties of the newly synthesised MTDs is a critical step in their development as a treatment for sepsis. As previously described (Section Microbial Invasions and Host Response), sepsis is often triggered by bacterial, fungal, or viral infections, with bacteria such as *E. coli* and *S. aureus* being the predominant pathogens [8]. Therefore, understanding the ability of the MTDs to target these pathogens is essential for ensuring their therapeutic potential and whether the compounds have broad-spectrum activity, targeting multiple types of pathogens, or narrow spectrum, focusing on specific bacteria.

Different methods are employed to assess the various aspects of antimicrobial activity of the novel compounds. For example, the MIC can be determined as the lowest concentration required to inhibit bacterial growth. This is vital information specifically for optimising dosing regimens in clinical settings. The time-kill kinetics assay offers insight into the bactericidal activity of the drug over time, showing how effectively and quickly the drug can reduce bacterial populations during infection. This information is particularly important in sepsis, where quick bacterial clearance can be lifesaving. Resazurin bacterial cell viability assays evaluate the drug's ability to inhibit bacterial metabolism by colour changes, confirming its ability against actively growing bacteria. Combining these assays gives a wide overview of the compound's initial antimicrobial activity, allowing for the determination of its potential as an antimicrobial agent. The assays are well-known and standardised approaches, allowing for comparability between similar research and current therapeutics (Table 4) [43,44].

Table 4 Overview of Antimicrobial Investigations - summary of principles and analysis of methods undertaken.

Assay	**Principle**	**Analysis**
Broth Microdilution	Serial dilution of drug incubated with bacterial strains. MIC determination.	Absorbance (625 nm)
Time Kill Kinetics	Plates spread at various intervals with bacteria.	Visually assess growth and count colonies
Resazurin	Change in colour (blue to pink) if metabolic activity is present.	Visual colourimetric

4.2.1 The 96-well Plate Microdilution

The 96-well plate microdilution assay is a well-known and versatile method for MIC determination of antimicrobial agents. The assay allows various samples to be screened simultaneously in a high-throughput format. This method is recommended by the CLSI, as it is a standardised method that allows for reproducibility and reliability when comparing MIC data in various studies [43]. Additionally, the method allows for various organisms to be investigated, including many bacterial and fungal strains, which add to the versatility of the assay.

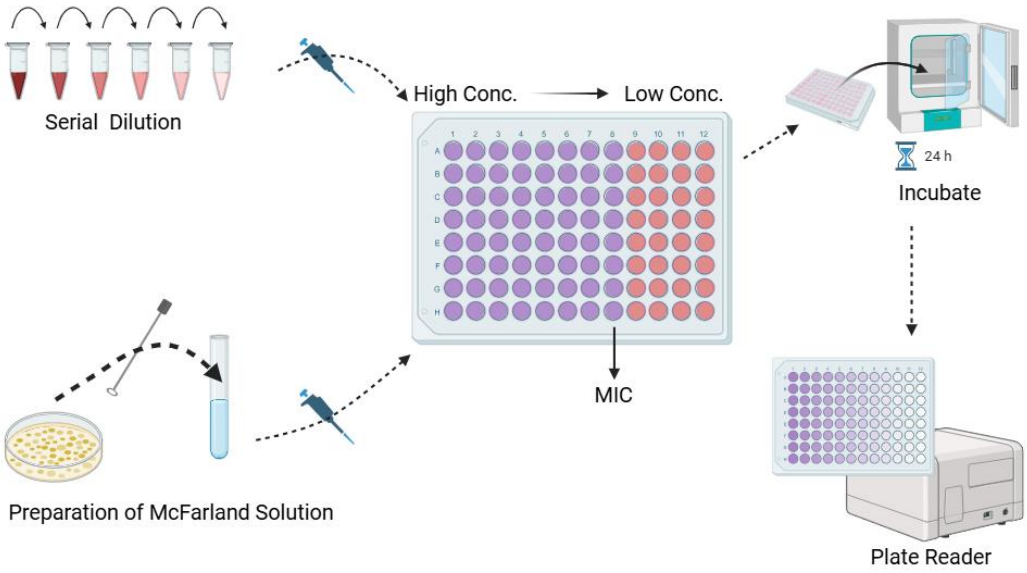

Figure 19 General overview of 96-well plate microdilution protocol and MIC determination.

The microdilution assay evaluates the antimicrobial potency of agents by using serial dilutions to identify the lowest concentration needed to inhibit the growth of specific microorganisms (Figure 19). During incubation, growth occurs in wells with insufficient antimicrobial concentration to inhibit the microorganism. Microbial growth is quantified by measuring OD with a plate reader, as greater turbidity indicates higher OD values. The MIC is defined as the lowest concentration of the antimicrobial agent that will inhibit growth.

In this study, the microdilution assay was performed to assess the antimicrobial properties of the synthesised MTD compounds against *E. coli* and *S. aureus* to determine each compound's MIC. This data, presented in graphs (Figures 20 & 21) and tables (Tables 5 & 6), provides insight into the potential of each compound (JW1-JW11) as antimicrobial agents. The antimicrobial activity of the compound's precursor materials can be found in Table 6.

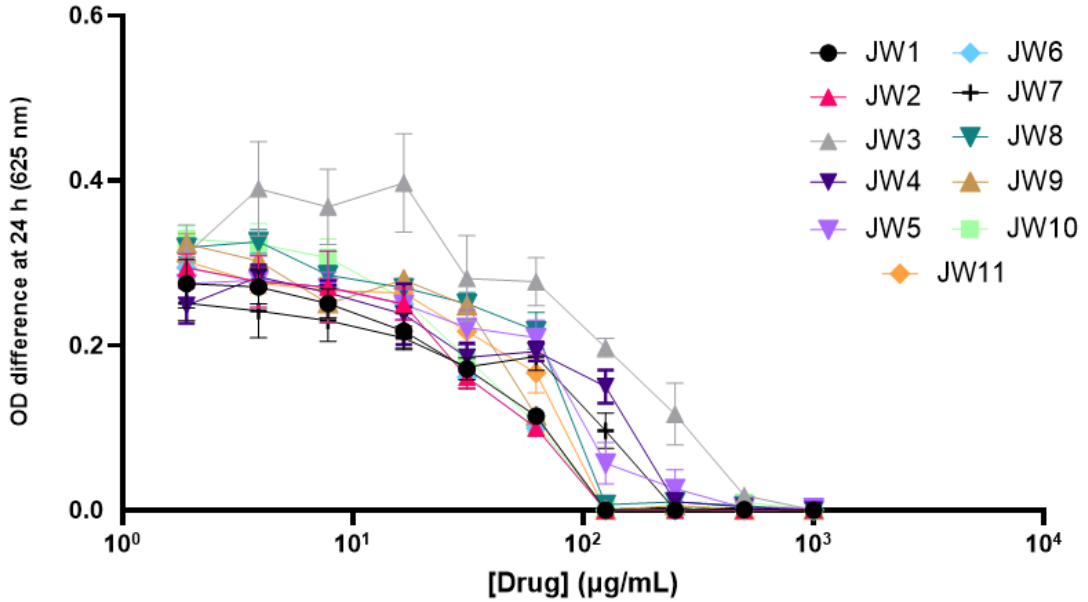

Figure 20 Microdilution assay. The dose-response curve of synthesised compounds (JW1-JW11) against E. coli over 24h at 37°c. Compound concentration ranged from 1.9-1000 µg/mL, and MIC was obtained as the lowest concentration to inhibit growth. OD difference of negative control MHB ranged from 1.0-1.2. Standard deviation (SD) represents the variation in the measurements of compound concentrations only, with a range from 0 to 0.05327 (n=3).

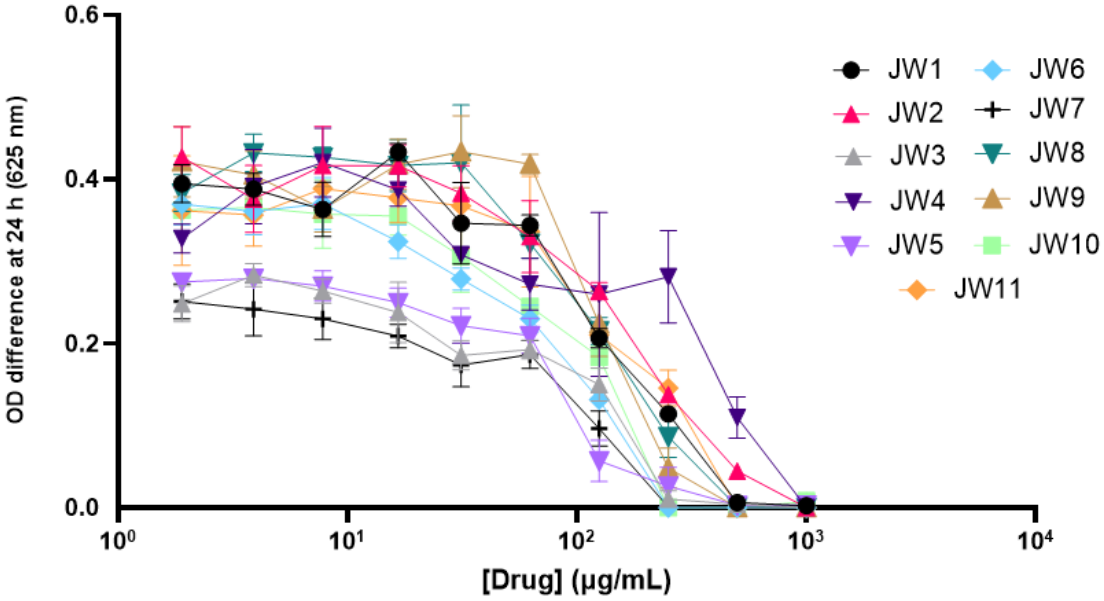

Figure 21 Microdilution assay. The dose-response curve of synthesised compounds (JW1-JW11) against S. aureus over 24h at 37°c. Compound concentration ranged from 1.9-1000 µg/mL, and MIC was obtained as the lowest concentration to inhibit growth. OD difference of negative control MHB ranged from 0.4-0.5. Standard deviation (SD) represents the variation in the measurements of compound concentrations only, with a range from 0 to 0.08919 (n=3).

The overall MIC values against *E. coli* ranged from 125-1000 µg/mL and 250-1000 µg/mL for *S. aureus*, showing a wide range in antimicrobial activity within the library. This suggests that the compound's structural additions substantially influence its ability and effectiveness against both bacterial strains. Compounds containing one (JW2) or two hydroxyl groups (JW3) (Figure 14) exhibited a higher MIC of 1000 µg/mL against *S. aureus*, suggesting that the hydroxyl groups had minimal effect on antimicrobial activity. This may be due to steric hindrance, which could impede the compound's ability to bind to its target sites [(84)]. In contrast, hydroxy and methoxy groups (Figure 14) in compounds JW6 and JW10 enhanced the antimicrobial activity, which can be seen by the low MIC of 250 µg/mL. Moreover, methoxy groups are known to increase lipophilicity in compounds, improving their ability to penetrate bacterial membranes, an ideal trait of effective antimicrobial agents [(48)]. Combining the two functional groups (-OH and -OCH_3) may also provide a synergistic effect, increasing the compound's hydrogen bonding and electron donation capacity [(49)].

The MIC of NPA was consistent with the MIC for some of the synthesised compounds, at 125 µg/mL against *E. coli* and 500µg/mL against *S. aureus*. This suggests that NPA upholds its antimicrobial activity after synthesis with the secondary parent compound. Therefore, it highlights using NPA as the compound's base, providing a stable scaffold with good antimicrobial properties for further modification and production of derivatives. This underscores the incorporation of NPA in all 11 synthesised compounds due to its potential as an effective antimicrobial agent and versatility between bacterial strains. A study investigating the potential of conjugating Naphthalimide with an AMP demonstrated that adding the Naphthalimide moiety reduced the MIC by half [(50)]. Although the AMP used in the study displayed considerably lower MIC than the JW compounds, likely due to its peptide composition or structure, the combination with Naphthalimide achieved enhanced antimicrobial activity, as seen in this study. The increased activity is likely attributed to Naphthalimide's membrane interactions and DNA intercalation, disrupting DNA replication and transcription, resulting in effectiveness against a broader range of pathogens [(50)].

Table 5 shows that JW1, JW2, JW6, and JW8-JW11 had MIC values of 125 µg/mL against *E. coli*, identical to NPA. This indicates that their modifications do not adversely affect the antimicrobial activity of the core NPA structure. Although these compounds feature a variety of structural differences on the phenyl ring (no substitutions, hydroxy groups, methoxy groups, and dimethyl amino groups) (Figure 14), they do not interfere with overall antimicrobial efficacy but rather improve (Table 5).

For instance, JW8 was synthesised from trans-cinnamaldehyde and NPA (Figure 14). Trans-cinnamaldehyde alone demonstrated some antimicrobial activity against *E. coli*, with a MIC of 250 µg/mL; however, it showed no effect on *S. aureus* (Table 6). Yet, the synthesis of JW8 effectively halved the MIC value against *E. coli* to 125 µg/mL (Table 5), substantially improving its effectiveness against *S. aureus* with a MIC of 500 µg/mL. This demonstrates that combining trans-cinnamaldehyde with NPA enhances the compound's ability to inhibit bacterial growth more effectively than trans-cinnamaldehyde alone.

Similarly, an enhancement in antimicrobial activity was observed with compounds JW9 and JW11. The starting materials for these compounds, 4-methoxycinnamaldehyde and 4-(dimethylamino)cinnamaldehyde (Figure 14), had MIC values against *E. coli* of 500 µg/mL and 1000 µg/mL, respectively. However, after their synthesis with NPA, the MIC values for JW9 and JW11 decreased to 125 µg/mL (Tables 5 and 6). This notable reduction indicates that pairing with NPA substantially boosts their antimicrobial efficacy. This was also the case for JW10, which was synthesised by combining NPA with coniferaldehyde. It showed an MIC of 500 µg/mL against *S. aureus*. After synthesis with NPA, the MIC decreased to 250 µg/mL, suggesting that adding NPA provided some benefit but not as much as observed with JW9 and 11 (Tables 5 and 6).

In contrast, JW4 (MIC of 1000 µg/mL) and JW5 (MIC of 500 µg/mL) demonstrated comparatively higher MIC values against *E. coli* compared to other sister compounds and NPA (MIC of 125 µg/mL). This may be due to the specific modifications present in JW4 and JW5 (i.e., bulky substituents/electron-withdrawing groups), potentially inhibiting the antimicrobial effectiveness of the core NPA structure. Supporting these observations, Neto et al. [(53)] reported a MIC of ≥1024 µg/mL against *S. aureus*, slightly higher than the concentration range used in this research. The authors further investigated the combination of benzaldehyde with the antibiotic Norfloxacin, which lowered the MIC of Norfloxacin from 287 µg/mL to 256 µg/mL, a slight improvement in antimicrobial activity. In contrast, NPA and benzaldehyde (JW1) synthesis improved the antimicrobial activity, reducing the MIC from >1000 µg/mL to 500 µg/mL.

A study by Friedman M et al. [(51)] researched the antimicrobial effectiveness of 35 benzaldehydes against various foodborne pathogens, including *E. coli*, evaluating the antibacterial activity of the compounds and the hydroxy and methoxy substitutes on the phenyl ring. Although this article used different investigative methods than that of this research project and results cannot be directly compared, the study highlighted the significance of the specific functional groups and their position. With findings that the addition of a methoxy group to the phenyl rings had no benefit to activity, this is further supported by the higher MIC of JW5 with the addition of one methoxy group and no hydroxy group resulted in a higher MIC of 500 µg/mL and in JW7 with the addition of two methoxy groups increased the MIC to 250 µg/mL suggesting that further addition decreased activity. The study also found that hydroxy and methoxy substitutions showed mixed impacts on antimicrobial activity. Compounds JW6 and JW10, which contain both substitutions, there was no further improvement in the MIC against *E. coli compared to NPA*, but the presence of these groups increased the MIC against *S. aureus* to 250 µg/mL, two times greater than that of the NPA base compound. In summary, although both studies used different approaches, the result showed the impact of the varying functional groups and their combination, supporting further optimisation and investigation into the compound's design.

Overall, the MIC data obtained demonstrated various antimicrobial activity from the library of MTD compounds. The base, NPA, used in the synthesis of all MTD compounds shows good potential as an antimicrobial agent; further modification and optimisation of the compounds could lead to increased activity using the

combination of functional groups, such as the presence of both hydroxyl and methoxy in JW6 and JW10, increasing the antimicrobial activity of NPA. Further studies will focus on the mechanism of action and investigation against several other sepsis-causing bacteria. The analysis highlights the importance of exploring the type and position of different structures and functional groups to guide further advancement in drug discovery of new antimicrobial agents.

Table 5 Comparative List of Compounds MIC against both E. coli and S. aureus

COMPOUND[1]	**MIC *E. coli* (µg/mL)**	**MIC *S. aureus* (µg/mL)**
JW1	125	500
JW2	125	1000
JW3	250	1000
JW4	1000	500
JW5	500	1000
JW6	125	250
JW7	250	1000
JW8	125	500
JW9	125	500
JW10	125	250
JW11	125	500
Gentamicin[2]	6.25	3.13

Table 6 Comparative List of Compounds Starting Material MIC against E. coli and S. aureus.

COMPOUND[3]	**MIC *E. coli* (µg/mL)**	**MIC *S. aureus* (µg/mL)**
NPA	125	500
Benzaldehyde	-	-
4-hydroxybenzaldehyde	-	-
3,4-dihydroxybenzaldehyde	-	-
3,4,5-trihydroxy benzaldehyde	-	-
4-anisaldehyde	-	-
Vanillin	-	-
Syringaldehyde	-	-
Trans Cinnamaldehyde	250	-
4-methoxycinnamaldehyde	500	-
Coniferaldehyde	-	500
4-(dimethylamino)cinnamaldehyde	1000	-

[1] Concentration range for JW compounds: 1.9-1000 *µg/mL*.
[2] Concentration range for Gentamicin: 0.2-100 *µg/mL*.
[3] Concentration range for parent compounds: 1.9-1000 *µg/mL*.

Gentamicin (aminoglycoside antibiotic) was chosen as the positive control for this study due to its broad activity against *E. coli*, *P. aeruginosa*, and *S. aureus*. Figure 22 shows the MIC determination for Gentamicin against *E. coli* at 6.25 µg/mL and *S. aureus* at 3.13 µg/mL. These MICs are considerably lower than the JW compounds, with the lowest MIC being 124 µg/mL and 250 µg/mL, respectively. Like other aminoglycosides, Gentamicin binds to RNA or 30s subunits in the cytoplasm of bacterial cells, disturbing mRNA translation and leading to non-functional protein formation. This compromises the permeability of the bacterial membrane. The JW compounds may act with a mechanism different from that of Gentamicin, or they do not contain the same level of antimicrobial activity as standard antibiotics [52]. The JW compounds are also in their initial stages of evaluation and modification; therefore, as the research progresses to improve on the current therapeutic potential.

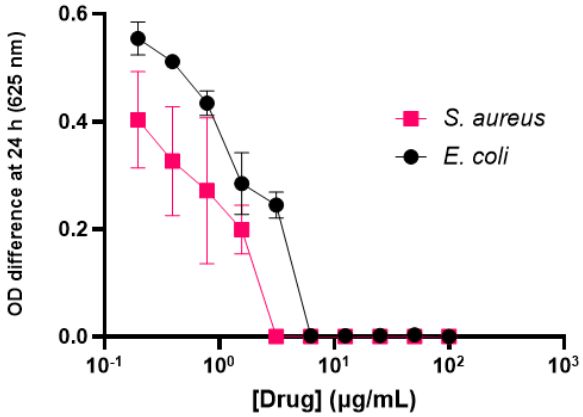

Figure 22 MIC determination for positive control and comparison of known antibiotic Gentamicin against E. coli and S. aureus. Concentration range for Gentamicin: 0.2-100 µg/mL. (n=3)

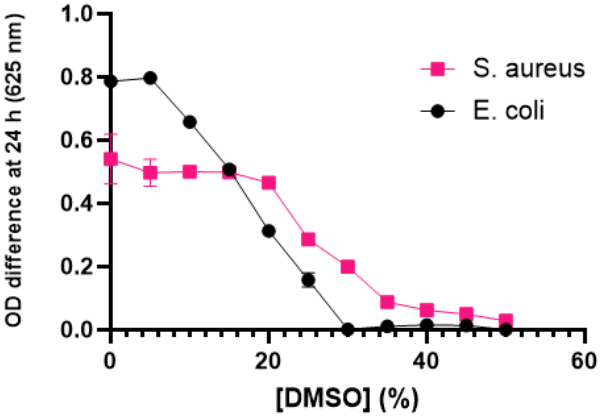

Figure 23 MIC determination for positive control and comparison of known solvent DMSO against E. coli and S. aureus. (n=3)

Figure 23 shows the MIC determination for DMSO, a widely used solvent in antimicrobial investigations due to its ability to dissolve both hydrophilic and hydrophobic compounds [73]. Many similar studies utilise DMSO as a solvent, such as Vafina, G. [72], investigate the antimicrobial and antifungal activity of Maleopimaric-Acid Derivatives. The MIC for DMSO against *E. coli* was 30%, and

S. aureus 35%; therefore, the use of DMSO as a solvent in the antimicrobial investigation had no impact on the activity of the compound as the compounds were dissolved in 10% DMSO, which is below the lowest concentration DMSO will inhibit the growth of either bacterial strain.

4.2.2 Resazurin Assay

The resazurin assay was used to investigate the viability of bacterial cells after exposure to a range of JW compounds at varying concentrations and to confirm the MIC. The resazurin dye (blue) is reduced to resorufin (pink) in the presence of metabolically active cells (Figure 24) [(44)]. Since antimicrobial compounds may be bactericidal (killing the bacteria) or bacteriostatic (inhibiting their growth), it is crucial to determine whether the cells are merely inhibited or dead [(74)]. Figure 25 shows images of the 96-well plates used in the assay with a range of compounds against tested bacteria. The first image shows JW3 against *E. coli*, and the first three rows show the blue resazurin for concentrations 1000, 500 and 250 µg/mL, confirming the MIC (Table 5); the plate also shows that after reaching the MIC, the resazurin dye is then reduced to resorufin, vivid pink colour. This shows that the bacteria within the pink wells are metabolically active. The reduction reaction of the assay is primarily due to mitochondrial reductases or NADP/NADPH, indicating that the cell is viable. In contrast, the blue wells show no active metabolism of the bacterial cells, resulting in no reduction in resazurin; the cells either have reduced metabolic activity or have been killed (bactericidal) [(44)].

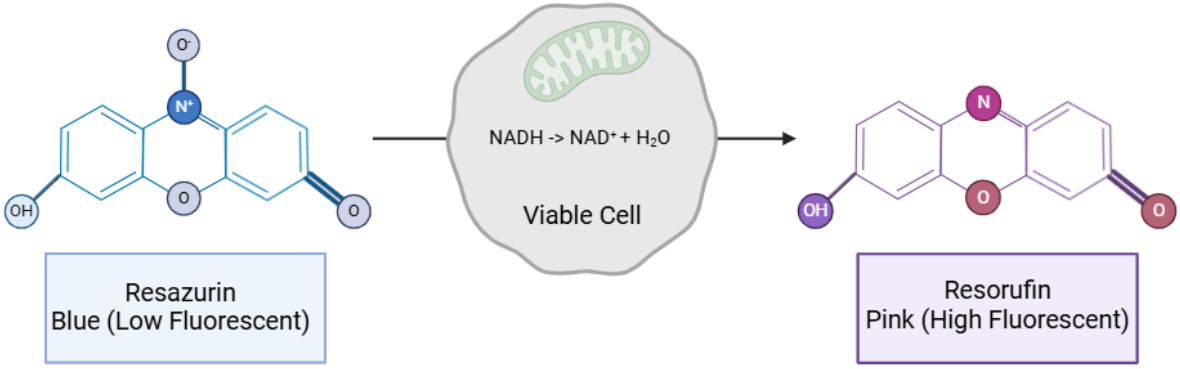

Figure 24 The principal reaction of the Resazurin assay. Showing the reduction of resazurin to resorufin [(44)].

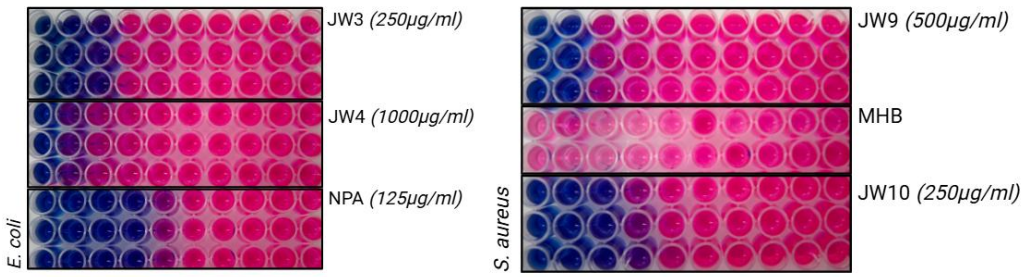

Figure 25 Images of resazurin assay for compounds JW3, JW4 and NPA against E. coli and JW9, JW10 and negative control MHB against S. aureus. Confirming MIC against E. coli: JW3 250 µg/mL, JW4 1000 µg/mL and NPA 125 µg/mL. Confirming MIC against S. aureus: JW9 500 µg/mL, JW10 250 µg/mL and control using MHB showing no antimicrobial activity.

4.2.3 Time-Kill Assay

The time-kill kinetics assay is a widely used technique that provides a dynamic assessment of antimicrobial activity against selected bacterial strains over a set period of time. In contrast with the 96-well plate method for MIC determination, the time-kill assay provides additional information into the rate and overall extent of the compound's antimicrobial properties at different concentrations. The assay can also determine whether the compounds are bacteriostatic (inhibits bacterial growth) or bactericidal (kills bacteria). Therefore, providing valuable information on the time and concentration required for antimicrobial activity is essential for optimising and developing clinical therapeutics. The theory of the assay is based on monitoring microbial growth after exposure to the test antimicrobial over a prolonged period. Samples are taken at multiple intervals and plated before incubating and counting colony-forming units (CFU). The CFU can then be plotted against time, and the interaction between the test antimicrobial and bacterial species can be observed [45].

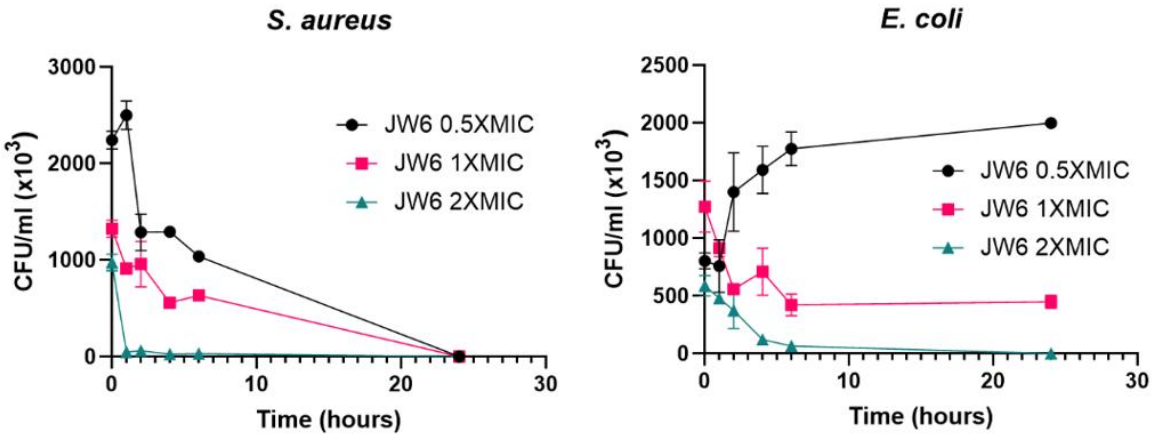

Figure 26 Time-kill plots for JW6 against both S. aureus (MIC 250 µg/mL) and E. coli (MIC 125 µg/mL) in MHB. The concentration range is 0.5, 1, and 2 x MIC; samples are collected at 0, 1, 2, 4, 6, and 24 hours. (n=3)

The time-dependent relationship between the compounds and bacteria was evaluated at 0.5x, 1x and 2x MIC concentrations. For compounds JW6 and JW10 against *E. coli*, 62.5 µg/mL, 125 µg/mL, and 250 µg/mL were employed and for *S. aureus*, 125 µg/mL, 250 µg/mL, and 500 µg/mL, respectively. Understanding the time/dose-dependent relationship is vital in a clinical setting to ensure the correct dosage is given to the patient, effectively wiping out the infection and minimising the risk of resistance.

Figure 26 shows the time-kill plot for JW6 against both evaluated bacterial strains. Against *S. aureus*, all concentrations resulted in no viable bacterial growth at 24 hours, with a rapid reduction in CFU with 2x MIC within 2 hours and slowly decreasing up to 24 hours. The 0.5x and 1x MIC show a similar trend: Within 2 hours, the CFU drops but is less effective than the higher 2x MIC dosage. This indicates that JW6 has strong antibacterial activity against *S. aureus*, killing the bacteria within 24 hours at low and high doses. Similar but less effective trends can be seen for JW6 against *E. coli,* where 1x and 2x MIC showed a significant reduction in CFU over time, but 1x MIC failed to wipe out

the infection within 24 hours. The 0.5x MIC dose showed slight inhibition within the first two hours. However, the antimicrobial activity at this concentration could not inhibit growth over a prolonged period, resulting in a substantially higher CFU reading. These results suggest that JW6 exhibits greater effectiveness against the Gram-positive *S. aureus* than the Gram-negative *E. coli*, potentially due to differences in bacterial cell wall structures or mechanisms like efflux pumps, which are more complex in *E. coli* and protect against antimicrobial agents [75].

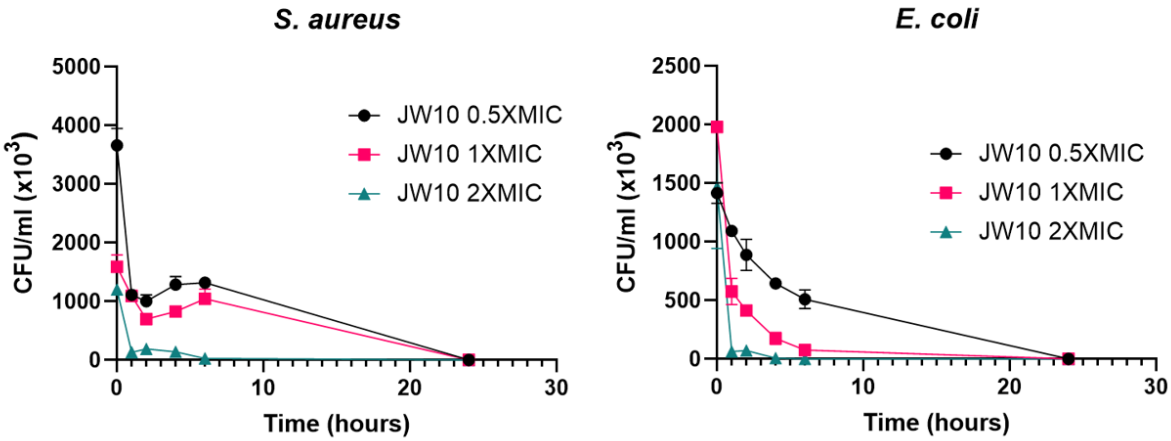

Figure 27 Time-kill plots for JW10 against both S. aureus (MIC 250 µg/mL) and E. coli (MIC 125 µg/mL) in MHB. The concentration range is 0.5, 1, and 2 x MIC; samples are collected at 0, 1, 2, 4, 6, and 24 hours. (n=3)

Time-kill plots for JW10 against both tested bacterial strains are shown in Figure 27. JW10 showed strong antibacterial activities against both strains, particularly *E. coli*, showing a sharp decline within 2 hours at 2x MIC dose before clearing the infection within 4 hours. The 1x and 0.5x MIC also showed good antimicrobial activity, resulting in no CFU present at 24 hours, with a continuous decline throughout. Against *S. aureus at* 2x MIC, JW10 showed strong activity with a rapid decrease from 0-2 hours before clearing the infection at 6 hours. The 1x and 2x MIC also showed good and similar activity, with 1x MIC showing slightly better inhibition, but both dosages resulted in no viable bacteria cells from growth at 24 hours.

Both compounds showed good inhibition against bacterial strains across all dosages, except for JW6 against *S. aureus* at a lower dose. This demonstrates the rapid and effective nature in which the compounds at low concentrations can kill the bacteria, preventing further growth. Additionally, this suggests that the compounds are bactericidal, meaning they kill rather than inhibit growth, as shown by the lack of viable cells to produce colonies in Figures 26 and 27.

The time-kill assay underscores the rapid and effective nature of compounds JW6 and JW10, demonstrating their ability to kill the bacteria at low concentrations and prevent further growth. The bactericidal nature of the compounds highlights their potential as therapeutics for combating bacterial infections, warranting further investigation into the mechanisms and optimisation of these compounds.

4.3 Antioxidant Investigations

Antioxidants help reduce inflammation by acting as free radical scavengers and reducing ROS. They can also inhibit the metabolic enzymes and factors involved in inflammation, protect against OS, reduce oxidative damage, and modulate proinflammatory gene expression. Phenolic compounds such as the proposed can interact with ROS and reactive nitrogen species (RNS), which prevents a chain reaction and protects cell viability. Oxidative stress is the imbalance of ROS, RNS, and antioxidants (Figure 28). ROS have a significant impact on immune cell dysfunction during sepsis. Free radicals, including anionic ($O_2^-$and OH^-) and non-ionic species (H_2O_2, HOCl, and NO.), significantly contribute to sepsis development [47]. Neutrophils and macrophages are key production sites of ROS. The body has built-in antioxidant defences to control ROS production; during sepsis, the overproduction of ROS overwhelms the defences, resulting in inflammation and cellular damage. In normal circumstances, ROS is successfully checked by the body's defences. NADPH oxidase can also generate ROS *via* phagocytosis, vital in defence against invading microbes. ROS also can modulate immune signals, contributing to the progression of sepsis and damage to tissues and organs [46].

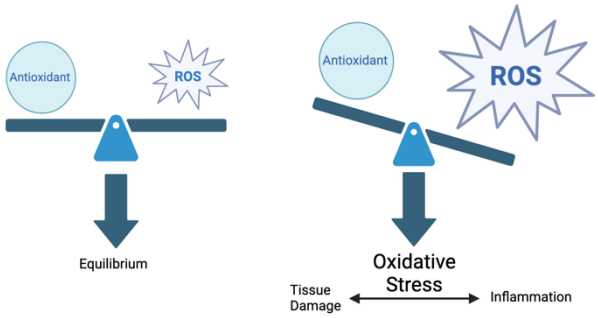

Figure 28 This diagram shows the unbalance of oxidative equilibrium, which leads to tissue damage and inflammation through excessive ROS production [46].

The MTD compounds' antioxidant potential and starting materials were evaluated using DPPH and FRAP assays. The DPPH assay assesses compounds' hydrogen-donating or single electron transfer capacity to neutralise DPPH free radicals, indicating free radical scavenging capability. The FRAP assay, on the other hand, measures the ability of compounds to reduce ferric (Fe^{3+}) to ferrous (Fe^{2+}) ions, reflecting electron donation potential [76]. Together, these assays comprehensively analyse the antioxidant mechanisms in early MTD development stages, offering insights into the effects of various structural modifications.

In vitro antioxidant testing further explores the single electron transfer (SET) and hydrogen atom transfer (HAT) mechanisms, which are influenced by structure, properties, and solubility factors. The SET mechanism, common in redox reactions, forms radical ions, while the HAT mechanism, often found in chain reactions like enzymatic processes, creates a new radical and a neutral molecule [38]. The combined use of DPPH and FRAP assays enables a thorough assessment of these mechanisms, facilitating a more complete evaluation of the antioxidant capacity of the compounds (Table 7).

Table 7 Overview of Antioxidant Investigations. Basic summary of DPPH and FRAP mechanisms and analysis.

Assay	Principle	Mechanism	Analysis
DPPH	Free radicals reduced in the presence of antioxidants	SET + HAT	Colourimetric
FRAP	Reduction reaction Fe (III) complex	SET	Colourimetric

DPPH is a colourimetric assay with the principle of a reduction reaction with free radicals based on HAT and SET mechanisms. The DPPH radical contains an unpaired valence electron on the nitrogen bridge (Figure 29), which is stable at room temperature. When adding antioxidants to the assay, they interact with the DPPH radicals, reducing and stabilising them. The reduction reaction in this process leads to a vivid colour change, shifting from purple to yellow/colourless solution. The colour change can then be measured using a UV/Vis spectrophotometer at 490 nm to obtain a reliable and straightforward assessment of the sample's antioxidant capacity [38].

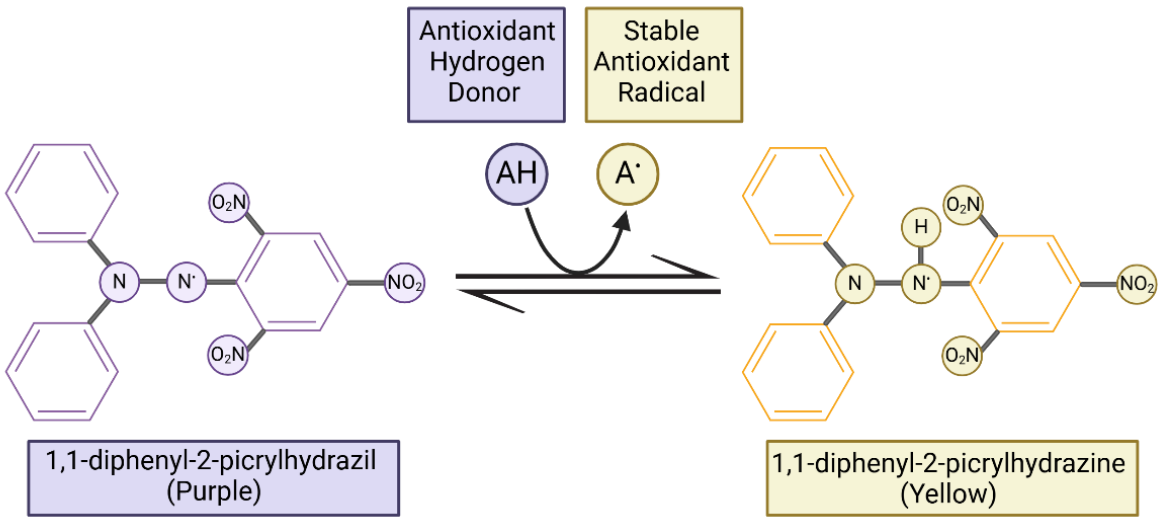

Figure 29 Reduction Reaction Scheme of DPPH radical [38].

In the DPPH assay, the results are presented as the IC_{50} (Half Maximal Inhibitory Concentration), which represents the concentration of an antioxidant required to inhibit 50% of DPPH radical activity. The IC_{50} is calculated by isolating and plotting 3 points which overlap with 50% absorbance. The equation of the line is then used to determine IC_{50} [77]. An example can be found in Figure 30.

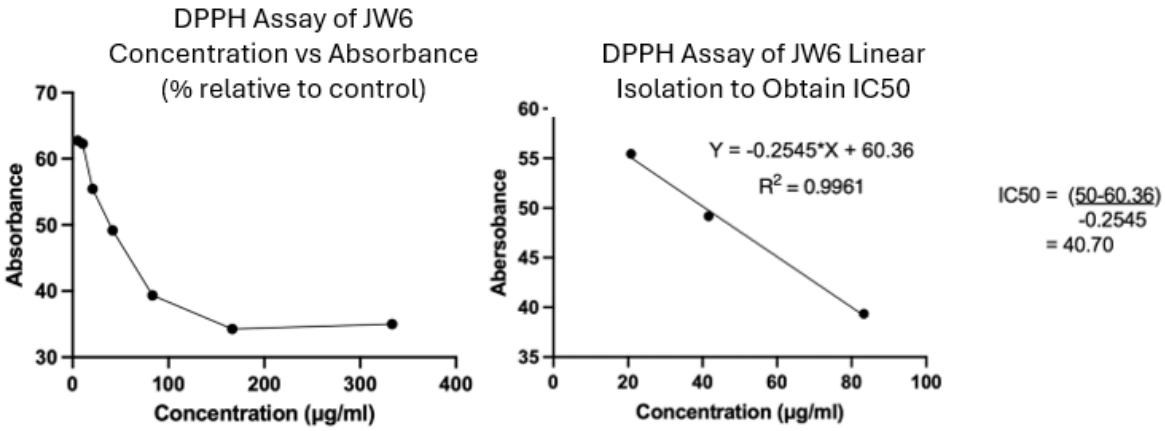

Figure 30 Example of IC_{50} determination of JW6 in the DPPH Assay: Plot and Calculations.

The ferric ion-reducing antioxidant power (FRAP) is based on the antioxidant compound's ability to reduce ferric ions (Fe^{3+}) to the ferrous ions (Fe^{2+}) via the SET mechanism under acidic conditions (Figure 31). The reaction occurs when the antioxidant sample donates an electron to the ferric ion, forming a coloured ferrous complex (ferric tripyridyltriazine (Fe^{3+}-TPTZ)). The complex is then reduced to ferrous tripyridyltriazine (Fe^{2+}-TPTZ), resulting in a vivid blue colour [38]. FRAP is also a colourimetric assay, and the colour change is measured using a spectrophotometer at 595 nm. The greater the blue intensity, the greater the antioxidant sample. This assay provides a rapid and reliable assessment and can be used on various potential antioxidants.

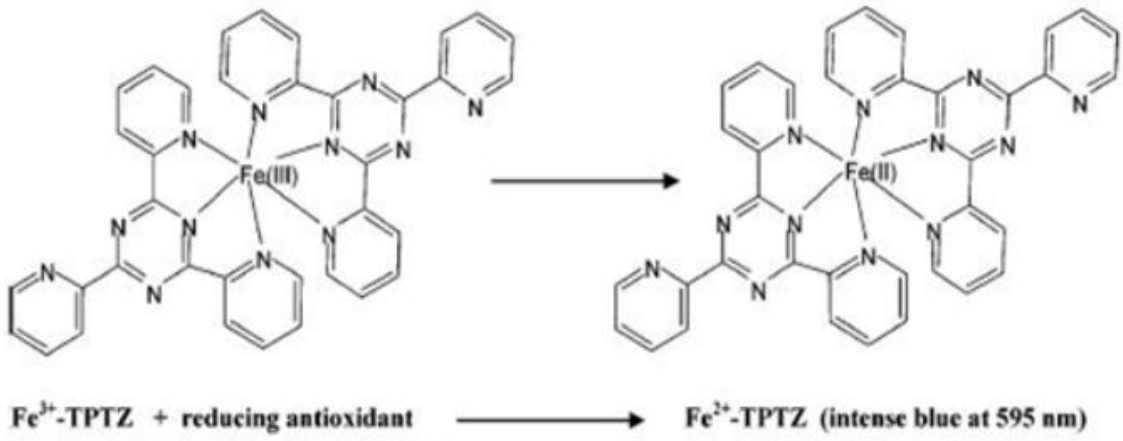

Figure 31 The chemical reaction of the FRAP assay [94]

In the FRAP assay, the results are presented as TE, which is the sample's antioxidant capacity compared to the standard Trolox. All antioxidant data is in Table 8, allowing for a comparison of each compound across both assays.
To compare the results, the slope of the antioxidant sample curve is divided by the slope of the Trolox curve; if TE > 1, the antioxidant sample is stronger than Trolox, as shown in Figure 32.

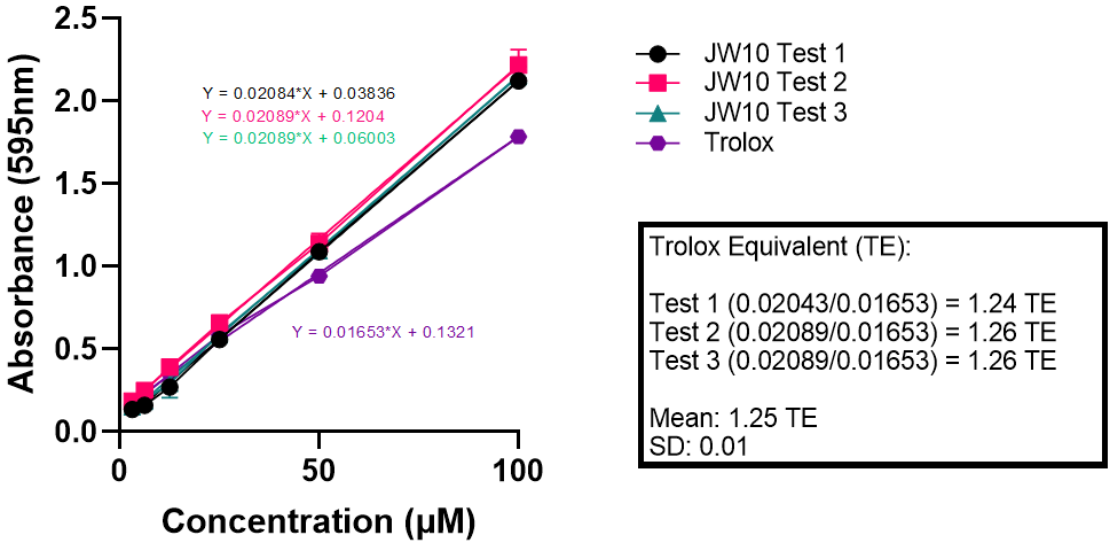

Figure 32 Example of FRAP Assay - Trolox calibration curve and sample curve of JW10 with calculations for TE.

Table 8 Antioxidant Investigations of the JW compounds in the DPPH assay, shown as IC_{50}, and in the FRAP assay, shown as TE. (n=3)

Compound	DPPH (IC_{50} µM) (Mean ± SD)	FRAP (TE) (Mean ± SD)
JW1	>100	0.0009 ± 0.001
JW2	>100	0.01 ± 0.005
JW3	>100	2.34 ± 0.03
JW4	>100	2.29 ± 0.06
JW5	>100	0.60 ± 0.05
JW6	40.70 ± 5.9	0.2 ± 0.07
JW7	54.87 ± 1.0	0.94 ± 0.002
JW8	>100	0.01 ± 0.008
JW9	>100	0.002 ± 0.002
JW10	38.90 ± 0.24	1.25 ± 0.01
JW11	>100	0.59 ± 0.06
Gallic Acid	61.81 ± 0.49	2.9 ± 0.1

Table 9 T-test analysis of antioxidant investigation against known antioxidant gallic acid.

***T- TEST* (*p*-value)**	**DPPH *(p < 0.05)***	**FRAP *(p < 0.05)***
JW1	X	0.0004
JW2	X	0.0004
JW3	X	0.0067
JW4	X	0.0018
JW5	X	<0.0001
JW6	0.0312	<0.0001
JW7	0.0026	0.0009
JW8	X	0.0004
JW9	X	0.0004
JW10	<0.0001	0.0011
JW11	X	<0.0001

The results obtained from the DPPH and FRAP assays provide valuable information on the antioxidant properties of the JW compounds compared to the reference standard gallic acid. The DPPH assay measures the compound's ability to scavenge free radicals (SET & HAT mechanisms). Compounds JW1-5, JW8, JW9 and JW11 all exhibited IC_{50} values greater than 100 µM, indicating low free radical scavenging activity (Table 8). In contrast, compounds JW6, JW7 and JW10 showed notably lower IC_{50} values of 40.70 ± 5.9 µM, 54.87 ± 1.0 µM and 38.90 ± 0.24 µM, respectively (Table 8). These compounds have good activity for neutralising the DPPH radicals; therefore, they have good antioxidant activity within this investigation, particularly JW10, compared to Gallic acid, a well-known antioxidant with an IC_{50} of 61.81 ± 0.49 µM (Table 8). This suggests that the presence of both hydroxy and methoxy groups is essential for effective free radical scavenging activity, as all three compounds (JW6, JW7, and JW10) contain these functional groups.

The FRAP assay evaluates the compound's electron donation (SET mechanism). Of the compounds that showed promising activity in the DPPH assay (JW6, 7 & 10), only JW10 showed a relatively strong reducing capacity in the FRAP assay with a TE of 1.25 ± 0.01. In contrast to the DPPH assay, all compounds showed activity. Compounds JW1, 2, 6, 8 and 9 showed considerably lower TE of below 0.5; compounds JW5, 7 and 11 showed slightly higher TE of 0.5-1.0, and compounds JW3 and JW4 showed the strongest activity of TE 2.34 ± 0.03 and 2.29 ± 0.06 respectively. The strong activity of JW3 and JW4 is likely due to the presence of two hydroxy and three hydroxy groups on the phenyl ring, increasing the compound's electron donation ability (Table 8).

As previously mentioned, both assays employ different mechanisms. DPPH primarily assesses HAT mechanisms, whereas FRAP employs SET [38]. This shows that most compounds have antioxidant activity in the SET mechanism, excluding JW6, 7, and 10, which show activity throughout both antioxidant mechanisms. Similar results were obtained from Blaikie et al, [33], which investigated the antioxidant potential of naphthalimide-based compounds linked with vanillin

(similar structurally to JW6, Figure 14). The studied compounds showed activity of 1a 62.00 ± 5.06 IC_{50} (µM), 0.26 ± 0.02 TE, 1b 70.00 ± 2.64 IC_{50} (µM) 0.34 ± 0.01 TE and Vanillin 7915.00 ± 24.00 IC_{50} (µM) 0.02 ± 0.01 TE [33]. These compounds exhibit strong activity in comparison to their parent compound, vanillin. Compared to the compound used in this study, JW6, 7 and 10 all exhibited stronger activity in the DPPH assay and similar results in the FRAP assay. Compounds 1a and 1b were synthesised and evaluated for the potential as MTD therapeutics for Alzheimer's; this competitive analysis underscores the potential for the JW compounds as they continue to be evaluated and optimised.

The *p-values* from the T-test indicate the statistical significance of the compound's effect on DPPH and FRAP assay results compared to control gallic acid. Table 9 highlights the significant p-values and shows which groups exhibit statistically significant antioxidant activity, offering insight into the compound's efficacy in both assays. The strong antioxidant properties of the JW compounds, particularly JW 6 and 10's free radical scavenging ability, coupled with their strong antimicrobial activity and JW3 and 4's neutralisation *via* electron transfer, reinforce their potential as potential MTD therapeutics for sepsis. The compounds could potentially neutralise ROS and restore the antioxidant balance during sepsis, reducing further damage to tissue and organs.

Table 10 displays the antioxidant investigation for the parent compounds of the JW compounds. In the DPPH assay, the synthesis of compounds 3,4-dihydroxybenzaldehyde with NPA (JW3) and 3,4,5-trihydroxybenzaldehyde with NPA (JW4) decreased the parent compounds antioxidant potential considerably, suggesting that the synthesis of JW3 and 4 showed no synergy and caused a disturbance in the compound’s mechanism. In contrast, the synthesis of NPA with vanillin (JW6), syringaldehyde (JW7) and coniferaldehyde (JW10) increased the parent compounds’ free radical scavenging activity considerably, similar to the impact seen in the Vanillin based study [33]. The FRAP assay had varied advantages and disadvantages after synthesis with NPA. Benzaldehyde (JW1), 4-hydroxybenzaldehyde (JW2), vanillin (JW6) and 4-methoxycinnamaldehyde (JW9) all had decreased antioxidant activity. Whereas 3,4,5-trihydroxybenzaldehyde (JW4), 4-anisaldehyde (JW5), trans cinnamaldehyde (JW8), coniferaldehyde (JW10), and 4-(dimethylamino)cinnamaldehyde (JW11) had increased antioxidant activity. There is no clear correlation between the decrease or increase in activity, so further investigations are required to assess the changes in activity. NPA showed little to no antioxidant activity across both investigations, suggesting that it plays a synergistic and hindering role in the compound's activity. However, due to its strong antimicrobial properties, it is still necessary for the potential MTD.

Table 10 Antioxidant Investigations of the JW compounds' parent compounds are shown as IC_{50} in the DPPH assay and as TE in the FRAP assay. (n=3)

Compound	DPPH (IC_{50} µM) (Mean ± SD)	FRAP (TE) (Mean ± SD)
Benzaldehyde	>100	2.76 ± 0.06
4-hydroxybenzaldehyde	>100	2.72 ± 0.55
3,4-dihydroxybenzaldehyde	50.41 ± 2.83	1.72 ± 0.02
3,4,5-trihydroxy benzaldehyde	55 ± 3.2	-
4-anisaldehyde	>100	-
Vanillin	>100	1.55 ± 0.77
Syringaldehyde	>100	0.13 ± 0.01
Trans Cinnamaldehyde	>100	-
4-methoxycinnamaldehyde	>100	0.02 ± 0.61
Coniferaldehyde	>100	1.14 ± 0.62
4-(dimethylamino)cinnamaldehyde	>100	0.01 ± 0.01
NPA	>100	0.01 ± 0

4.4 Clot Lysis Investigation

One of the critical complications associated with sepsis is the disruption of normal blood coagulation processes. During sepsis, the overactivation of the immune system can cause an imbalance between pro-coagulant and anti-coagulant factors, leading to excessive clot formation or DIC (Figure 1). This abnormal clotting impairs blood flow to vital organs, contributing to MODS and increasing mortality risk. DIC is a common development in sepsis when widespread clotting in the patient's blood vessels occurs, leading to ischemia and organ failure that is followed by excessive fibrinolysis, and this can then lead to severe bleeding [13].

The role of the clot lysis assay in the research is to evaluate the anticoagulant and pro-fibrinolytic activity of the novel compounds. This will determine whether the novel compounds' fibrinolytic properties would be beneficial in treating sepsis. Compounds that possess this ability may prevent the microvascular thrombosis that is associated with DIC, serving potential therapeutic benefits such as reducing organ failure and severe bleeding while improving patient survival rates.

The clot lysis assay allows for an evaluation of fibrin formation and potential breakdown. There are many versions of this assay, but all have similar procedures, where plasma is mixed with a coagulation activator (thrombin or tissue factor), calcium, and phospholipids to prompt clot lysis. As the fibrin clot is formed, the turbidity of the sample increases and, in turn, decreases as the clot is lysed in the 96-well plate. Absorbance is measured continuously after adding the activator mix over a chosen time (4 hours). A clot-lysis curve is then produced, and from this, the initial fibrin formation, maximum absorbance, and 50% lysis time can be obtained [40].

The activation mix is produced by combining thrombin and calcium chloride ($CaCl_2$). Thrombin, an enzyme, can convert fibrinogen to fibrin, resulting in clot formation. In the assay, thrombin initiates and activates the plasma, initiating the in vivo clotting process. $CaCl_2$ is used as part of the activation mix to enable the clotting process by activating clotting factors. The calcium ions are essential cofactors for many enzymes in the clotting cascade. Therefore, the activation mix is crucial for the clotting cascade initiation, with both components working together to trigger clot formation [40].

Each reagent in the assay is chosen for its specific role in the replication of the clot formation and breakdown (fibrinolysis) process. TBST Buffer (10 mM TRIS, 140 mM NaCl, 0.01% Tween20, pH 7.4) is employed in the assay to maintain pH and ionic strength and reduce non-specific protein interactions. The phospholipids substitute the cell membrane surface required to build the clot complex, thereby enhancing the clot formation process and providing a surface for enzymatic reactions in the clotting cascade. Finally, tissue plasminogen activator (tPA), a serine protease, converts plasminogen to plasmin, a type of enzyme responsible for fibrin clot lysis. Adding tPA initiates fibrinolysis, allowing the clot breakdown to be measured over time [40].

Figure 33 demonstrates the assay process: the absorbance increases as the clot is formed before reaching the maximum absorbance, at which point clot lysis is initiated. The assay controls provide essential context for interpretation, where the buffer serves as a negative control baseline; the absorbance for the plasma-only control initially increases as the clot forms and remains as the clot stabilizes, mimicking natural clotting behaviour. Similarly, the plasma and phospholipid control follow the same trend. However, adding the phospholipids provides a surface for platelet adhesion and activation and enhances the clot formation, resulting in a greater max absorbance and overall clotting time. The final control contains plasma, phospholipids, and tPA, which stimulate the clot lysis process. Therefore, the absorbance increases as the clot is formed and decreases due to its breakdown.

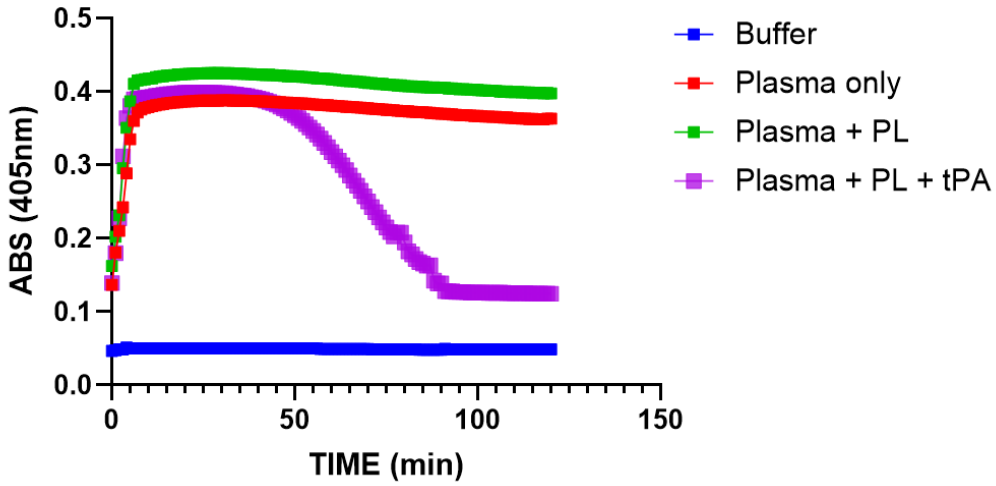

Figure 33 Clot Lysis plot showing absorbance at 405 nm for assay controls.

The 50% lysis time is calculated by normalising the absorbance for each sample independently to percentages, then highlighting the first time each sample fell below 50% and noting the time this occurred (minutes). The 50% lysis time for each sample and replicate was plotted in a scatter graph (Figure 34).

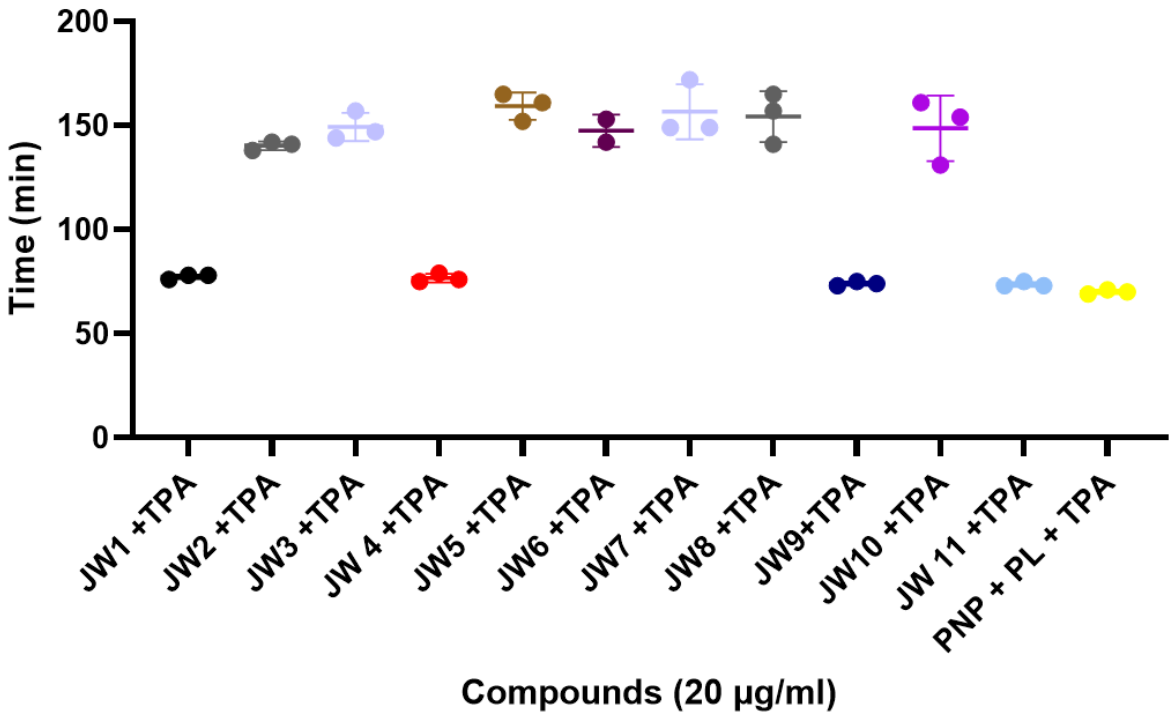

Figure 34 50% Clot Lysis Time of Synthesised Compounds at 20 µg/mL Concentration. This figure shows the time required for each compound to achieve 50% clot lysis, highlighting statistically significant differences ($p < 0.05$) in anticoagulant activity compared to the control group (PNP + PL + tPA), as determined by an unpaired t-test (Table 11). (n=3)

Table 11 Unpaired t-test for 50% clot lysis statistical analysis.

Comparison of Clot Lysis Times and Statistical Significance for Various Compounds (T-Test)											
JW Compounds	1	2	3	4	5	6	7	8	9	10	11
***p*-value**	0.0012	<0.0001	0.002	0.017	0.0015	<0.0001	0.0075	0.0066	0.008	0.0127	0.0148

Figure 34 demonstrates the 50% clot lysis times of JW compounds in the presence of tPA at a concentration of 20 µg/mL. Showing a range of responses indicating how the different compounds influence the clot lysis process, which is vital in understanding their anticoagulant properties.

JW1, 4, 9, and 11 show considerably lower 50% clot lysis times (Figure 34). The control sample for the assay containing plasma, phospholipids and tPA had the lowest 50% lysis time, but these showed similar abilities (Figure 34). The remaining compounds had 50% clot lysis times of around 150 minutes. This indicates that these compounds have a comparatively lower ability to break down clots, leading to a longer degradation period. It is also possible that these compounds delay clot degradation and compete with tPA to stabilise the clot rather than initiate degradation [78]. Further investigation into the mechanisms of action and thrombotic activity of the compounds is required to fully assess the

coagulant nature of the compounds. Overall, the 50% clot lysis time analysis and the significant *p*-value analysis (Table 11) provide a good framework for the initial investigation into these compounds as potential MTD therapeutics. While some of the compounds suggest undesired prothrombotic activity due to their prolonged clot lysis times, this characteristic could be useful in other therapeutic contexts, such as haemostatic agents or in conditions where slower clot breakdown is beneficial [79].

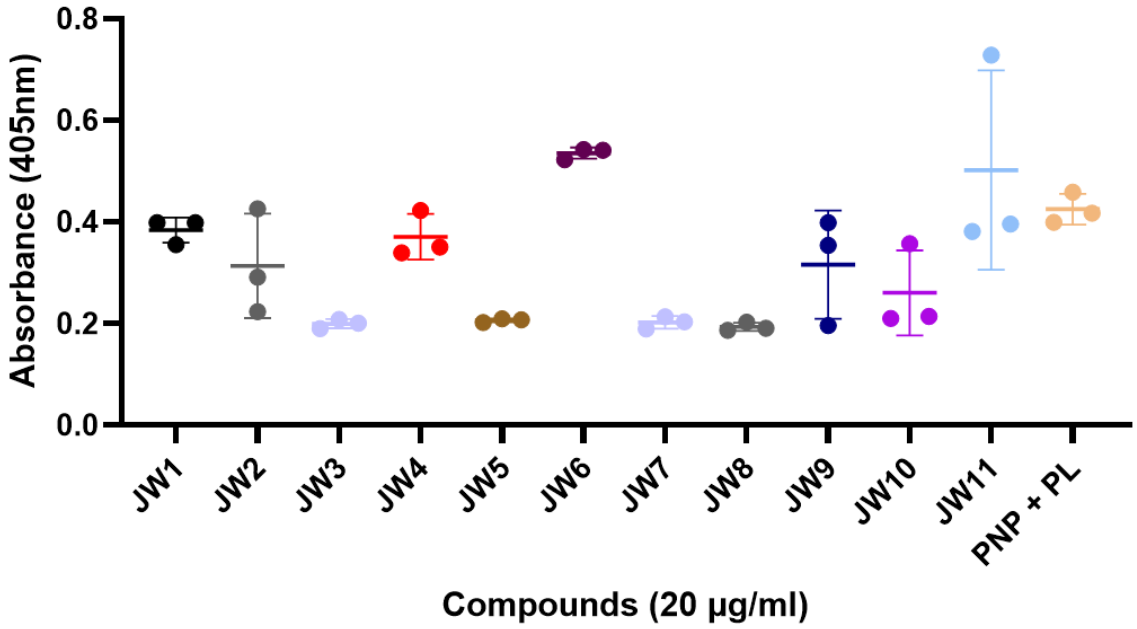

Figure 35 Presents the maximum absorbance readings at 405 nm for the JW compounds in the context of clot formation and lysis. The control PNP + PL mimics normal clot formation, with a maximum absorbance of 0.4. (n=3)

The maximum absorbance (Figure 35) measures peak clot formation size and density. It is calculated by normalising the absorbance for each sample independently to percentages. Highlighting the first time each sample was equal to 100% and returning to the raw data to collect the absorbance. The lower maximum absorbance of JW3, 5, 7, and 8 indicates that clot formation has been reduced and the coagulation process has been inhibited; this can also be seen in JW1, 2, 4 and 9-11, where the maximum absorbance is reduced slightly in comparison to the control, although it is not as effective. In contrast, JW6 showed a much higher maximum absorbance greater than its sister compounds. The high maximum absorbance and a higher 50% lysis further reinforced the potential of prothrombotic activity where the compound increases clot formation and stability rather than decreasing size and promoting lysis.

The range of functional groups within the library showed increased and decreased activity within the clot lysis assay. Compounds with no additional groups of the aldehyde rings JW1 and JW8 showed differing activity; JW1, with the incorporation of one double bond within the compound, had a lower 50% lysis time but a greater maximum absorbance compared to JW8 with two double bonds, which showed a greater 50% lysis time and low maximum absorbance. Compounds JW2, with one hydroxyl group and JW3, with two hydroxyl groups,

showed a higher 50% lysis time compared to JW4, which contains three hydroxyl groups, indicating that the larger compound with three hydroxyl groups, increased the compound's ability to lyse the clot. The hydroxyl-only compounds showed moderate activity in reducing clot formation, with JW3 showing greater activity, producing a smaller, less dense clot. Compounds JW5 and JW9 contain a methoxy group (Figure 14). Both compounds showed reduced max absorbance, producing a smaller clot, but the additional double bond in JW9 may increase the compound's reactivity, resulting in a lower 50% lysis time. Compounds JW6 and JW10 showed a higher 50% lysis time; however, they show considerable differences in maximum absorbance. JW6 resulted in the highest absorbance (Figure 34) within the JW compounds investigated, coupled with the extended clot lysis time, suggesting that this compound promotes clot formation and stability rather than reducing and lysing the clot. In contrast, JW10, the analogue of JW6 with the addition of a double bond, showed good activity in reducing clot formation (Figure 35); the extended lysis time is possible due to the compounds hindering/competing with tPA to lyse the clot. JW7 is one of the library's largest compounds, with two methoxy groups and one hydroxy group (Figure 14). It showed similar activity to JW3 (two hydroxyl groups) and JW5 (one methoxy group), suggesting that combining multiple functional groups had no beneficial or negative impact on the compound's activity, providing no additional synergistic effects. JW11 differs from the other compounds by having a dimethyl amino group. It showed moderate maximum absorbance and a good clot lysis time. The dimethyl amino group may contribute to a balance between clot formation and lysis. This is possible due to the compound’s electron donation and hydrogen bonding potential. Overall, compounds JW4 and JW9 showed promising activity within both assay analyses but require further analysis to determine the extent and mechanism of this activity.

A study explored the efficacy of a single-site mutant (M5) of pro-urokinase (pro-UK) combined with tPA in promoting thrombosis. ProUK is an inactive precursor urokinase (UK), an enzyme crucial for the fibrinolytic pathway [(54)]. The study resulted in clot lysis times of 55 minutes for tPA and 48 minutes for M5. When combined at a lower dosage, the clot lysis time was reduced to a mean of 47 minutes [(54)]. In comparison, the JW compounds 1, 4, 9 and 11 showed 50% lysis times of around 70-80 minutes; while this result is slightly higher than that of the mentioned study, it suggested the JW compounds still show therapeutic potential and with further optimisation and investigation the compounds anticoagulant ability may improve to competitive times. The study also emphasised the synergy effects of combining low doses; in future work, evaluating the combination of these drugs could improve overall activity [(54)].

5. Next Steps and Future Work

Regarding the synthesis aspect of this research, the next steps would include exploring the structural substitutions and their position, building on the initial work carried out, and creating a larger database for potential MTD compounds. This would allow for a larger and wider range of potential compounds, gathering information on the existing promising compounds, such as the combination of hydroxy and methoxy groups or the addition of a secondary aldehyde to the compound, allowing for a larger range of activity as seen in [33] where the newly synthesised compound with its naphthalimide base was synthesised incorporating two vanillin aldehydes (compound 2a) showed over 3-fold higher activity in DPPH assay compound to the mono vanillin compound (1a and 1b). Currently, the JW compounds are hydrophobic; therefore, converting them into salts to increase their solubility and stability may aid in their handling and allow for a wider range of investigations to be conducted at higher concentrations. However, [55] reported that quaternary salts showed reduced activity and that the electron pair within the studied compounds was vital for activity. This study also reported that the key to increasing antioxidant activity was linked to increasing the number of vanillin moieties in the compound. Further optimisation of the compounds may be supported with *In Silico* methods, therefore screening a larger range of potential modifications and improving the compound's activity regarding antimicrobial, anti-inflammatory and anticoagulant targets in sepsis.

Future work will also include further mechanisms of action studies to investigate how the JW compounds inhibit or kill bacteria in antimicrobial investigations, such as membrane permeability assays using propidium iodine dye [56]. Membrane-targeting antimicrobials are particularly beneficial as they reduce the risk of resistance developing; instead of interacting with the bacterial components, the compounds compromise the structure of the bacterial cell, leading to lysis and death. Scanning electron microscope (SEM) could also be used to elucidate the compound's antimicrobial mechanism of action by visually assessing the effect of the JW compounds on bacterial cell morphology, revealing any structural damage or leakage [57].

For the antioxidant mechanisms of the compounds, further investigations, such as the oxygen radical absorbance capacity (ORAC) assay, to assay the compounds to protect fluorescein from oxidative degradation by peroxyl radicals via the HAT mechanism [58].

Several assays could explore the anticoagulant mechanism, showing the compound's impact on the various coagulation pathways. For example, Activated Partial Thromboplastin Time (aPTT) and Prothrombin Time (PT) assays measure the time taken for a clot to form under certain conditions of the intrinsic and extrinsic coagulation pathways to identify further if the compounds prevent clot formation. Other assays include Thrombin Time (TT), to look at the conversion from fibrinogen to fibrin and factor-specific assay to determine if the JW compounds inhibit coagulation factors such as Factor Xa to inhibit clot formation [59]. These mechanistic studies will provide a comprehensive insight into how the JW compounds exert their proven activity.

The toxicity of the JW compounds will also be investigated on RAW macrophage cells lines, using the MTT (3-[4,5-dimethylthiazol-2-yl]-2,5 diphenyl tetrazolium

bromide) assay to confirm the compounds' toxicity and cell viability post-exposure [60]. As the research is developing an MTD designed for sepsis, this cell or related line would be the most beneficial choice. Macrophages are cells that play a role in initiating and regulating the natural immune response. During sepsis, the production of macrophages increases, which in turn increases ROS production, mimicking on a small scale the processes of sepsis [61].

6. Conclusion

Sepsis is a complex and multifaceted condition, with increasing mortality rates partly due to the rise in AMR and lack of specific treatments. The development of the proposed MTD is a promising advancement and strategy to address the challenges of the condition, including the antimicrobial, antioxidant, and anticoagulant aspects. The JW compounds evaluated in this research show promising activity in all areas for MTD candidates. Most of the compounds showed strong antimicrobial activity with JW6 and JW7 as lead compounds, providing a synergistic effect with incorporating NPA, showing a MIC of 125 µg/mL against *E. coli* and 250 µg/mL against *S. aureus.* These two compounds also exhibited strong antioxidant activity, particularly with the HAT mechanism reinforcing their potential not only as antimicrobial agents but also with potential anti-inflammatory properties by neutralising ROS and restoring the antioxidant balance disrupted in sepsis.

Although the lead compounds JW6 and JW10 showed promising antimicrobial and antioxidant activity, they did not show good activity within the clot lysis assay, with JW6 indicating prothrombic activity and JW10 showing moderate fibrinolytic activity, with reduced clot formation and a 50% lysis time of ~150 minutes. Compounds like JW11 showed a greater fibrinolytic ability, reducing the 50% clotting time to ~70 minutes and reducing clot density. As mentioned above, further investigation into the anticoagulant abilities of the compounds is required to fully assess and understand the mechanisms and potential of their activity.

In conclusion, the initial evaluation of these compounds shows potential. However, further optimisation and investigation are required to understand how the compounds function through the mechanism of action studies and whether they show toxicity towards animal cell lines for a more comprehensive analysis. The ongoing analysis will contribute to advancing the MTD approach for sepsis by potentially offering a combined synergistic therapeutic to a life-threatening condition, improving patient outcomes.

7. Acknowledgements

I want to thank my supervisors at Robert Gordon University, Dr. Aakash Welgamage Don, Professor Paul Kong Thoo Lin, and Dr. Graeme Kay, for their guidance, encouragement, and feedback throughout this research project.

I would also like to thank the RGU technical and support staff for their assistance in the laboratories.

Unless stated, all figures and graphs were produced using GraphPad Prism and Biorender software.

8. References

1. Arora J, Mendelson AA, Fox-Robichaud A. Sepsis: Network Pathophysiology and Implications for Early Diagnosis. American Journal of Physiology-Regulatory, Integrative and Comparative Physiology [Internet]. 2023 May 1 [cited 2024 Aug 29];324(5): R613–24. Available from: https://journals.physiology.org/doi/full/10.1152/ajpregu.00003.2023

2. McMullan RR, McAuley DF, O'Kane CM, Silversides JA. Vascular Leak in sepsis: Physiological Basis and Potential Therapeutic Advances. Critical Care. 2024 Mar 23;28(1).

3. Abdulkhaleq LA, Assi MA, Abdullah R, Zamri-Saad M, Taufiq-Yap YH, Hezmee MNM. The Crucial Roles of Inflammatory Mediators in inflammation: a Review. Veterinary World [Internet]. 2018 May [cited 2024 Sep 30];11(5):627–35. Available from: https://www.ncbi.nlm.nih.gov/pmc/articles/PMC5993766/

4. Singer M, Deutschman CS, Seymour CW. The Third International Consensus Definitions for Sepsis and Septic Shock (Sepsis-3). The Third International Consensus Definitions for Sepsis and Septic Shock (Sepsis-3) [Internet]. 2016 Feb 23 [cited 2023 Nov 13];315(8):801–10. Available from: https://www.ncbi.nlm.nih.gov/pmc/articles/PMC4968574/

5. The UK Sepsis Trust. References and Sources | Sepsis Statistics [Internet]. The UK Sepsis Trust. [cited 2023 Nov 1]. Available from: https://sepsistrust.org/about/about-sepsis/references-and-sources/#:~:text=Up%20to%2048%2C000%20deaths%20in%20the%20UK%20every%20year&text=The%20IHME%20study%20again%20corroborated

6. Jarczak D, Kluge S, Nierhaus A. Sepsis—Pathophysiology and Therapeutic Concepts. Frontiers in Medicine [Internet]. 2021 [cited 2024 Sep 30];8(1):1–22. Available from: https://www.frontiersin.org/articles/10.3389/fmed.2021.628302/full

7. CDC. What is Sepsis? [Internet]. Centres for Disease Control and Prevention. 2023 [cited 2024 Apr 23]. Available from: https://www.cdc.gov/sepsis/what-is-sepsis.html#:~:text=It%20is%20a%20life%2Dthreatening,%2C%20skin%2C%20or%20gastrointestinal%20tract.

8. Ramachandran G. Gram-positive and gram-negative Bacterial Toxins in Sepsis. Virulence [Internet]. 2013 Nov 5 [cited 2023 Oct 30];5(1):213–8. Available from: https://www.ncbi.nlm.nih.gov/pmc/articles/PMC3916377/

9. Cao M, Wang G, Xie J. Immune Dysregulation in sepsis: Experiences, Lessons, and Perspectives. Cell Death Discovery [Internet]. 2023 Dec 19 [cited 2024 Sep 30];9(1):1–

10. Hotchkiss RS, Coopersmith CM, McDunn JE, Ferguson TA. The Sepsis seesaw: Tilting toward Immunosuppression. Nature Medicine. 2009 May;15(5):496–7.

11.Cicchinelli S, Pignataro G, Gemma S, Piccioni A, Picozzi D, Ojetti V, et al. PAMPs and DAMPs in Sepsis: A Review of Their Molecular Features and Potential Clinical Implications. International Journal of Molecular Sciences [Internet]. 2024 Jan 1 [cited 2024 Sep 30];25(2):962. Available from: https://www.mdpi.com/1422-0067/25/2/962

12. Denning NL, Aziz M, Gurien SD, Wang P. DAMPs and NETs in Sepsis. Frontiers in Immunology. 2019 Oct 30;10.

13. Giustozzi M, Ehrlinder H, Bongiovanni D, Borovac JA, Guerreiro RA, Gąsecka A, et al. Coagulopathy and sepsis: Pathophysiology, Clinical Manifestations and Treatment. Blood Reviews. 2021 Nov; 50:100864.

14. Hu Q, Hao C, Tang S. From Sepsis to Acute Respiratory Distress Syndrome (ARDS): Emerging Preventive Strategies Based on Molecular and Genetic Research. Bioscience Reports [Internet]. 2020 [cited 2024 Sep 30];40(5). Available from: https://www.ncbi.nlm.nih.gov/pmc/articles/PMC7199454/

15. Tsantes AG, Parastatidou S, Tsantes EA, Bonova E, Tsante KA, Mantzios PG, et al. Sepsis-Induced Coagulopathy: An Update on Pathophysiology, Biomarkers, and Current Guidelines. Life [Internet]. 2023 Feb 1 [cited 2024 Sep 30];13(2):350. Available from: https://www.mdpi.com/2075-1729/13/2/350

16. Xu X, Wang Y, Tao Y, Dang W, Yang B, Li Y. Role of Platelets in Sepsis. Biomolecules & Biomedicine. 2024 Jan 18.

17. Ahsanullah Unar, Bertolino L, Patauner F, Gallo R, Emanuele Durante-Mangoni. Pathophysiology of Disseminated Intravascular Coagulation in Sepsis: A Clinically Focused Overview. Cells. 2023 Aug 22;12(17):2120–0.

18. Schmidt EP, Yang Y, Janssen WJ, Gandjeva A, Perez MJ, Barthel L, et al. The Pulmonary Endothelial Glycocalyx Regulates Neutrophil Adhesion and Lung Injury during Experimental Sepsis. Nature Medicine [Internet]. 2012 Aug 1 [cited 2024 Sep 30];18(8):1217–23. Available from: https://pubmed.ncbi.nlm.nih.gov/22820644/

19. Semeraro N, Ammollo CT, Semeraro F, Colucci M. Sepsis-Associated Disseminated Intravascular Coagulation and Thromboembolic Disease. Mediterranean Journal of Hematology and Infectious Diseases. 2010 Aug 6;2(3): e2010024.

20. Zhang H, Wang Y, Qu M, Li W, Wu D, Cata JP, et al. Neutrophil, Neutrophil Extracellular Traps and Endothelial Cell Dysfunction in Sepsis. Clinical and Translational Medicine. 2023 Jan;13(1).

21. Mithal LB, Arshad M, Swigart LR, Khanolkar A, Ahmed A, Coates BM. Mechanisms and Modulation of sepsis-induced Immune Dysfunction in Children. Pediatric Research. 2021 Dec 24;91(2):447–53.

22. Hotchkiss RS, Coopersmith CM, McDunn JE, Ferguson TA. The Sepsis seesaw: Tilting toward Immunosuppression. Nature Medicine. 2009 May;15(5):496–7.

23. Boucher J, Carpenter D. Sepsis: Symptoms, Assessment, Diagnosis, and the Hour-1 Bundle in Patients with Cancer. Clinical Journal of Oncology Nursing. 2020 Feb 1;24(1):99–102.

24. Mayo Clinic. Sepsis - Symptoms and Causes [Internet]. Mayo Clinic. 2023 [cited 2024 Sep 30]. Available from: https://www.mayoclinic.org/diseases-conditions/sepsis/symptoms-causes/syc-20351214

25. NICE. Antibiotic therapy, Intravenous Fluid and Oxygen | Suspected sepsis: recognition, Diagnosis and Early Management | Guidance | NICE [Internet]. www.nice.org.uk. 2024 [cited 2024 Sep 30]. Available from: https://www.nice.org.uk/guidance/ng51/chapter/Antibiotic-therapy-intravenous-fluid-and-oxygen

26. Strich JR, Heil EL, Masur H. Considerations for Empiric Antimicrobial Therapy in Sepsis and Septic Shock in an Era of Antimicrobial Resistance. The Journal of Infectious Diseases [Internet]. 2020 Jul 21 [cited 2024 Sep 30];222(Supplement_2): S119–31. Available from: https://www.ncbi.nlm.nih.gov/pmc/articles/PMC7372215/

27. World Health Organization. Global Antimicrobial Resistance and Use Surveillance System (GLASS) Report 2022. World Health Organization; 2022.

28. Browne K, Chakraborty S, Chen R, Willcox MD, Black DS, Walsh WR, et al. A New Era of Antibiotics: The Clinical Potential of Antimicrobial Peptides. International Journal of Molecular Sciences [Internet]. 2020 Jan 1 [cited 2024 Sep 5];21(19):7047. Available from: https://www.mdpi.com/1422-0067/21/19/7047/htm

29. Leong K, Gaglani B, Khanna AK, McCurdy MT. Novel Diagnostics and Therapeutics in Sepsis. Biomedicines [Internet]. 2021 Mar 18 [cited 2024 Sep 5];9(3):311. Available from: https://www.ncbi.nlm.nih.gov/pmc/articles/PMC8003067/

30. Tracey KJ, Fong Y, Hesse DG, Manogue KR, Lee AT, Kuo GC, et al. Anti-cachectin/TNF Monoclonal Antibodies Prevent Septic Shock during Lethal Bacteraemia. Nature [Internet]. 1987 Dec 17 [cited 2024 Sep 30];330(6149):662–4. Available from: https://pubmed.ncbi.nlm.nih.gov/3317066/

31. Hornberg J. Simple Drugs Do Not Cure Complex Diseases: The Need for Multi-Targeted Drugs. In: Designing Multi-Target Drugs. 2012. p. 1–13.

32. Kumar D, Patil VM, Wu D, Nanasaheb Thorat. Deciphering Drug Targets for Alzheimer's Disease. Springer Nature; 2023.

33. Blaikie L, Kay G, Kong Thoo Lin P. Synthesis, and in Vitro Evaluation of Vanillin Derivatives as Multi-target Therapeutics for the Treatment of Alzheimer's Disease. Bioorganic & Medicinal Chemistry Letters [Internet]. 2020 Nov [cited 2024 Sep 30];30(21):127505. Available from: https://doi.org/10.1016/j.bmcl.2020.127505

34. Dr. Priyanka Chandra. Description of Various Assay Procedures for Determination of Antioxidant Activity [Internet]. Biotecharticles.com. 2016 [cited 2024 Sep 30]. Available from: https://www.biotecharticles.com/Applications-Article/Description-of-Various-Assay-Procedures-for-Determination-of-Antioxidant-Activity-3712.html

35. Luo YL, Kishore B, Vijaya Kumar Kannekanti, Zhou CH, Cai GX. Novel Benzimidazole Derived Naphthalimide Triazoles: Synthesis, Antimicrobial Activity, and Interactions with Calf Thymus DNA. Science China-chemistry. 2015 Jan 20;58(3):483–94.

36. Kumar N, Goel N. Phenolic acids: Natural Versatile Molecules with Promising Therapeutic Applications. Biotechnology Reports [Internet]. 2019 Dec 1 [cited 2024 Sep 11];24(e00370): e00370. Available from: https://www.ncbi.nlm.nih.gov/pmc/articles/PMC6734135/

37. Takó M, Kerekes EB, Zambrano C, Kotogán A, Papp T, Krisch J, et al. Plant Phenolics and Phenolic-Enriched Extracts as Antimicrobial Agents against Food-Contaminating Microorganisms. Antioxidants [Internet]. 2020 Feb 18 [cited 2024 Sep 11];9(2):165. Available from: https://www.ncbi.nlm.nih.gov/pmc/articles/PMC7070704/

38. Chen J, Yang J, Ma L, Li J, Shahzad N, Kim CK. Structure-antioxidant Activity Relationship of methoxy, Phenolic hydroxyl, and Carboxylic Acid Groups of Phenolic Acids. Scientific Reports [Internet]. 2020 Feb 13 [cited 2024 Sep 11];10(1). Available from: https://www.nature.com/articles/s41598-020-59451-z

39. Thebti A, Meddeb A, Ben Salem I, Bakary C, Ayari S, Rezgui F, et al. Antimicrobial Activities and Mode of Flavonoid Actions. Antibiotics [Internet]. 2023 Feb 1 [cited 2024 Sep 11];12(2):225. Available from: https://www.mdpi.com/2079-6382/12/2/225

40. Larsen JB, Hvas AM. Fibrin Clot Formation and Lysis in Plasma. Methods and Protocols. 2020 Sep 25;3(4):67.

41. Fatemeh Khashami. Chemical shift, NMR Spectroscopy and beyond. Chemical shift, NMR Spectroscopy and beyond. 2023 Oct 24;107–20.

42. Willoughby PH, Jansma MJ, Hoye TR. A Guide to Small-Molecule Structure Assignment through Computation of (^{1}H and ^{13}C) NMR Chemical Shifts. Nature Protocols. 2014 Feb 20;9(3):643–60.

43. National Committee for Clinical Laboratory Standards. Methods for dilution antimicrobial susceptibility tests for bacteria that grow aerobically: approved standard. 9th ed. Vol. 32. Wayne, Pa. National Committee for Clinical Laboratory Standards (Nccls; 2003.

44. Petiti J, Revel L, Divieto C. Standard Operating Procedure to Optimize Resazurin-Based Viability Assays. Biosensors [Internet]. 2024 Mar 26 [cited 2024 May 10];14(4):156–6. Available from: https://www.ncbi.nlm.nih.gov/pmc/articles/PMC11048620/

45. Adusei EBA, Adosraku RK, Oppong-Kyekyeku J, Amengor CDK, Jibira Y. Resistance Modulation Action, Time-Kill Kinetics Assay, and Inhibition of Biofilm Formation Effects of Plumbagin from Plumbago Zeylanica Linn. Journal of Tropical Medicine [Internet]. 2019 Nov 26 [cited 2024 Sep 24]; 2019:1–8. Available from: https://www.ncbi.nlm.nih.gov/pmc/articles/PMC6899278/

46. Kumar S, Saxena J, Srivastava VK, Kaushik S, Singh H, Abo-EL-Sooud K, et al. The Interplay of Oxidative Stress and ROS Scavenging: Antioxidants as a Therapeutic Potential in Sepsis. Vaccines [Internet]. 2022 Sep 20 [cited 2024 Sep 13];10(10):1575. Available from: https://www.ncbi.nlm.nih.gov/pmc/articles/PMC9609850/#:~:text=Oxidative%20stress%20resulting%20from%20the%20disproportion%20of%20oxidants,%28ROS%29%20leading%20to%20the%20reduction%20of%20oxidative%20stress.

47. Kehrer JP. The Haber-Weiss Reaction and Mechanisms of Toxicity. Toxicology [Internet]. 2000 Aug 14 [cited 2024 Sep 13];149(1):43–50. Available from: https://pubmed.ncbi.nlm.nih.gov/10963860/

48. Chiodi D, Ishihara Y. The Role of the Methoxy Group in Approved Drugs. European Journal of Medicinal Chemistry. 2024 Apr 1;116364–4.

49. Chen J, Yang J, Ma L, Li J, Shahzad N, Kim CK. Structure-antioxidant Activity Relationship of methoxy, Phenolic hydroxyl, and Carboxylic Acid Groups of Phenolic Acids. Scientific Reports. 2020 Feb 13;10(1).

50. Carretero GPB, Saraiva GKV, Rodrigues MA, Kiyota S, Bemquerer MP, Chaimovich H, et al. Naphthalimide-Containing BP100 Leads to Higher Model Membranes Interactions and Antimicrobial Activity. Biomolecules. 2021 Apr 8;11(4):542.

51. FRIEDMAN M, HENIKA PR, MANDRELL RE. Antibacterial Activities of Phenolic Benzaldehydes and Benzoic Acids against Campylobacter jejuni, Escherichia coli, Listeria monocytogenes, and Salmonella enterica. Journal of Food Protection. 2003 Oct 1;66(10):1811–21.

52. Chaves BJ, Tadi P. Gentamicin [Internet]. PubMed. Treasure Island (FL): StatPearls Publishing; 2021 [cited 2024 Oct 1]. Available from: https://www.ncbi.nlm.nih.gov/books/NBK557550

53. Neto LJ de L, Ramos AGB, Freitas TS de, Barbosa CR dos S, de Sousa Júnior DL, Siyadatpanah A, et al. Evaluation of Benzaldehyde as an Antibiotic Modulator and Its Toxic Effect against Drosophila Melanogaster. Molecules. 2021 Sep 13;26(18):5570.

54. Pannell R, Li S, Gurewich V. Highly Effective Fibrinolysis by a Sequential Synergistic Combination of Mini-Dose tPA plus Low-Dose Mutant proUK. Brophy JM, editor. PLOS ONE. 2015 Mar 26;10(3): e0122018.

55. Scipioni M, Kay G, Megson I, Kong Thoo Lin P. Novel Vanillin derivatives: Synthesis, antioxidant, DNA and Cellular Protection Properties. European Journal of Medicinal Chemistry. 2018 Jan; 143:745–54.

56. Chen YY, Gopala L, Bheemanaboina RRY, Liu HB, Cheng Y, Geng RX, et al. Novel Naphthalimide Aminothiazoles as Potential Multitargeting Antimicrobial Agents. ACS Medicinal Chemistry Letters. 2017 Dec 7;8(12):1331–5.

57. Zhang PL, Laiche MH, Li YL, Gao WW, Lin JM, Zhou CH. An Unanticipated Discovery of Novel Naphthalimidopropanediols as Potential Broad-spectrum Antibacterial Members. European Journal of Medicinal Chemistry [Internet]. 2022 Nov 5 [cited 2024 Oct 2]; 241:114657. Available from: https://www.sciencedirect.com/science/article/pii/S0223523422005591

58. Silvestrini A, Meucci E, Ricerca BM, Mancini A. Total Antioxidant Capacity: Biochemical Aspects and Clinical Significance. International Journal of Molecular Sciences. 2023 Jul 1;24(13):10978–8.

59. Zaidi SRH, Rout P. Interpretation of Blood Clotting Studies, and Values (PT, PTT, aPTT, INR, Anti-Factor Xa, D-Dimer) [Internet]. PubMed. Treasure Island (FL): StatPearls Publishing; 2024 [cited 2024 Oct 2]. Available from: https://www.ncbi.nlm.nih.gov/books/NBK604215/

60. Dipak Kumar Sahoo, Wong D, Anil Patani, Biswaranjan Paital, Virendra Kumar Yadav, Patel A, et al. Exploring the Role of Antioxidants in sepsis-associated Oxidative Stress: A Comprehensive Review. Frontiers in cellular and infection microbiology. 2024 Mar 6;14.

61. Chen X, Liu Y, Gao Y, Shou S, Chai Y. The Roles of Macrophage Polarization in the Host Immune Response to Sepsis. International Immunopharmacology. 2021 Jul; 96:107791.

62. Rudd KE, Johnson SC, Agesa KM, Shackelford KA, Tsoi D, Kievlan DR, et al. Global, regional, and National Sepsis Incidence and mortality, 1990–2017: Analysis for the Global Burden of Disease Study. The Lancet. 2020 Jan 18;395(10219):200–11.

63. Gotts JE, Matthay MA. Sepsis: Pathophysiology and Clinical Management. BMJ [Internet]. 2016 May 23 [cited 2024 Oct 7];353(353). Available from: https://www.bmj.com/content/353/bmj.i1585
64.
Chousterman BG, Swirski FK, Weber GF. Cytokine Storm and Sepsis Disease Pathogenesis. Seminars in Immunopathology. 2017 May 29;39(5):517–28.

65. Sahu SK, Kulkarni DH, Ozanturk AN, Ma L, Kulkarni HS. Emerging Roles of the Complement System in Host–pathogen Interactions. Trends in Microbiology [Internet]. 2022 Apr [cited 2024 Oct 7];30(4):390–402. Available from: https://www.cell.com/trends/microbiology/fulltext/S0966-842X%2821%2900213-4?dgcid=raven_jbs_etoc_email

66. Sang Y, Roest M, de Laat B, de Groot PG, Huskens D. Interplay between Platelets and Coagulation. Blood Reviews [Internet]. 2020 Jul 12 [cited 2024 Oct 7];46. Available from: https://www.ncbi.nlm.nih.gov/pmc/articles/PMC7354275/

67. Vardon-Bounes F, Ruiz S, Gratacap MP, Garcia C, Payrastre B, Minville V. Platelets Are Critical Key Players in Sepsis. International Journal of Molecular Sciences. 2019 Jul 16;20(14):3494.

68. Pierrakos C, Velissaris D, Bisdorff M, Marshall JC, Vincent JL. Biomarkers of sepsis: Time for a Reappraisal. Critical Care. 2020 Jun 5;24(1).

69. Dey S, Manogaran D, Manogaran S, Schaefer HF. Substituent Effects on the Aromaticity of benzene—An Approach Based on Interaction Coordinates. The Journal of Chemical Physics. 2019 Jun 7;150(21):214108.

70. Savin KA. Reactions of Nucleophiles and Bases. Writing Reaction Mechanisms in Organic Chemistry. 2014;93–159.

71. Miljković M. Relative Reactivity of Hydroxyl Groups in Monosaccharides. Carbohydrates. 2009 Aug 3;113–42.

72. Guglielmi P, Pontecorvi V, Rotondi G. Natural Compounds and Extracts as Novel Antimicrobial Agents. Expert Opinion on Therapeutic Patents. 2020 Dec 1;30(12):949–62.

73. Tunçer S, Gurbanov R, Sheraj I, Solel E, Esenturk O, Banerjee S. Low Dose Dimethyl Sulfoxide Driven Gross Molecular Changes Have the Potential to Interfere with Various Cellular Processes. Scientific Reports. 2018 Oct 4;8(1):14828.

74. Longhin EM, El Yamani N, Rundén-Pran E, Dusinska M. The Alamar Blue Assay in the Context of Safety Testing of Nanomaterials. Frontiers in Toxicology. 2022 Sep 28;4.

75. Smith WPJ, Wucher BR, Nadell CD, Foster KR. Bacterial defences: mechanisms, Evolution and Antimicrobial Resistance. Nature Reviews Microbiology [Internet]. 2023 Apr 24 [cited 2024 Oct 17]; 21:1–16. Available from: https://www.nature.com/articles/s41579-023-00877-3

76. Munteanu IG, Apetrei C. Analytical Methods Used in Determining Antioxidant Activity: a Review. International Journal of Molecular Sciences. 2021 Mar 25;22(7):3380.

77. Baliyan S, Mukherjee R, Priyadarshini A, Vibhuti A, Gupta A, Pandey RP, et al. Determination of Antioxidants by DPPH Radical Scavenging Activity and Quantitative Phytochemical Analysis of Ficus Religiosa. Molecules [Internet]. 2022 Feb 16 [cited 2024 Oct 17];27(4):1326. Available from: https://www.ncbi.nlm.nih.gov/pmc/articles/PMC8878429/

78. Kearney KJ, Pechlivani N, King R, Tiede C, Phoenix F, Cheah R, et al. Affimer Proteins as a Tool to Modulate Fibrinolysis, Stabilize the Blood clot, and Reduce Bleeding Complications. Blood. 2019 Mar 14;133(11):1233–44.

79. Khoshmohabat H, Paydar S, Kazemi HM, Dalfardi B. Overview of Agents Used for Emergency Hemostasis. Trauma Monthly [Internet]. 2016 Feb 6 [cited 2024 Oct 17];21(1). Available from: https://www.ncbi.nlm.nih.gov/pmc/articles/PMC4869418/

80. Borges A, Bento L. Organ Crosstalk and Dysfunction in Sepsis. Annals of Intensive Care. 2024 Sep 19;14(1).

82. Wright BA, Sarpong R. Molecular Complexity as a Driving Force for the Advancement of Organic Synthesis. Nature Reviews Chemistry. 2024 Sep 9.

83. Abel, Gaspar E. 1.1. Separation, Purification, and Identification of the Components of a Mixture. The Royal Society of Chemistry eBooks. 2016 Dec 16;1–5.

84. Huemer M, Mairpady Shambat S, Brugger SD, Zinkernagel AS. Antibiotic Resistance and Persistence—Implications for Human Health and Treatment Perspectives. EMBO Reports [Internet]. 2020 Dec 3 [cited 2024 Oct 17];21(12). Available from: https://www.embopress.org/doi/full/10.15252/embr.202051034

85. National Mass Spectrometry Facility Swansea. Mass Spectrometry at Swansea University [Internet]. Swan.ac.uk. 2021 [cited 2024 Oct 18]. Available from: https://nmsf.swan.ac.uk/index.php?page=applications-and-instruments

86. Ramsay RR, Popovic-Nikolic MR, Nikolic K, Uliassi E, Bolognesi ML. A Perspective on Multi-target Drug Discovery and Design for Complex Diseases. Clinical and Translational Medicine. 2018 Jan 17;7(1).

87. Zschäbitz S, Grüllich C. Lenvantinib: A Tyrosine Kinase Inhibitor of VEGFR 1-3, FGFR 1-4, PDGFRα, KIT and RET. Recent Results in Cancer Research

Fortschritte Der Krebsforschung Progres Dans Les Recherches Sur Le Cancer [Internet]. 2018 [cited 2024 Oct 25]; 211:187–98. Available from: https://pubmed.ncbi.nlm.nih.gov/30069768/

88. Bolognesi ML, Cavalli A, Melchiorre C. Memoquin: a multi-target-directed Ligand as an Innovative Therapeutic Opportunity for Alzheimer's Disease. Neurotherapeutics. 2009 Jan;6(1):152–62.

89. Hsu WT, Porta L, Chang I-Jing, Dao QL, Tehrani BM, Hsu TC, et al. Association Between Aspirin Use and Sepsis Outcomes: A National Cohort Study. Anesthesia & Analgesia. 2022 Mar 4;135(1):110–7.

90. Toner P, McAuley DF, Shyamsundar M. Aspirin as a Potential Treatment in Sepsis or Acute Respiratory Distress Syndrome. Critical Care. 2015 Oct 23;19(1).

91. Inata Y. Should We Treat sepsis-induced DIC with anticoagulants? Journal of Intensive Care. 2020 Feb 14;8(1).

92. National Center for Biotechnology Information. Aspirin [Internet]. National Library of Medicine. PubChem; 2004 [cited 2024 Oct 31]. Available from: https://pubchem.ncbi.nlm.nih.gov/compound/aspirin

93. Casu B. Heparin Structure. Haemostasis. 1990;20 Suppl 1:62–73.

94. Ben-Moussa MT, Khelil K, Harkat H, Lakehal S, Hadef Y. Chemical composition, Antimicrobial and Antioxidant Activity of the Essential Oil of Brocchia Cinerea VIS. from Algeria. Batna Journal of Medical Sciences (BJMS). 2020 Nov 9;7(2):122–8.